

Conference on Advances in Topological Condensed Matter | (SMR 3980)

11 Nov 2024 - 15 Nov 2024
ICTP, Trieste, Italy

P01 - ACCIAI Matteo

Role of scaling dimensions in generalized noises in fractional quantum Hall tunnelling due to a temperature bias

P02 - ANAS OMER ABDELWAHAB MOHAMMED -

Topological phases of arbitrary number of coupled Su-Schrieffer-Heeger wires

P03 - ARAYA DAY Isidora Melania

Pymablock: an algorithm and a package for quasi-degenerate perturbation theory

P04 - ASSILI Mohamed

Dynamical chiral symmetry and symmetry-class conversion in Floquet topological insulators

P05 - BAU Nicolas

Local Z₂ topological markers: Theory and applications

P06 - BEHERA Sushant Kumar

Relativistic Insights into Electron Transport in Chiral Molecules

P07 - BEIRANVAND Razieh

Chirality Transfer Torques and Planar Hall current at the Ferromagnet/Normal interface of 3D Topological Insulators

P08 - BERADZE Bachana

Emergence of non-Abelian SU(2) invariance in Abelian frustrated fermionic ladders

P09 - BERNABEU GOMEZ Joan

Hysteresis of Dynamical Axion Insulators

P10 - BHATTACHARYYA Kuntal

Topological phase transition through electron-phonon interaction in an α -T₃ lattice

P11 - BUCCHERI Francesco

Dispersive drumhead states in nodal-line semimetal junctions

P12 - BUNNEY Matthew Thomas

Topological Superconductivity in Hexagonal Lattice Systems

P13 - CAVICCHI Lorenzo

Plasmons as proxies of orbital skyrmion textures: the case of twisted MoTe₂

P14 - CHERAGHCHI Hossein

Light-Induced Electronic States in Thin Topological Insulators

P15 - CHESI Stefano

Dynamics of spiral magnetic order in an electrically-biased Kondo chain

P16 - DAS Ankur

Topological Semimetals via Internal Symmetry

P17 - DAS Sanjib Kumar

From Local to Emergent Altermagnetism: Footprints of Free Fermions Band Topology

P18 - DEL POZO Frederick Carlos-Rodrigo

Topological signatures of a p-wave superconducting wire through light

P19 - DE Suman Jyoti

Magnon transmission across $|\nu=1|-1|1$ mono-layer graphene junction as a probe of electronic structure

P20 - FARIDI Azadeh

Valley-contrasting magnetoresistance beyond the relaxation-time approximation

P21 - FAVATA Roberta

Topological phase diagram of two-band fermionic chain in presence of Hubbard interaction

P22 - FORTIN Clement

Non-Hermitian Topological Phase Transition of the Bosonic Kitaev Chain

P23 - GHORAI Koushik

Planar Hall Effect in Quasi-Two-Dimensional Materials

P24 - GHOSH Arnob Kumar

Local and energy-resolved topological invariants for Floquet systems

P25 - GHOSH Sudeep Kumar

Spin-triplet superconductivity in topological semimetals

P26 - GIRI Debasmita

Skyrmion Stripes in Twisted Double Bilayer Graphene

P27 - HUA Jiannan

Layer-polarized ferromagnetism and electrical switching of chirality in rhombohedral multilayer graphene

P28 - HUAMANI CORREA Jorge Luis

The Development of Adjustable Exceptional Points in p - wave Altermagnets

P29 - KOBIALKA Aksel Wit

Topological superconductivity in Fibonacci quasicrystals

P30 - KUMARI Rekha

Josephson-Current Signatures of Unpaired Floquet Majorana Bound States

P31 - LAHIRI Srijata

Competing topological phases in a non-Hermitian time-reversal symmetry-broken Bernevig-Hughes-Zhang model

P32 - LIN Hengfu

Spin-orbit splitting and piezoelectric properties of Janus Ge_2XY ($X \neq Y = \text{P, As, Sb and Bi}$)

P33 - LIU Tianyu

Poster: "Fermi arcs and Landau levels in superconducting topological semimetals" Talk: "Pseudo Electromagnetic Fields in Dirac Matter"

P34 - MARTINAZZO Rocco

Dynamics of the molecular geometric phase

P35 - MENICHETTI Guido

Giant chirality-induced spin polarization in twisted transition metal dichalcogenides

P36 - MIDYA Bikashkali

Topological phase transition in non-Hermitian gauge fields

P37 - MILES Sebastian

Interaction-induced strong zero modes in short quantum dot chains with time-reversal symmetry

P38 - MOHAMMADI Fatemeh

\mathbb{Z}_2 Topological Order in Strongly Correlated Systems

P39 - MONDAL Sayan

Superconducting Diode Effect in Josephson Junction with Zeeman Field and Rashba Spin-Orbit Coupling

P40 - PANU Carlo

Heat-charge separation in a hybrid superconducting quantum Hall setup

P41 - PEZO LOPEZ Armando Arquimedes

Theory of spin and orbital charge conversion at the surface states of $\text{Bi}_{1-x}\text{Sb}_x$ topological insulator

P42 - PICCIONI Davide

Insulating and metallic phases in the 1D Hubbard-Su-Schrieffer-Heeger model: Insights from a backflow-inspired variational wave function

P43 - RAVICHANDRAN Ranjith Kumar

Signatures of topological phase transition on a quantum critical line

P44 - REDDY Aidan Patrick

Non-Abelian fractionalization in topological minibands

P45 - REHMAN Majeed Ur

Emerging Spintronic and Valleytronic Phenomena in Non-Centrosymmetric Variants of the Kane-Mele $\text{X}_4\text{Y}_2\text{Z}_6$ Materials Family (X=Pt, Pd, Ni; Y=Hg, Zn, Cd; Z=S, Se, Te).

P46 - RITU -

Generic control of measurement-induced topological phase transitions

P47 - ROY KARMAKAR Abhirup

First-principles study of photocurrents in non-centrosymmetric magnetic Weyl semimetal CeAlSi

P48 - RÜEGG Luca

Dualities of paired quantum Hall bilayer states at total filling $1/2 + 1/2$

P49 - RUSSOMANNO Angelo

Kitaev ring threaded by a magnetic flux: Topological gap, Anderson localization of quasiparticles, and divergence of supercurrent derivative.

P50 - SALEHI Morteza

Transverse chirality current in the magnetic Weyl semimetal/ superconductor junction

P51 - SHAH Muzamil

Topological characterization of monolayer jacutingaite

P52 - SHARMA Hemant Kumar

Emerging topology in a hybrid SSH model due to the competition between higher order hopping and spin-orbit coupling

P53 - SINGH Arushi

Characterization of Silicon Carbide Biphenylene Network Through GW-BSE Simulations

P54 - SINGH Mukhtiyar

Investigating Topological Phase Transition in Rare-Earth Monopnictide Semimetals: A first-principles Approach

P55 - SINGH Poorva

Exploring Novel Topological Phases in 3D Materials: Theoretical Insights and Predictions

P56 - TAKAHASHI Hidemitsu

Evidence of Magnetism Induced by Drumhead Surface States in the Dirac Line-Nodal Semimetal CaAgP

P57 - TIRANDARI Mehraneh

Dependence of the conserved quantities in tilted Dirac material on the amount of tilting

P58 - TORRES LUNA Juan Daniel

Probing valley phenomena with gate-defined valley splitters

P59 - TRAVERSO Simone

Emerging Majorana bound states in superconducting Haldane nanoribbons

P60 - TRUONG Bill

Shuttling of Majorana zero modes in disordered and noisy topological superconducting wires

P61 - VERMA Sonu

Topological phase transitions of generalized Brillouin zones in Hermitian and non-Hermitian systems

P62 - VIMAL Vimallesh Kumar

Geometric measure of entanglement in systems with poor man's Majorana modes

P63 - VOSOUGHI NIA Sakineh

Dynamical Hall responses of disordered superconductors

P64 - YALAVALLI RAMACHANDRA SUBRAY HEDGE Kartik

Quantum geometric analysis of non-Hermitian Kitaev chain with long-range couplings

P65 - ZHANG Xiaofei

Topological defects in Rydberg-dressed Bose gases with spin-orbit coupling

P66 - ZIJDERVELD Ronja Johanna

Scattering theory of higher order topological insulators

Role of scaling dimensions in generalized noises in fractional quantum Hall tunnelling due to a temperature bias

M. Acciai^{1,2}, **G. Zhang**³, and **C. Spånslätt**^{1,4}

¹*Department of Microtechnology and Nanoscience (MC2), Chalmers University of Technology, S-412 96 Göteborg, Sweden*

²*Scuola Internazionale Superiore di Studi Avanzati, Via Bonomea 265, 34136, Trieste, Italy*

³*Beijing Academy of Quantum Information Sciences, Beijing 100193, China*

⁴*Department of Engineering and Physics, Karlstad University, Karlstad, Sweden*

Continued improvement of heat control in mesoscopic conductors [1] brings novel tools for probing strongly correlated electron phenomena. In particular, heat transport in the fractional quantum Hall effect has recently attracted a lot of interest. Indeed, heat conductance measurements provide crucial information (typically not accessible by charge transport) about the edge structure, such as the number of edge channels and their chirality [2], thus distinguishing between candidate edge theories and, in principle, bulk topological orders. In addition, the analysis of charge fluctuations (or noise) due to temperature biases [3,4] (rather than the more common voltage-bias scenario) has recently emerged as an additional tool to probe the properties of fractional quantum Hall tunneling [5].

Motivated by these advances, we comprehensively study transport due to a temperature bias in a quantum point contact device in the fractional quantum Hall regime. We compute the charge-current noise (so-called delta-T noise), heat-current noise, and mixed noise and elucidate how these observables can be used to infer strongly correlated properties of the device [6]. Our main focus is the extraction of so-called scaling dimensions of the tunneling anyonic quasiparticles [7,8], of critical importance to correctly infer their anyonic exchange statistics.

[1] J. P. Pekola, B. Karimi, *Rev. Mod. Phys.* **93**, 041001 (2021).

[2] M. Banerjee, M. Heiblum, V. Umansky, D. E. Feldman, Y. Oreg, A. Stern, *Nature* **559**, 205 (2018).

[3] O. S. Lumbroso, L. Simine, A. Nitzan, D. Segal, O. Tal, *Nature* **562**, 240 (2018).

[4] S. Larocque, E. Pinsolle, C. Lupien, B. Reulet, *Phys. Rev. Lett.* **125**, 106801 (2020).

[5] N. Schiller, Y. Oreg, K. Snizhko, *Phys. Rev. B* **105**, 165150 (2022).

[6] M. Acciai, G. Zhang, C. Spånslätt, arXiv:2408.04525 (2024).

[7] A. Veillon, C. Piquard, P. Glidic, Y. Sato, A. Aassime, A. Cavanna, Y. Jin, U. Gennser, A. Anthore, F. Pierre, *Nature* **632**, 517 (2024).

[8] N. Schiller, T. Alkalay, C. Hong, V. Umansky, M. Heiblum, Y. Oreg, K. Snizhko, arXiv:2403.17097 (2024).

Topological phases of arbitrary number of coupled Su-Schrieffer-Heeger wires

Anas Abdelwahab¹

¹ *Leibniz Universität Hannover, Germany*

We consider arbitrary number N_w of Su-Schrieffer-Heeger (SSH) wires coupled with single particle perpendicular or diagonal hopping. Both systems respect the symmetries of the BDI class. We investigate the topological phases of these two systems with respect to the dimerization and the wire-wire coupling. Perpendicularly coupled even number of wires have either gappless or trivial topological phases. For odd number of wires they have gappless, trivial and nontrivial topological phases with winding number $w = 1$. The diagonally coupled wires have topological phases that depend on the number of wires, dimerization and the wire-wire coupling. The values of winding numbers are in the range $0 \leq w \leq N_w$. Critical lines in the phase diagrams of diagonally coupled SSH ladders reveal topological gappless phases [1, 2]. The topological phases of single SSH wire is adiabatically connected to the symmetry-protected-topological (SPT) phases in the corresponding dimerized spin- $\frac{1}{2}$ wire [3]. We discuss implications of the topological phases in the coupled SSH wires on SPT phases in their corresponding coupled spin- $\frac{1}{2}$ wires. We discuss possibilities of constructing W states [4] at the edges of coupled SSH wires with open boundary conditions.

- [1] Ruben Verresen, Ryan Thorngren, Nick G. Jones, and Frank Pollmann, Phys. Rev. X **11**, 041059 (2021).
- [2] Ruben Verresen, arXiv:2003.05453.
- [3] David Mikhail, Benoit Voisin, Dominique Didier St Medar, Gilles Buchs, Sven Rogge, and Stephan Rachel, Phys. Rev. B **106**, 195408 (2022).
- [4] W. Dür, G. Vidal, and J. I. Cirac Phys. Rev. A **62**, 062314 (2000).

Pymablock: an algorithm and a package for quasi-degenerate perturbation theory

Isidora Raya Day², Sebastian Miles¹, Hugo K. Kerstens², Daniel Varjas^{3,4}, Anton R. Khmerov²

¹ QuTech, Delft University of Technology, Delft 2600 GA, The Netherlands

² Kavli Institute of Nanoscience, Delft University of Technology, P.O. Box 4056, 2600 GA Delft, The Netherlands

³ Max Planck Institute for the Physics of Complex Systems, Nothnitzer Strasse 38, 01187 Dresden, Germany

⁴ Institute for Theoretical Solid State Physics, IFW Dresden and Wurzburg-Dresden Cluster of Excellence ct.qmat, Helmholtzstr. 20, 01069 Dresden, Germany

A common technique in the study of complex quantum-mechanical systems is to reduce the number of degrees of freedom in the Hamiltonian by using quasi-degenerate perturbation theory. While the Schrieffer–Wolff transformation achieves this and constructs an effective Hamiltonian, its scaling is suboptimal, and implementing it efficiently is both challenging and error-prone. We introduce an algorithm for constructing an equivalent effective Hamiltonian as well as a Python package, Pymablock, that implements it. Our algorithm combines an optimal asymptotic scaling with a range of other improvements. The package supports numerical and analytical calculations of any order and it is designed to be interoperable with any other packages for specifying the Hamiltonian. We demonstrate how the package handles constructing a $k \cdot p$ model, analyses a superconducting qubit, and computes the low-energy spectrum of a large tight-binding model. We also compare its performance with reference calculations and demonstrate its efficiency.

[1] I. Raya Day, S. Miles, H. K. Kerstens, D. Varjas, A. R. Khmerov, arXiv: 2404.03728 (2024).

Dynamical chiral symmetry and symmetry-class conversion in Floquet topological insulators

Mohamed Assili, and Panagiotis Kotetes

CAS Key Laboratory of Theoretical Physics, Institute of Theoretical Physics, Chinese Academy of Sciences, Beijing 100190, China

In this work, we discuss properties with no static counterpart arising in Floquet topological insulators with a dynamical chiral symmetry (DCS), i.e., a chiral symmetry which is present while driving [1]. We explore the topological properties of Floquet insulators possessing a DCS which either does or does not survive upon taking the static limit. We consider the case of harmonic drives and employ a general framework using the quasienergy operator in frequency space [2]. We find that for a DCS with no static analog, the presence of driving has a negligible impact on the topological phases associated with zero quasienergy. In stark contrast, topological gaps can open at π quasienergy and mainly occur at momenta where the driving perturbation vanishes. We confirm the above general predictions for an extended Kitaev chain model in the BDI symmetry class. Another possibility that opens up when adding the drive, while preserving chiral symmetry, is symmetry-class conversion. We demonstrate such an effect for a static CI class Hamiltonian which is topologically trivial in one dimension. By considering a suitable driving, we obtain a CI \rightarrow AIII transition, which now enables the system to harbor topological π modes. Notably, the arising topological phases strongly depend on whether or not the DCS has a static analog. Our results bring Floquet insulators with nonstandard DCS forward as ideal candidate platforms for engineering and manipulating topological π modes [3].

[1] T. Oka and H. Aoki, Photovoltaic Hall effect in graphene, *Phys.Rev. B* **79**, 081406 (2009).

[2] A. Eckardt and E. Anisimovas, High-frequency approximation for periodically driven quantum systems from a Floquet-space perspective, *New J. Phys.* **17**, 093039 (2015).

[3] L. Zhou and J. Gong, Floquet topological phases in a spin-1/2 double kicked rotor, *Phys. Rev. A* **97**, 063603 (2018).

Local \mathbb{Z}_2 topological markers: Theory and applications

N. Baù¹, R. Favata¹ A. Marrazzo²

¹*Dipartimento di Fisica, Università di Trieste, Strada Costiera 11, I-34151 Trieste, Italy*

²*Scuola Internazionale Superiore di Studi Avanzati (SISSA), Via Bonomea 265, I-34136 Trieste, Italy*

Topological invariants are global properties of the ground-state wave function, typically defined as winding numbers in reciprocal space. Over the years, a number of topological markers have been introduced, allowing to probe the topological order locally in real space even for disordered and inhomogeneous systems [1]. Here, I will address time-reversal symmetric systems in two dimensions and introduce two local \mathbb{Z}_2 topological markers [2]. The first formulation is based on a generalization of the spin-Chern number [3] while the second one is based solely on time-reversal symmetry [4]. Then, I will introduce a formulation of the local Chern marker for extended systems with periodic boundary conditions [5, 6], and extend it to the aforementioned \mathbb{Z}_2 markers [7]. Finally, I will show numerical simulations to validate the approach, including pristine, disordered and inhomogeneous systems, such as topological/trivial heterojunctions, and I will apply our framework to study topological phase transitions driven by Anderson disorder [8].

- [1] Raffaello Bianco and Raffaele Resta, Phys. Rev. B 84, 241106(R) (2011)
- [2] Nicolas Baù and Antimo Marrazzo, Phys. Rev. B 110, 054203 (2024)
- [3] Emil Prodan, Phys. Rev. B 80, 125327 (2009)
- [4] Alexey A. Soluyanov and David Vanderbilt, Phys. Rev. B 85, 115415 (2012)
- [5] Nicolas Baù and Antimo Marrazzo, Phys. Rev. B 109, 014206 (2024)
- [6] Davide Ceresoli and Raffaele Resta, Phys. Rev. B 76, 012405 (2007)
- [7] Roberta Favata and Antimo Marrazzo, Electron. Struct. 5 014005 (2023)
- [8] Roberta Favata, Nicolas Baù and Antimo Marrazzo, in preparation

Relativistic Insights into Electron Transport in Chiral Molecules

Sushant Kumar Behera¹, Ruggero Sala², Abhirup Roy Karmakar³, Rocco Martinazzo³ and Matteo Cococcioni¹

¹*Department of Physics, Università degli Studi di Pavia, 27100 Pavia, Italy.*

²*Department of Chemistry, Università degli Studi di Pavia, 27100 Pavia, Italy.*

³*Department of Chemistry, Università degli studi di Milano, 20133 Milano, Italy*

The Chirality-Induced Spin Selectivity (CISS) effect refers to the ability of chiral molecules and crystals to preferentially transmit spin-polarized currents, a phenomenon first observed in 1999 [1]. Despite its promising technological applications in spintronics and electron transfer, a comprehensive understanding of the underlying mechanisms remains elusive [2,3]. It is widely believed that the effect arises from enhanced spin-orbit coupling (SOC) in chiral molecules [4,5]. However, the magnitude of the SOC needed to explain the experimental evidence far exceeds the one that can be computed from the usual atomic average for the involved species (most frequently, light atoms). Using the relativistic implementation of DFT contained in the DIRAC code we study how the structural chirality of a molecule reflects itself on the chirality of its outermost electrons, and how the distribution of this quantity is changed by an applied external electric field. By approaching a magnetic molecule to the chiral one we also study how the decay of the spin polarisation depends on its degree of chirality. Finally employ the Landauer-Imry-Büttiker formalism to assess how spin-dependent transmission depends on the twist angle of the structure. While qualitatively consistent with observations, our results point to the need for more advanced exchange-correlation functionals, able to capture the effect of a more general definition of SOC, e.g. through the dependence on the spin current density.

[1] K. Ray, S. P. Ananthavel, D. H. Waldeck, *Science* **283**, 814 (1999).

[2] F. Evers, *et al.* *Adv. Mater.* **34**, 2106629 (2022).

[3] S. Dalum, P. Hedegård, *Nano Lett.* **19**, 5253 (2019).

[4] X. Zhao, *et al.* *Phys. Rev. Lett.* **133**, 036201 (2024).

[5] Y. Adhikari, *et al.* *Nat. Commun.* **14**, 5163 (2023).

Chirality Transfer Torques and Planar Hall current at the Ferromagnet/Normal interface of 3D Topological Insulators

Razieh Beiranvand¹ Morteza Salehi²







¹*Physics department, Faculty of Basic Science, Ayatollah Borujerdi University, Borujerd, Iran.*

²*Physics departemtn, Faculty of Basic Science, Bu-Ali Sina University, Hamadan, Iran.*

In-plane magnetization on the surface of three-dimensional topological insulators (3D TIs) tunes the Dirac cone's location in the k -space. We theoretically show that a normal/ferromagnetic junction on the surface of 3D TIs bends the propagation direction of Dirac fermions when the magnetization has a component perpendicular to the junction. This effect leads to a Hall conductance, which flows parallel to the interface. Also, it creates an indirect gap that manifests itself in the longitudinal conductance of the junction. The sign of Hall conductance is related to the in-plane magnetization direction. Based on this effect, we propose a set up to detect it experimentally. Moreover, this bending effect imposes a torque on the junction called current transfer torque (CTT). We show the z -component of CTT is non-zero in the presence of bending effect. Also, its value and direction that can be used in fabricating new devices are related to the Hall conductance.

[1] Razieh Beiranvand and Morteza Salehi, *J. Phys. Cond. Matt.* **33**, 32541 (2021).

Emergence of non-Abelian SU(2) invariance in Abelian frustrated fermionic ladders

Bachana Beradze ^{1,2}, Mikheil Tsitsishvili ^{3,4}, Emanuele Tirrito ^{3,5}, Marcello Dalmonte ^{3,4},
Titas Chanda ^{3,6,*} and Alexander Nersesyan ^{1,2,3,†}

¹*Andronikashvili Institute of Physics, 0177 Tbilisi, Georgia*

²*Ilia State University, 0162 Tbilisi, Georgia*

³*The Abdus Salam International Centre for Theoretical Physics (ICTP), 34151 Trieste, Italy*

⁴*International School for Advanced Studies (SISSA), 34136 Trieste, Italy*

⁵*Pitaevskii BEC Center, CNR-INO and Dipartimento di Fisica, Università di Trento, Trento, I-38123, Italy*

⁶*Department of Physics, Indian Institute of Technology Indore, Indore 453552, India*



(Received 16 May 2023; revised 24 July 2023; accepted 10 August 2023; published 21 August 2023)

We consider a system of interacting spinless fermions on a two-leg triangular ladder with $\pi/2$ magnetic flux per triangular plaquette. Microscopically, the system exhibits a U(1) symmetry corresponding to the conservation of total fermionic charge and a discrete \mathbb{Z}_2 symmetry—a product of parity transformation and chain permutation. Using bosonization, we show that, in the low-energy limit, the system is described by the quantum double-frequency sine-Gordon model. On the basis of this correspondence, a rich phase diagram of the system is obtained. It includes trivial and topological band insulators for weak interactions, separated by a Gaussian critical line, whereas at larger interactions a strongly correlated phase with spontaneously broken \mathbb{Z}_2 symmetry sets in, exhibiting a net charge imbalance and nonzero total current. At the intersection of the three phases, the system features a critical point with an emergent SU(2) symmetry. This non-Abelian symmetry, absent in the microscopic description, is realized at low energies as a combined effect of the magnetic flux, frustration, and many-body correlations. The criticality belongs to the SU(2)₁ Wess-Zumino-Novikov-Witten universality class. The critical point bifurcates into two Ising critical lines that separate the band insulators from the strong-coupling symmetry broken phase. We establish an analytical connection between the low-energy description of our model around the critical bifurcation point on one hand and the Ashkin-Teller model and a weakly dimerized XXZ spin-1/2 chain on the other. We complement our field-theory understanding via tensor network simulations, providing compelling quantitative evidences of all bosonization predictions. Our findings are of interest to up-to-date cold atom experiments utilizing Rydberg dressing that have already demonstrated correlated ladder dynamics.

DOI: [10.1103/PhysRevB.108.075146](https://doi.org/10.1103/PhysRevB.108.075146)

I. INTRODUCTION

Experimental setups involving ultracold atoms, trapped in optical tweezer arrays and laser coupled to highly excited Rydberg states, have demonstrated, in recent years, the remarkable potential for simulating strongly correlated quantum phases of many-body systems under controllable experimental conditions [1–7]. Rydberg atom platforms, where large and long-lived van der Waals-type interactions between Rydberg states can extend over relatively long distances (tunable even up to a few microns), provide unique opportunities to probe the many-body system at single-site levels with high experimental precision and control [8]—a feat that is unattainable in conventional cold atoms in optical lattices governed by Hubbard-like physics (see, e.g., Ref. [9]).

In a typical experimental scenario of optical tweezer arrays, Rydberg states are populated with the dynamics between the Rydberg states being much faster compared to the respective atomic motion. Such a setup of Rydberg arrays is often described by interacting spin-1/2 models [10,11] paving the

way to study frustrated magnetism in a controllable laboratory setting [12–15] and offers various fascinating phenomena both in one- (1D) and two- (2D) dimensional settings (see, e.g., Refs. [1,7,13–20]).

In an alternative experimental scenario, the ground states of trapped ultracold atoms in optical lattices are weakly coupled to virtually populated Rydberg states—the so-called Rydberg dressing—resulting in generalized Hubbard-like systems with tunable long-range interactions [21–24]. The dynamics of such Rydberg dressed systems lies in the intermediate regime between the conventional Hubbard models describing ultracold atoms on optical lattices and the frozen Rydberg gases trapped in optical tweezers. In 1D with a single bosonic field, Rydberg dressed systems show exotic critical behavior like cluster Luttinger liquids [25] and emergent supersymmetric critical transition [26]. In 2D settings, these systems are associated with anomalous dynamics and glassy behavior [27,28]. Along with these theoretical endeavors, the many-body dynamics of Hubbard models with long-range Rydberg-dressed interactions in 2D has been realized in a recent experiment [29].

While the aforementioned cases are mostly focused on either 1D or 2D geometries, in this work, we consider the

*titas.hri@gmail.com

†alex.a.nersesyan@gmail.com

intermediate regime between these two—a ladder geometry that can accommodate interactions and magnetic terms possible in 2D geometries, while simultaneously being tractable by analytical and numerical methods that are suitable for 1D systems. In recent years, ladder systems with Rydberg dynamics have been subjected to various theoretical works, which includes coupled-cluster Luttinger liquids and coupled supersymmetric critical transitions [30–32], Ising criticality by order-by-disorder mechanism [33], chiral three-state Potts criticality [34], among many others. Another interesting scenario that is being explored over the years in the ladder systems involves the effect of external (synthetic) magnetic flux [35–50], where vortex phases, topological properties, chiral boundary currents, topological Lifshitz transitions, etc., have been investigated.

In the present work, we consider the scenario of an optical lattice system on a two-leg triangular ladder geometry where ultracold spinless fermions are trapped and subjected to a synthetic magnetic flux by means of Raman-assisted tunneling [51–54]. Moreover, the fermions can be coupled to Rydberg states (i.e., the Rydberg dressing) by off-resonant laser driving that can trigger controllable interactions between the fermions. The system exhibits a $U(1)$ symmetry corresponding to the conservation of total fermion number and a discrete \mathbb{Z}_2 symmetry coming from the joint operation of parity transformation and chain inversion. This minimal setting beyond 1D allows for the exploration of the interplay between the magnetic flux, interactions, and the geometrical frustrations and the associated emerging phenomena that can be investigated using well-established analytical and numerical techniques.

In a recent paper [55], by considering the triangular ladder system with an asymmetric single-particle hopping across zigzaglike interchain links in the noninteracting limit, the effect of the interplay between geometric frustration and magnetic flux has been thoroughly investigated focusing on the single-particle band structures. Due to the breakdown of $k \rightarrow \pi - k$ particle-hole symmetry, two isolated low-energy Dirac-like excitations with different masses emerge. This leads to a sequence of Lifshitz transitions on the variation of magnetic flux in the vicinity of the critical flux value of $\pi/2$ per triangular plaquette. The Lifshitz points for fixed chemical potential and fixed particle density belong to different universality classes. In the maximally frustrated case (i.e., the scenario of symmetric hopping across zigzag interchain links), the Dirac-like excitations at the boundary of the Brillouin zone become gapless, rendering the system very susceptible to possible many-body interactions.

In this work, by utilizing a combination of field-theoretical approaches based on bosonization [56,57] and numerical simulations based on tensor networks (TN) [58–60], we extend this exploration by introducing many-body correlations among the fermions in the form of interchain nearest-neighbor interactions. Our particular interest is in the understanding of the interplay between geometrical frustration, an external synthetic flux of $\pi/2$ per triangular plaquette, and many-body correlations.

We find that the system is described by the double-frequency sine-Gordon (DSG) model at low energies. This enables us to predict a rich phase diagram that consists of triv-

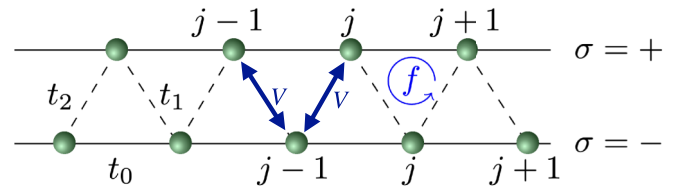


FIG. 1. Spinless fermions on a two-leg triangular ladder. The integer j labels the diatomic unit cells. t_0 , t_1 , and t_2 denote the amplitudes of single-particle nearest-neighbor hopping along the chains and between them. We consider $f = 1/2$ flux per triangular plaquettes (in units of π) and interchain nearest-neighbor interaction of strength V .

ial and topological band insulators at weak interactions and an insulating phase with spontaneously broken \mathbb{Z}_2 symmetry at strong couplings. The analytical predictions coming from the phenomenological analysis of the DSG model are validated by large-scale TN simulations: Crucially, we combine both matrix-product-state and tree tensor network simulations [58–60], that, as we detail below, demonstrate complementary capabilities in probing different parts of the phase diagram. We show that the trivial and topological band insulators are separated by a Gaussian critical line, that terminates with a Berezinskii-Kosterlitz-Thouless (BKT) transition to the strong-coupling symmetry-broken phase. This critical endpoint bifurcates into two Ising critical lines that separate the band insulator phases from the strong-coupling \mathbb{Z}_2 symmetry-broken insulator phase.

The most exciting physics lies in the low-energy description of the critical endpoint of the Gaussian critical line that bifurcates into two Ising critical lines. At this critical endpoint, the system exhibits enlarged non-Abelian $SU(2)$ symmetry that is entirely absent in the microscopic description of the system, which only respects Abelian $\mathbb{Z}_2 \times U(1)$ symmetry. Indeed, starting with our model of interacting spinless fermions on a flux-ladder and applying the usual Jordan-Wigner (JW) transformation along the zigzag path (see Fig. 1), one would arrive at a lattice spin model which is not $SU(2)$ invariant. The emergence of non-Abelian $SU(2)$ symmetry arises due to the combined effects of the synthetic magnetic flux, interactions, and the geometrical frustrations, taking place only in the low-energy limit. At this limit, operators that explicitly violate this non-Abelian symmetry become *irrelevant* in the renormalization group sense as their scaling dimensions are greater than the space-time dimension of 2. We show that this critical endpoint belongs to the $SU(2)_1$ Wess-Zumino-Novikov-Witten (WZNW) universality class [56,61]. Furthermore, we draw an analytical connection of the low-energy description around this critical bifurcation point to the Ashkin-Teller model [62–65] and a weakly dimerized XXZ spin-1/2 chain.

The paper is organized as follows. In Sec. II we introduce the fermionic system on two-leg triangular ladder geometry and state its symmetry properties, and give a brief overview of the results of this work. In Sec. III, we provide the analytical low-energy description of the system using bosonization in terms of the DSG model, and predict the phase diagram, including $SU(2)_1$ WZNW bifurcation criticality, by phenomenological analysis of the DSG model. Section IV

discusses the connection between the low-energy description of the $SU(2)_1$ WZNW criticality in this frustrated fermionic ladder with the Ashkin-Teller model and a weakly dimerized XXZ spin-1/2 chain. We validate the predictions of field-theoretical analytical treatments by performing numerical simulations based on tensor-network algorithms in Sec. V. Finally, we conclude with Sec. VI.

II. THE SYSTEM

We consider a paradigmatic spinless fermionic system on a two-leg triangular ladder in the presence of external magnetic flux as shown in Fig. 1. Its Hamiltonian is given by

$$\begin{aligned} H &= H_0 + H_{\text{int}}, \\ H_0 &= -t_0 \sum_{j,\sigma=\pm} (e^{-i\pi\sigma f} c_{j,\sigma}^\dagger c_{j+1,\sigma} + \text{H.c.}) \\ &\quad - \sum_j (t_1 c_{j,+}^\dagger c_{j,-} + t_2 c_{j,+}^\dagger c_{j-1,-} + \text{H.c.}), \\ H_{\text{int}} &= V \sum_j \hat{n}_{j,+} (\hat{n}_{j,-} + \hat{n}_{j-1,-}). \end{aligned} \quad (1)$$

Here $c_{j,\sigma}$ and $c_{j,\sigma}^\dagger$ are annihilation and creation operators for a spinless fermion on the chain $\sigma = \pm$ with j labeling diatomic unit cells, $\hat{n}_{j,\sigma} = c_{j,\sigma}^\dagger c_{j,\sigma}$ are occupation number operators, t_0 and $t_{1,2}$ are the intra- and interchain tunneling amplitudes, and $f = \Phi_{\square}/\phi_0$ is the magnetic flux per triangular plaquette measured in units of the flux quantum $\phi_0 = hc/e$. H_{int} stands for the nearest-neighbor density-density interaction of amplitude V between fermions residing on top and bottom chains. We work at the regime of half-filling.

The dynamics we are interested in is relevant to cold atom gases in optical lattices, in the presence of off-resonant laser drive to Rydberg states (the Rydberg dressing) [21–24]. In particular, laser-dressing to p states generated a strong anisotropic interaction: The latter can be made very strong vertically, and very weak horizontally, realizing the interaction pattern described by H_{int} [12,26]. Such couplings have been recently realized experimentally in Ref. [29], while distance selection (which could also be utilized for our case here) has also been demonstrated in Ref. [66]. The tunneling dynamics can instead be engineered utilizing laser-assisted tunneling [51]. We note that the system is also relevant for experiments with trapped ions [67].

The properties of the noninteracting flux-ladder model H_0 have been recently studied in detail in Ref. [55]. It has been shown that in the regime of weak interchain hopping, $0 < t_{1,2} \ll t_0$, the effect of the geometric frustration is most pronounced in the limit $|t_1 - t_2| \ll t_1 + t_2$ and $f \rightarrow \frac{1}{2}$. At $f = \frac{1}{2}$ the low-energy excitations, as described by the dispersion relations

$$\omega(k)_{\pm} = \pm \sqrt{4t_0^2 \sin^2 k + t_1^2 + t_2^2 + 2t_1 t_2 \cos k}, \quad (2)$$

are represented by two branches of massive Dirac fermions, with momenta close to $k = 0$ and $k = \pi$ in the Brillouin zone, and with masses $M = t_1 + t_2$ and $m = t_1 - t_2$, respectively. We will be referring to them as *heavy* (M) and *light* (m) fermionic sectors. The degree of frustration in the noninter-

acting case can be quantified by the ratio $\delta = t_2/t_1 = (M - m)/(M + m)$. The model is maximally frustrated in the $m \rightarrow 0$ limit. At $f = 1/2$ the ground state of a half-filled ladder with $m \neq 0$ is insulating. Under the same conditions with $m = 0$, the presence of a Dirac node at $k = \pi$ renders the spectrum of the ladder gapless. Such a system is very susceptible to correlations between the particles. Consequently, we will be considering $f = \frac{1}{2}$ regime only.

The Hamiltonian Eq. (1) possesses a \mathbb{Z}_2 symmetry which we label by \mathcal{P} : It is a product of parity transformation ($j \rightarrow -j$) and permutation of the chains ($\sigma \rightarrow -\sigma$). Obviously, H has a global $U(1)$ symmetry related to the conservation of the total particle number. However, except for the limit of two decoupled chains ($t_1 = t_2 = 0$, $f = 0$), the total fermionic Hamiltonian H does not display an apparent $SU(2)$ symmetry for any values of the parameters of the model. One of the main results of this paper is the demonstration that, in fact, in the massless case ($m = t_1 - t_2 = 0$) at a certain value of the coupling constant V the system occurs in a critical state with central charge $c = 1$, where it is characterized by the non-Abelian $SU(2)$ symmetry.

In a symmetric flux ladder ($m = 0$) at $f = 1/2$, at some critical value V_c of the interaction constant, the system undergoes a transition from a Tomonaga-Luttinger (TL) liquid phase ($V < V_c$) to a long-range ordered phase ($V > V_c$) with a spontaneously broken discrete \mathcal{P} symmetry. The ordered phase is characterized by a finite interchain charge transfer and a nonzero spontaneous current along the ladder. Starting from the broken-symmetry phase and increasing the zigzag asymmetry m or decreasing V , one observes two Ising critical lines (with central charge $c = 1/2$), signifying transitions to two band insulator phases, one of them being topological ($m < 0$) while the other nontopological ($m > 0$). We show, both analytically and numerically, that the two Ising critical lines merge at an Ashkin-Teller (AT) bifurcation point $V = V_c$, $m = 0$, as shown in Fig. 2. We show, both analytically and numerically, that at this point the symmetry of the underlying criticality is promoted to $SU(2)_1$ WZNW universality class. The emergence of this $SU(2)$ criticality is a remarkable property of the originally Abelian model of spinless fermions on a triangular ladder, emerging at low energies as a combined effect of frustration, flux, and correlations.

III. ANALYTICAL APPROACH TO A WEAKLY COUPLED FLUX LADDER: EFFECTIVE BOSONIZED MODEL

In our analytical treatment of the interacting model, we concentrate on the limit of weak repulsive interaction, $V \ll W$, with $W = 2t_0$ being the ultraviolet energy cutoff. In the low-energy range, i.e., $E \sim |m| \ll M \ll W$, the most important states reside in the light sector. Interaction H_{int} induces scattering processes within and between the light and heavy sectors. In the low-energy range under consideration, the interaction in the heavy sector is of minor importance, because the finite mass M cuts off infrared divergences of the scattering amplitudes. Integrating out the heavy modes reduces to renormalization of the parameters of the effective Hamiltonian of the light sector. Assuming that all these renormalizations are taken into account, in what follows we will concentrate

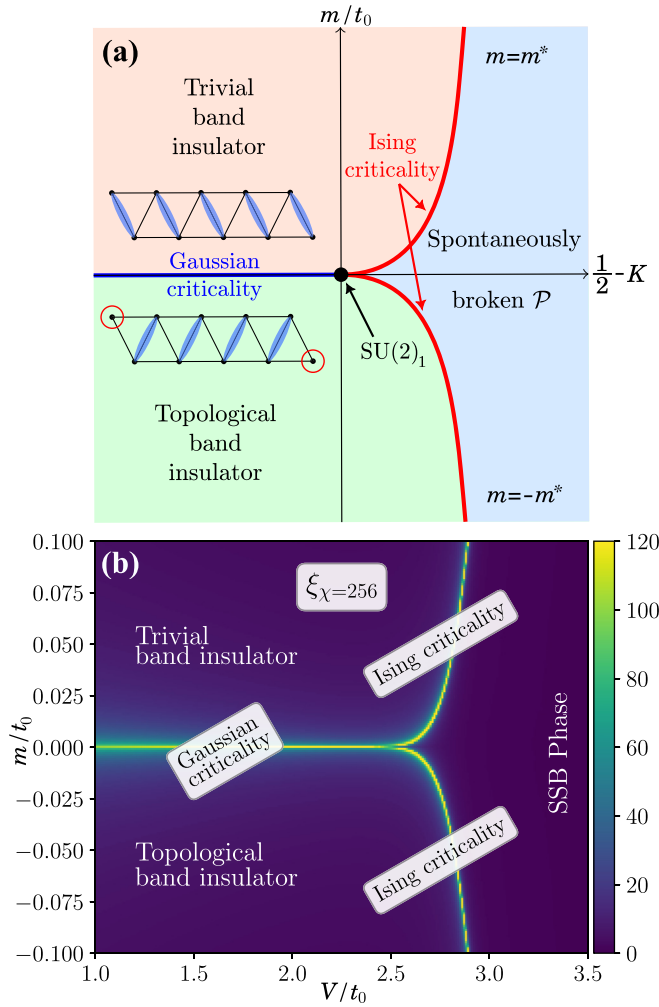


FIG. 2. (a) The phase diagram of the DSG model [Eq. (13)] that dictates that low-energy description of the lattice Hamiltonian (1). The blue line corresponds to U(1) Gaussian criticality with $c = 1$. The black dot at the origin is the $SU(2)_1$ critical point with $c = 1$. Two red lines are the Ising criticalities with $m = \pm m^*$ critical lines and $c = 1/2$. In the band insulator phases, shaded in orange and green, the dimerization is nonzero along t_1 and t_2 links. The orange and green regions correspond to trivial and topological (see Appendix B) band insulator phases, respectively. The region shaded in blue corresponds to the phase with spontaneously broken \mathcal{P} symmetry—a combination of parity and chain interchange operations. This phase is characterized by the nonzero total current along the chains, which is proportional to the charge imbalance between the chains. (b) The phase diagram of the lattice Hamiltonian (1) obtained by iDMRG simulations. We plot the correlation length ξ_χ for the iMPS bond dimension $\chi = 256$ in the $(m, V/t_0)$ plane (see Sec. V for details). Diverging values of the correlation length clearly indicate that the critical line at $m = 0$ bifurcates into two critical lines at around $V/t_0 \simeq 2.45$ akin to the DSG model. Apart from these critical lines, all the phases are gapped, and these phases are trivial and topological band insulators, and twofold degenerate spontaneous symmetry-broken (SSB) phase.

on the fermionic modes with momenta $k \sim \pi$ and small mass gap m .

We define the continuum limit for the lattice fermionic operators by using the correspondence

$$c_{j\sigma} \rightarrow \sqrt{a_0}(-1)^j \Psi_\sigma(x), \quad (\sigma = \pm), \quad (3)$$

where $\Psi_\sigma(x)$ are slowly varying fermionic fields describing single-particle excitations with momenta close to the zone boundary $k = \pi$, and a_0 is the lattice constant along the chain which we set to 1. Accordingly, in the light sector, the unperturbed Hamiltonian density of the light fermionic modes takes the following continuum form:

$$\mathcal{H}_0(x) = \Psi^\dagger(x)[-iv_F(\hat{\sigma}_3 + \tau\hat{\sigma}_2) + m\hat{\sigma}_1]\Psi(x),$$

$$\text{with } \Psi = \begin{pmatrix} \Psi_+ \\ \Psi_- \end{pmatrix}, \quad (4)$$

where $\tau = t_2/W = (M - m)/2W$ is proportional to the frustration parameter δ . The kinetic energy in Eq. (4) is brought to a canonical Dirac form by an $SU(2)$ rotation of the spinor Ψ around the $\hat{\sigma}_1$ axis,

$$\Psi(x) = U\chi(x), \quad \chi = \begin{pmatrix} R \\ L \end{pmatrix}, \quad U = u + iv\hat{\sigma}_1$$

$$u^2 - v^2 \equiv \cos \gamma = \frac{1}{\sqrt{1 + \tau^2}}, \quad (5)$$

$$2uv \equiv \sin \gamma = \frac{\tau}{\sqrt{1 + \tau^2}},$$

with $u^2 + v^2 = 1$. As a consequence, in the rotated (band) basis the Hamiltonian \mathcal{H}_0 becomes

$$\mathcal{H}_0(x) = \chi^\dagger(x)(-i\tilde{v}\hat{\sigma}_3\partial_x - m\hat{\sigma}_1)\chi(x), \quad (6)$$

where $\tilde{v} = v_F\sqrt{1 + \tau^2}$ is the renormalized velocity. It is important to realize that the role of the frustration parameter τ is not exhausted by the above velocity renormalization of the single-particle excitations. As we show below, in the continuum limit, frustration in the τ^2V -order generates pair-hopping scattering processes which, in the rotated basis, are responsible for the onset of a strong-coupling phase with broken \mathcal{P} symmetry.

In Appendix A, we provide the expressions for the particle densities on each chain valid in the continuum limit in both chain and band representations. Using this expression and neglecting perturbative corrections to the frustration parameter τ (being of the order $g^n\tau$, $n \geq 1$), we obtain the continuum version of H_{int} :

$$H_{\text{int}} = \int dx \{ \lambda (: J_R^2 : + : J_L^2 :) + 2gJ_RJ_L + \lambda\mathcal{O}_{\text{ph}} \}. \quad (7)$$

Here

$$\mathcal{O}_{\text{ph}}(x) =: (R^\dagger L)_x (R^\dagger L)_{x+a} : + \text{H.c.} \quad (8)$$

is the interband pair-hopping operator, $J_{R,L}(x)$ are the chiral (right and left) components of the particle density—the U(1) chiral currents—see Appendix A,

$$\lambda = \frac{\tau^2 g}{2(1 + \tau^2)}, \quad (9)$$

and $g = Va_0$ is a coupling constant (a_0 being the lattice constant along the chains). Recasting the kinetic energy of the fermions as a quadratic form of the chiral currents [56], we

arrive at the following effective continuum model describing interacting fermions in the rotated basis of states:

$$\begin{aligned} \mathcal{H}(x) &= \mathcal{H}_0(x) + \mathcal{H}_{\text{int}}(x) \\ &= \pi v^* [: J_R^2(x) : + : J_L^2(x) :] \\ &\quad - mB(x) + 2gJ_R(x)J_L(x) + \lambda\mathcal{O}_{\text{ph}}(x), \end{aligned} \quad (10)$$

where the Dirac-mass operator $B(x)$ is defined in Eq. (A4) and Eq. (A9) and $v^* = \tilde{v} + \lambda/\pi$ is the Fermi velocity with an extra renormalization caused by interactions. Using the transformation properties of the fermionic fields, chiral currents, and mass bilinears under \mathcal{P} [see Appendix A, Eqs. (A12)], we find that $[\mathcal{H}, \mathcal{P}] = 0$.

Bosonization of the model Eq. (10) is based on the well-know Fermi-Bose correspondence [56,57]:

$$\begin{aligned} J_{R,L}(x) &= \frac{1}{\sqrt{\pi}} \partial_x \varphi_{R,L}(x), \quad \varphi_{R,L}(x) = \frac{1}{2} [\pm \Phi(x) + \Theta(x)], \\ R^\dagger(x)L(x) &= -\frac{i}{2\pi\alpha} e^{-i\sqrt{4\pi}\Phi(x)}, \end{aligned} \quad (11)$$

where $\varphi_{R,L}$ are chiral bosonic fields, $\Phi(x)$ and $\Theta(x)$ are the scalar field and its dual counterpart, and $\alpha \sim a_0$ is the short-distance cutoff of the bosonic theory. The fields Φ and Θ can be conveniently rescaled, $\Phi \rightarrow \sqrt{K}\Phi$, $\Theta \rightarrow \Theta/\sqrt{K}$, where

$$K = 1 - \frac{g}{2\pi v^*} + O(g^2) \quad (12)$$

is the so-called Luttinger-liquid interaction parameter. It decreases on increasing the interchain repulsion g ; however, its parametrization Eq. (12) is only universal at small values of g . Since the model at hand is not integrable, the exact analytical expression of $K = K(g)$ beyond the weak-coupling limit is not known. We need to rely on numerical tools to get the dependence of K at large values of g (see Sec. VC). Nevertheless, below we treat K as an independent phenomenological parameter of the model. Collecting all the terms we arrive at the fully bosonized effective Hamiltonian which has the structure of the DSG model [62,63]:

$$\begin{aligned} \mathcal{H}(x) &= \frac{v_c}{2} [: \Pi^2(x) : + : [\partial_x \Phi(x)]^2 :] \\ &\quad + \left(\frac{m}{\pi\alpha} \right) : \sin \sqrt{4\pi K} \Phi(x) : \\ &\quad - \frac{\lambda}{2(\pi\alpha)^2} : \cos \sqrt{16\pi K} \Phi(x) :, \end{aligned} \quad (13)$$

where $\Pi(x) = \partial_x \Theta(x)$ is the momentum canonically conjugate to the field $\Phi(x)$, and $v_c = v^*[1 + O(g^2)]$. The first two terms in Eq. (13) represent the Gaussian part of the Hamiltonian, while the remaining nonlinear terms contribute to the potential $\mathcal{U}[\Phi]$ whose profile is determined by the relative strength and signs of the λ and m perturbations. In a strong-coupling regime, the field Φ gets localized in one of the infinitely degenerate vacua of $\mathcal{U}[\Phi]$ thus determining the phase of the system. It is to be noted that when, in addition to V , the interaction also includes nearest-neighbor coupling along the chain— $V_0 \hat{n}_{j,\sigma} \hat{n}_{j+1,\sigma}$ —the DSG model (13) maintains its structure with a slightly modified velocity v_c and the parameter λ replaced by $\lambda = \tau^2(g - g_0)/2(1 + \tau^2)$, where $g_0 = V_0 a_0$.

Using Eqs. (A6)–(A9) and the rules Eq. (11), we derive the bosonized expressions of the local physical operators which will be used when discussing the correlation effects:

$$\rho_{\text{tot}}(x) = \sum_{\sigma} \rho_{\sigma}(x) = \sqrt{\frac{K}{\pi}} \partial_x \Phi(x), \quad (14)$$

$$\begin{aligned} \rho_{\text{rel}}(x) &= \sum_{\sigma} \sigma \rho_{\sigma}(x) = \frac{1}{v_F} j_0(x), \\ &= -\frac{1}{\sqrt{1 + \tau^2}} \left[\frac{1}{\sqrt{\pi K}} \partial_x \Theta(x) \right. \\ &\quad \left. - \left(\frac{\tau}{\pi\alpha} \right) : \cos \sqrt{4\pi K} \Phi(x) : \right], \end{aligned} \quad (15)$$

$$\begin{aligned} j_z(x) &= -\frac{v_F}{\sqrt{1 + \tau^2}} \left[\frac{\tau^2}{\sqrt{\pi K}} \partial_x \Theta(x) \right. \\ &\quad \left. + \left(\frac{\tau}{\pi\alpha} \right) : \cos \sqrt{4\pi K} \Phi(x) : \right], \end{aligned} \quad (16)$$

$$B(x) = -\frac{1}{\pi\alpha} : \sin \sqrt{4\pi K} \Phi(x) :. \quad (17)$$

A. Correlation effects

The relevance of the two operators entering the nonlinear potential $\mathcal{U}(\Phi)$ of the DSG model (13) is determined by their scaling dimensions: $d_m = K$ and $d_{\lambda} = 4K$. We will be mainly concerned with the case of a repulsive interchain interaction, $g > 0$, $K < 1$, and briefly comment on the attractive case $g < 0$, $K > 1$. At $K > 1/2$ the λ term in (13), which describes interband pair-hopping processes, is irrelevant, and the properties of the model are determined by the single-particle mass perturbation. It is well known [57] that, in one-dimensional models with short-range repulsive interactions, increasing local repulsion between the particles to push K to small-enough values may not be enough; longer-range interaction should be also invoked. Therefore, we will phenomenologically assume that interaction in the model is generalized in such a way that the regime with $K < 1/2$, where the λ perturbation becomes relevant, is feasible. In this case, the DSG model (13) describes the interplay of correlations and single-particle perturbations. Below we discuss the possible realization of different ground-state phases of the system.

1. $m = 0$ regime

This is the case of a symmetric triangular flux ladder ($t_1 = t_2$, i.e., $m = 0$) in which bare fermions with momenta $k \sim \pi$ are massless. The effective Hamiltonian Eq. (13) reduces to a standard sine-Gordon (SG) model:

$$\begin{aligned} \mathcal{H}(x) &= \frac{v_c}{2} \{ \Pi^2(x) + [\partial_x \Phi(x)]^2 \} \\ &\quad - \frac{\lambda}{2(\pi\alpha)^2} : \cos \sqrt{16\pi K} \Phi(x) :. \end{aligned} \quad (18)$$

When interchain repulsion V is not strong enough and $K > 1/2$, the λ perturbation is irrelevant, and in the infrared limit the Hamiltonian Eq. (18) flows to a Gaussian model. The latter describes a Tomonaga-Luttinger liquid phase with a gapless spectrum of collective excitations and power-law correlations with K -dependent critical exponents. As follows from the

definitions Eqs. (14)–(17), strong quantum fluctuations suppress any kind of ordering in the system, including charge imbalance between the legs of the ladder, dimerization along the zigzag links, and net current in the ground state. Within the range $1/2 < K < 1$, the τ -proportional part of the relative density Eq. (15) contributes to dominant correlations in the model: At distances $|x| > \alpha(K|\tau|)^{-\frac{1}{2(1-K)}}$ the corresponding correlation function follows the power law

$$\langle \rho_{\text{rel}}(x)\rho_{\text{rel}}(0) \rangle \simeq \frac{1}{2(\pi\alpha)^2} \frac{\tau^2}{1+\tau^2} \left(\frac{\alpha}{|x|} \right)^{2K}. \quad (19)$$

At $K < 1/2$, the λ perturbation in Eq. (18) becomes relevant and the model flows towards strong-coupling with a dynamical generation of a mass gap

$$m_\lambda \sim \frac{v_c}{\alpha} \left(\frac{|\lambda|}{v_c} \right)^{1/2(1-2K)}, \quad (K < 1/2). \quad (20)$$

Since $\lambda > 0$, the field Φ is locked in one of the infinitely degenerate vacuum values

$$\langle \Phi \rangle_l = \frac{1}{2} \sqrt{\frac{\pi}{K}} l, \quad l \in \mathbb{Z}. \quad (21)$$

Therefore $\langle B_1 \rangle = \langle B_2 \rangle = 0$, but the average relative density turns out to be nonzero,

$$\langle \rho_{\text{rel}} \rangle_\lambda = \pm \rho_0, \quad \rho_0 \sim |\tau|^{\frac{1-K}{1-2K}}. \quad (22)$$

According to Eqs. (15) and (16), the population imbalance between the chains is accompanied by a spontaneous generation of a net current,

$$\langle j_0 \rangle_\lambda = \langle j_z \rangle_\lambda = \frac{v_F}{\pi\alpha} \frac{\tau}{1+\tau^2} \langle : \cos \sqrt{4\pi K} \Phi(x) : \rangle_\lambda. \quad (23)$$

The spontaneous relative density, and hence the current, are nonanalytic functions of the frustration parameter τ . Being zero at $K > 1/2$, they exponentially increase on decreasing K in the region $K < 1/2$ following the law Eq. (22). The quantum phase transition taking place at $K = 1/2$ belongs to the BKT universality class [56,57].

Elementary excitations of the charge-transfer phase are topological quantum solitons of the SG model Eq. (18). They carry the mass given by Eq. (20) and a fractional fermionic number $Q_s = 1/2$. This number is identified with the topological charge of the soliton which interpolates between neighboring vacua of the cosine potential $\cos \sqrt{16\pi K} \Phi$:

$$Q_s = \sqrt{\frac{K}{\pi}} \int_{-\infty}^{\infty} dx \partial_x \Phi(x) = \frac{1}{2}. \quad (24)$$

2. $m \neq 0$ regime with $K > \frac{1}{2}$

At $K > 1/2$ and $m \neq 0$ the interband pair-hopping processes are irrelevant, and the effective theory is given by the SG model,

$$\mathcal{H}(x) = \frac{v_c}{2} [\Pi^2(x) + (\partial_x \Phi(x))^2] + \left(\frac{m}{\pi\alpha} \right) : \sin \sqrt{4\pi K} \Phi(x) :. \quad (25)$$

It describes a bosonized version of the theory of marginally perturbed massive fermions—the so-called massive Thirring

model [68]. The scalar field Φ is locked in one of the infinitely degenerate vacua,

$$\langle \Phi \rangle_l^{\text{vac}} = \sqrt{\frac{\pi}{K}} \left[-\frac{1}{4} \text{sgn}(m) + l \right], \quad l \in \mathbb{Z}. \quad (26)$$

Equation (26) displays two subsets of the vacua corresponding to different signs of m , each subset describing a band insulator. The excitation spectrum has a mass gap m_s :

$$m_s = C(K) \left(\frac{v_c}{\alpha} \right) \left(\frac{|m|\alpha}{v_c} \right)^{1/(2-K)} \text{sgn}(m), \quad (27)$$

where $C(K)$ is a dimensionless constant tending to 1 as $K \rightarrow 1$. The mass term in Eq. (25) explicitly breaks parity and, according to Eqs. (A9) and (17), leads to a finite dimerization $\langle B \rangle$ of the zigzag bonds of the ladder,

$$\langle B \rangle \sim |m_s|^K \text{sgn}(m) \sim |m|^{K/(2-K)} \text{sgn}(m). \quad (28)$$

The quantum soliton of the SG model Eq. (25) carries the mass m_s and topological charge $Q_F = 1$ and thus is identified as the fundamental fermion of the related massive Thirring model [68]. In the ground state $\langle \partial_x \Phi \rangle = \langle \partial_x \Theta \rangle = 0$. Moreover, for the vacuum values of the field Φ given by Eq. (26) the average $\langle \cos \sqrt{4\pi K} \Phi \rangle$ vanishes. So at $\rho = 1$ and $m \neq 0$ the total and relative densities remain unaffected by the flux. Correlations of the relative density are short ranged.

Thus, at $m \neq 0$ the SG model Eq. (25) describes band insulator phases. Their thermodynamic properties depend only on the magnitude of the spectral gap $|m_s|$, while their topological properties are determined by the sign of the bare mass m . With the sign of the “heavy” mass fixed ($M > 0$), the band insulator phase at $m > 0$ is topologically trivial, whereas the corresponding phase at $m < 0$ is topologically nontrivial. This conclusion has been reached in Ref. [55] by inspecting the 2×2 matrix structure of the Bloch Hamiltonian describing bulk properties of the noninteracting model. In the present paper, we provide extra support to this conclusion by studying boundary zero-energy states of a semi-infinite triangular asymmetric flux ladder. The corresponding calculations are given in Appendix B.

A more complete characterization of the two band insulating phases described by the SG model in Eq. (25) is extracted from the mass dependence of nonlocal order parameters [69]—the parity (\hat{O}_P) and string-order (\hat{O}_S) operators:

$$\hat{O}_P(j) = \exp \left(i\pi \sum_{k \leq j} \delta \hat{n}_k \right), \quad \hat{O}_S(j) = \hat{O}_P(j) \delta \hat{n}_j. \quad (29)$$

Here j labels the diatomic unit cells of the ladder, and $\delta \hat{n}_j = \sum_\sigma : c_{j\sigma}^\dagger c_{j\sigma} :$ is the density fluctuation on the zigzag rung j . Nonlocal string and parity orders have been considered earlier for interacting bosons [70–73] to specify the differences between the Mott and Haldane insulator gapped phases. It was shown that the two nonlocal order parameters are dual to each other [71]: $\langle \hat{O}_P \rangle \neq 0$, $\langle \hat{O}_S \rangle = 0$ for the Mott insulator, and $\langle \hat{O}_P \rangle = 0$, $\langle \hat{O}_S \rangle \neq 0$ for the Haldane insulator. Nonlocal parity and string order have been shown to characterize strongly correlated states of interacting fermions in strictly one-dimensional systems [74,75], as well as in fermionic ladder models [76–78]. Significant progress in the

direct measurement of nonlocal parity and string correlations in low-dimensional ultracold Fermi and Bose systems has recently been reported [17,79–82].

The string and parity order parameters, Eqs. (29), being nonlocal in terms of the densities \hat{n}_k , admit a local representation in terms of vertex operators of the effective SG model. In both Bose [71] and Fermi [78] cases, the perturbation to the Gaussian Hamiltonian for the field Φ was defined as $m \cos \sqrt{4\pi K} \Phi$, with the Luttinger-liquid constant K being close to 1. Using Abelian bosonization, with such a definition, one shows that in the continuum limit

$$\hat{O}_P(x) \sim \sin \sqrt{\pi K} \Phi(x), \quad \hat{O}_S(x) \sim \cos \sqrt{\pi K} \Phi(x). \quad (30)$$

However, in the SG model of Eq. (25) the perturbation is of the form $m \sin \sqrt{4\pi K} \Phi$. Therefore the bosonic representation of the operators \hat{O}_P and \hat{O}_S must be modified. The sine transforms to a cosine under the shift $\Phi \rightarrow \Phi - (1/4)\sqrt{\pi/K}$, implying the following the redefinition of the nonlocal order parameters,

$$\begin{aligned} \hat{O}_P &\rightarrow \frac{1}{\sqrt{2}}(\sin \sqrt{\pi K} \Phi - \cos \sqrt{\pi K} \Phi), \\ \hat{O}_S &\rightarrow \frac{1}{\sqrt{2}}(\cos \sqrt{\pi K} \Phi + \sin \sqrt{\pi K} \Phi). \end{aligned} \quad (31)$$

Using the fact that in the ground state of the SG model (25) the vacuum values of the field Φ are given by Eq. (26), we conclude that the expectation values of \hat{O}_P and \hat{O}_S are given by

$$\begin{aligned} \langle \hat{O}_P(m; l) \rangle &= (-1)^{l-1} F(m) \theta(m), \\ \langle \hat{O}_S(m; l) \rangle &= (-1)^l F(m) \theta(-m), \end{aligned} \quad l \in \mathbb{Z}, \quad (32)$$

where at $|m|\alpha/v \ll 1$ (i.e., in the vicinity of the Gaussian line $m = 0$) and

$$F(m) \sim \left(\frac{|m|\alpha}{v} \right)^{\frac{K}{4(2-K)}}.$$

Thus, the band insulator phase with $m > 0$ ($t_1 > t_2$) is topologically trivial ($\langle \hat{O}_S \rangle = 0$) and characterized by a nonzero nonlocal parity order ($\langle \hat{O}_P \rangle \neq 0$), whereas the phase with $m < 0$ ($t_1 < t_2$) represents a topological insulator with a nonzero string order ($\langle \hat{O}_S \rangle \neq 0$) but lacks parity order ($\langle \hat{O}_P \rangle = 0$). Below, in Sec. VB, we provide numerical evidence for this conclusion.

3. $m \neq 0$ regime with $K < \frac{1}{2}$

The most interesting situation arises when both perturbations of the DSG model in Eq. (13) are relevant. This case can be realized when the interchain repulsion satisfies the condition $g \geq g_c$, where g_c is a nonuniversal value of the coupling constant such that $K(g_c) = 1/2$. At $\lambda > 0$ the DSG potential of Eq. (13) is shown in Fig. 3. It represents a sequence of double-well potentials of the \mathbb{Z}_2 -symmetric Ginzburg-Landau theory with the minima merging into ϕ^4 local wells at $2\pi\alpha m/\lambda = 4$. These semiclassical considerations lead to the conclusion that at $\lambda > 0$ the interplay of the two perturbations of the DSG model is resolved as the appearance of quantum criticalities belonging to the Ising universality class with central charge $c = 1/2$ [62]. In the

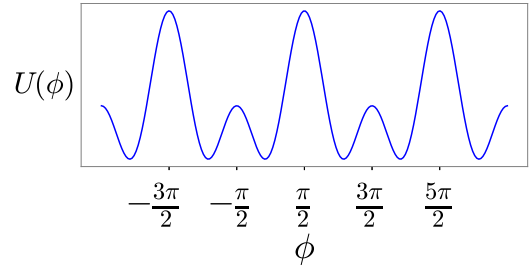


FIG. 3. A pictorial representation of the potential $U(\phi) = a \sin \phi - \cos 2\phi$, $\phi = \sqrt{4\pi K} \Phi$, $a = (2\pi\alpha)m/\lambda$.

following Sec. V, we confirm the existence of $c = 1/2$ criticalities for $m \neq 0$ at critical interaction strengths $V = V_c(m)$.

As pointed out in Ref. [62], at a quantum level, the infrared behavior of the DSG model is determined by the ratio of the mass gaps separately generated by each of the two perturbations in the absence of the other. The parameter $\varrho \sim |m_s/m_\lambda|$ controls the two perturbative regimes of the DSG model (13): $\varrho \rightarrow 0$ and $\varrho \rightarrow \infty$. The Ising transitions occur in a nonperturbative region where the two masses are of the same order. The condition $\varrho \sim 1$ gives an order-of-magnitude estimate of the critical curves on the plane (λ, m) :

$$m = \pm m^*(\lambda), \quad m^*(\lambda) \sim \frac{v_c}{\alpha} \left(\frac{\lambda}{v_c} \right)^{\frac{2-K}{2(1-2K)}}. \quad (33)$$

The two critical lines Eq. (33) separate the band-insulator phases, $|m| > m^*(\lambda)$, from the mixed phase occupying the region $-m^*(\lambda) < m < m^*(\lambda)$, in which charge imbalance coexists with dimerization of the zigzag bonds. As shown in Fig. 3, in the mixed phase the minima of the DSG potential decouple into two subsets,

$$\begin{aligned} (\Phi)_k^{\text{odd}} &= \frac{1}{2} \sqrt{\frac{\pi}{K}} \left(2k + 1 + \frac{\eta}{\pi} \right) \\ (\Phi)_k^{\text{even}} &= \frac{1}{2} \sqrt{\frac{\pi}{K}} \left(2k - \frac{\eta}{\pi} \right), \end{aligned} \quad (34)$$

where $k = 0, \pm 1, \pm 2, \dots$ and $\eta = a/4 = 2\pi\alpha m/4\lambda$. Accordingly, there are two types of massive topological excitations carrying η -dependent fractional charge. These kinks are associated with the vacuum-vacuum interset transitions $(\Phi)_k^{\text{odd}} \leftrightarrow (\Phi)_{k,k+1}^{\text{even}}$. The long kinks carry the charge $Q_+ = 1/2 + |\eta|/\pi$ and interpolate between the solitons of the $m = 0$ phase with spontaneously broken \mathcal{P} symmetry ($Q = 1/2$) and single-fermion excitations of the band-insulator phase ($Q = 1$). On the other hand, on approaching the Ising criticality, the short kinks with the topological quantum number $Q_- = 1/2 - |\eta|/\pi$ lose their charge and mass and transform to a neutral collective excitonic mode.

According to the analysis done in Ref. [63], in the vicinity of the critical lines Eq. (33) the gapped phases in the regions $|m| > m^*$ and $|m| < m^*$ are identified as Ising ordered and disordered phases, respectively. Near the transition the average relative density $\rho_{\text{rel}}(x)$ behaves as the disorder operator $\mu(x)$ of the underlying quantum Ising model [63]. Therefore, the phases realized at $|m| > m^*$ are the already discussed zigzag-dimerized insulating phases with equally populated

chains: $\langle : \rho_{\text{rel}} : \rangle = 0$. At $|m| < |m^*|$ the relative density acquires a finite expectation value which vanishes as

$$\langle : \rho_{\text{rel}} : \rangle \sim (|m^*| - |m|)^{1/8} \quad (35)$$

on approaching the critical point from below: $|m| \rightarrow |m^*| - 0$.

The two Ising critical lines merge at the point $m = 0, K = 1/2$ and, as shown in Fig. 2, transform to a Gaussian critical line $m = 0, K > 1/2$ which describes a Tomonaga-Luttinger liquid phase. In the next section, we show that the merging point of the Ising critical lines represents a bifurcation point of the AT model where the symmetry is enlarged to $SU(2)$.

IV. ASHKIN-TELLER AND DOUBLE-FREQUENCY SINE-GORDON MODELS: EQUIVALENCE TO A WEAKLY DIMERIZED XXZ SPIN-1/2 CHAIN

In this section, we elaborate on the relationship between the quantum 1D version of the AT model, staggered XXZ spin-1/2 chain, and the DSG model of Eq. (13) at K close to $1/2$. The relation between the AT model, considered in the scaling limit, and the DSG model of a scalar field has been anticipated in earlier studies [62–65]. Here we focus on the connection between the above two models on one hand, and an effective isotropic $S = 1/2$ Heisenberg chain, weakly perturbed by an explicit dimerization and exchange anisotropy, on the other.

The classical AT model describes two identical 2D Ising models coupled by a four-spin interaction. As is well known [83], by virtue of transfer matrix formalism, two-dimensional classical statistics can be viewed as an imaginary-time (i.e., Euclidean) version of quantum mechanics in $1 + 1$ dimensions. The quantum lattice version of the AT model was derived in [84]:

$$\begin{aligned} H_{\text{QAT}} = & -\frac{1}{4} \sum_{j=1}^N [(J_+ \sigma_{1,j}^z \sigma_{1,j+1}^z + J_- \sigma_{1,j}^x) \\ & + (J_+ \sigma_{2,j}^z \sigma_{2,j+1}^z + J_- \sigma_{2,j}^x) \\ & + q(J_+ \sigma_{1,j}^z \sigma_{1,j+1}^z \sigma_{2,j}^z \sigma_{2,j+1}^z + J_- \sigma_{1,j}^x \sigma_{2,j}^x)]. \quad (36) \end{aligned}$$

The Hamiltonian (36) describes two coupled quantum Ising chains. The relationship between the constants J_{\pm}, q and main parameters of the 2D AT model can be found in Ref. [84]. At $q = 1$, H_{QAT} possesses a hidden $SU(2)$ symmetry. Indeed, using a specially designed nonlocal unitary transformation it has been shown [84] that the quantum AT model (36) is exactly equivalent to a model of a staggered XXZ spin-1/2 chain:

$$H_S = \sum_{n=1}^{2N} [J_0 + (-1)^n J_1] (\mathbf{S}_n \cdot \mathbf{S}_{n+1} + \rho S_n^z S_{n+1}^z), \quad (37)$$

where $J_{0,1} = (J_{\pm} \pm J_{\mp})/2, \rho = q - 1$.

At $|J_{\pm}|, |\rho| \ll J$, the model in Eq. (37) occurs in the vicinity of the isotropic Heisenberg point, $J_{\pm} = \rho = 0$, where it is critical with the central charge $c = 1$ and whose properties in the scaling limit are described by the critical $SU(2)_1$ WZNW

model with a marginally irrelevant perturbation [85]:

$$\mathcal{H}_0 = \frac{2\pi v_s}{3} (: \mathbf{J}_R^2 : + : \mathbf{J}_L^2 :) - g_0 \mathbf{J}_R \cdot \mathbf{J}_L, \quad (38)$$

with $g_0 \sim v_s \sim J_0 a_0 > 0$. Here $\mathbf{J}_{R,L}$ are the generators of the chiral, level-1 $SU(2)$ Kac-Moody algebra (see for details the textbooks [61,86]). A finite ρ term in (37) introduces exchange anisotropy. The translationally invariant chain ($J_{\pm} = 0$) with $\rho < 0$ occurs in a Tomonaga-Luttinger liquid phase with ρ -dependent critical exponents [87], whereas at $\rho > 0$ the system enters a gapped Neel phase with a doubly degenerate ground state [88]. The Neel ordering is site-parity (P_S) symmetric but breaks spontaneously link parity (P_L). At $\rho = 0, J_{\pm} \neq 0$ the chain maintains spin-rotational symmetry but is explicitly dimerized. Its spectrum is massive. The J_{\pm} perturbation breaks P_S but preserves P_L .

So there are two, mutually incompatible by symmetry, “massive” directions at the $SU(2)$ critical point parametrized by the couplings J_{\pm} and ρ . Their competition gives rise to the splitting of the $SU(2)_1$ WZNW criticality into two Ising criticalities. For small values of J_{\pm} and ρ the low-energy properties of the model in Eq. (37) with both perturbations present can be adequately described in terms of a perturbed Gaussian theory with the structure of the DSG model [84]:

$$\begin{aligned} \mathcal{H}_{\text{DSG}} = & \frac{u_s}{2} [(\partial_x \Phi)^2 + (\partial_x \Theta)^2] \\ & + \frac{h}{\pi \alpha} \sin \sqrt{2\pi K_s} \Phi - \frac{g_{\perp}}{(2\pi \alpha)^2} \cos \sqrt{8\pi K_s} \Phi. \quad (39) \end{aligned}$$

This mapping is valid up to irrelevant corrections. In Eq. (39) u_s is a renormalized velocity, $h \sim J_{\pm}$,

$$K_s = \left(\frac{1 - g_{\parallel}/4\pi v_s}{1 + g_{\parallel}/4\pi v_s} \right)^{1/2} \simeq 1 - g_{\parallel}/4\pi v_s + \dots, \quad (40)$$

where $g_{\parallel} = g_0 - C_1 \alpha \rho$, $C_1 > 0$ being a nonuniversal numerical constant, and the coupling constant $g_{\perp} = g_0 + C_2 \alpha \rho$, $C_2 > 0$ being another constant.

We observe that, even though there is no direct mapping of the spin models (37) or (36) onto the original fermionic model (1), or vice versa, under the identifications

$$h = m, \quad g_{\perp} = 2\lambda, \quad K_s = 2K \quad (41)$$

the DSG models in Eq. (39) and Eq. (13) coincide. Thus we conclude that at $K \sim 1/2$ and small m , the DSG model (13), being derived as a field-theoretical limit of the original flux-ladder model, at the same time describes scaling properties a weakly dimerized spin-1/2 chain with a small exchange anisotropy. Let us stress again that while the QAT and spin-chain lattice Hamiltonians, Eqs. (36) and (37), are unitarily equivalent, the correspondence between the spin-chain Hamiltonian H_S and the field-theoretical model H_{DSG} in (39) only holds in the scaling limit. This fact renders the $SU(2)$ symmetry of our fermionic ladder model at the bifurcation point an *emergent* phenomenon.

Although the above discussion of model Eq. (39) concerned the vicinity of the XXX point, this model maintains its applicability to a broader region of the parameter space where $K_s < 1$. In particular, there exists a “decoupling” point $K_s = 1/2$ where the DSG model can be mapped onto two

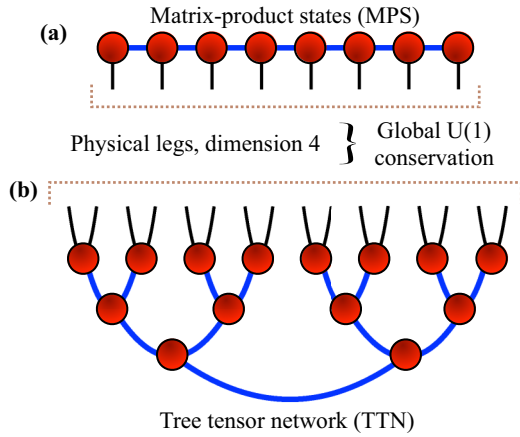


FIG. 4. TN ansatzes used in our numerical simulations. We use two different TN ansatzes, namely (a) the matrix-product state (MPS) and (b) the tree tensor network (TTN), for our analysis. In each case, the physical dimension is four, and we employ U(1) symmetric tensors [91,92] to conserve the total particle number. In our simulations, we group two sites along the rungs of the ladder (following the labeling in Fig. 1) to define the physical sites of the TN states.

noncritical (disordered) Ising models coupled by an interaction $h\sigma_1\sigma_2$ [62,63]. However, in that region, the two mutually dual Ising critical lines are well separated and their merging point is not accessible. On the contrary, the present discussion, relying on the equivalence with the staggered XXZ spin chain, treats the DSG model as a weakly perturbed SU(2)₁ WZNW model. In such an approach, the SU(2) symmetry emerging at the bifurcation point $K_s = 2K = 1$ of Gaussian line $m = 0$ into two Ising critical lines finds its natural explanation.

Thus, as follows from the above discussion, mapping of the original spinless fermionic flux-ladder model to the DSG field theory plays a central role in the present paper. While we are not in a position to determine the (nonlocal) generators of the hidden symmetry emerging at the critical point, the field theory analogy is fully consistent with all other our field theory predictions: We will then proceed in the next section with a numerical verification of our findings. We note that our case differs substantially from cases with emergent continuous Abelian symmetries that are already relatively well understood (for some recent examples, see Refs. [20,89,90]).

V. NUMERICAL TREATMENT

To validate the analytical approaches and extend the prediction to larger coupling strengths, we now employ state-of-the-art TN simulations, see Fig. 4. To mitigate any finite-size boundary effects, we evaluate the system either at the thermodynamic limit or at finite sizes with periodic boundary conditions (PBC), unless stated otherwise.

For infinite lattices, we employ the infinite density-matrix renormalization group (iDMRG) technique [93–98] based on the matrix-product state (MPS) ansatz [58,59] [Fig. 4(a)]. Specifically, we use the infinite variation of MPS known as the iMPS [99,100]. For the finite system sizes with PBC, we apply tree tensor network (TTN) methods [60,101,102] [Fig. 4(b)], which can, unlike MPS, handle PBC with similar computational cost and accuracy as open boundary conditions

(OBC) [102]. In the following, unless otherwise stated, we fix $t_0 = 1$ to set the energy unit of the system and consider $M = t_1 + t_2 = 0.2 < t_0$. We also consider the situation of repulsive interchain interaction, i.e., $V \geq 0$, and we analyze the phase diagram in the $(m/t_0, V/t_0)$ parameter space. The regime of repulsive interaction corresponds to $\lambda > 0$, via Eq. (9). For the scenario of attractive interactions, see Appendix C.

A. Phase diagram

To determine different phase transitions and differentiate different phases, we perform our numerical simulations over the $(m/t_0, V/t_0)$ plane and first consider the system correlation length ξ . The correlation length ξ_O corresponding to any local operator O_j is defined by the length scale associated with the correlation function:

$$\langle O_j O_{j+R} \rangle - \langle O_j \rangle \langle O_{j+R} \rangle \sim \exp(-R/\xi_O). \quad (42)$$

Then the system correlation length ξ of the quantum state is given by the maximum of these length scales as

$$\xi = \max(\xi_{O_1}, \xi_{O_2}, \dots). \quad (43)$$

For an iMPS ground state with bond dimension χ , the correlation length is $\xi_\chi = -1/\ln|\epsilon_2|$, where ϵ_2 is the second largest eigenvalue of the iMPS transfer matrix [100]. It is to be noted that in case of critical systems where the system correlation length diverges, ξ_χ is the length-scale artificially introduced by the finite iMPS bond dimension χ and usually $\xi_\chi \sim \chi^\beta$, with β being a scaling exponent.

In Fig. 2(b), we show the phase diagram of the system in the $(m/t_0, V/t_0)$ plane through the lens of correlation length for iMPS bond dimension $\chi = 256$. Clearly, we see a bifurcation of critical line at $m = 0$ into two critical lines at around $V/t_0 \simeq 2.45$ similarly to what has been seen in the Ashkin-Teller (AT) model, see Secs. III A 3 and IV. Although the bosonization approach is controlled only for weak-coupling regime $V/t_0 \ll 1$, it predicted, from the phenomenological treatment of the DSG model, the existence of the bifurcation point (Sec. IV) that appeared at relatively strong-coupling regime $V/t_0 \simeq 2.45$. Below we show that this bifurcation is indeed of the SU(2)₁ WZNW type, where a Gaussian critical line with central charge $c = 1$ (at $m = 0$ and $V/t_0 \lesssim 2.45$) bifurcates into two Ising transitions with $c = 1/2$ (for $m \neq 0$ and $V/t_0 \gtrsim 2.45$). Moreover, Fig. 2(b) also suggest that apart from the critical lines, all the three phases are gapped as they possess finite correlation lengths.

B. Characterization of different phases

The band insulator phases at lower values of V/t_0 undergo distinct types of zigzag dimerization as explained in Sec. III A 2. For $m > 0$, the dimerization occurs along t_1 links and the phase is a trivial band insulator. For $m < 0$ regime, the dimerization is along t_2 links, where the phase is a topological band insulator. To distinguish these two kinds of dimerization, we consider two rung tunneling amplitudes, $D_1 = \langle c_{j,+}^\dagger c_{j,-} + \text{H.c.} \rangle$ and $D_2 = \langle c_{j,+}^\dagger c_{j-1,-} + \text{H.c.} \rangle$, averaged over the site index j . The difference $D_1 - D_2$, as seen in Fig. 5(a), can indeed characterize these two band insulator phases.

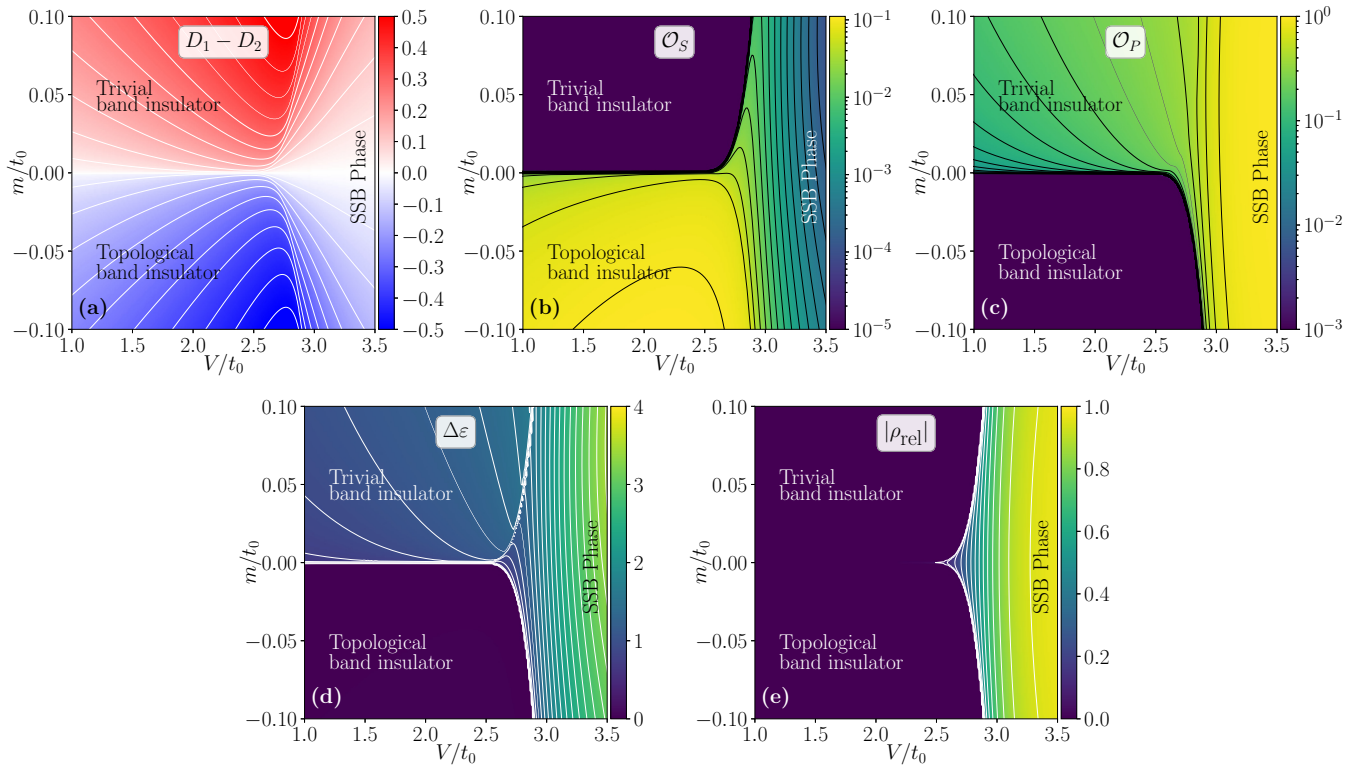


FIG. 5. The characterization of different phases of the repulsive triangular ladder in the $(m/t_0, V/t_0 > 0)$ plane. (a) We consider the difference between two different rung tunneling amplitudes $D_1 = \langle c_{j,+}^\dagger c_{j,-} + \text{H.c.} \rangle$ and $D_2 = \langle c_{j,+}^\dagger c_{j-1,-} + \text{H.c.} \rangle$, respectively. This difference highlights the different types of zigzag dimerization in the band insulator phases. [(b) and (c)] The nonlocal string (\mathcal{O}_S) and parity (\mathcal{O}_P) correlation functions as defined in Eqs. (44). \mathcal{O}_S is zero (nonzero) while \mathcal{O}_P is nonzero (zero) in the trivial (topological) band insulator phase. Both become nonvanishing in the large- V/t_0 symmetry-broken phase. (d) The entanglement gap $\Delta\varepsilon = \varepsilon_1 - \varepsilon_0$, where ε_0 and ε_1 are the ground- and first-excited-state energies of the entanglement Hamiltonian $H_l^E = -\ln \rho_l$, respectively, is plotted in the parameter space. Vanishing values $\Delta\varepsilon$ in the band insulator phase for $m < 0$ dictates the topological nature of this phase. (e) The relative density $\rho_{\text{rel}} = \langle \hat{n}_{j,+} - \hat{n}_{j,-} \rangle$ between the legs serves as an order parameter for the \mathbb{Z}_2 symmetry-breaking associated with \mathcal{P} symmetry. The order parameter ρ_{rel} becomes nonvanishing in the twofold degenerate \mathbb{Z}_2 -broken phase for $V > V_c$. Here we have used iDMRG simulations with bond dimension $\chi = 256$.

In Sec. III A 2, we have shown by analyzing the nonlocal string and parity order parameters that the band insulator phase for $m < 0$ has a topological nature, while the same for $m > 0$ is trivial. Here we numerically verify this analytical result by examining string (\mathcal{O}_S) and parity (\mathcal{O}_P) correlation functions defined as [69–73]:

$$\begin{aligned} \mathcal{O}_S &= \lim_{|i-j| \rightarrow \infty} \langle \hat{\mathcal{O}}_S(i) \hat{\mathcal{O}}_S(j) \rangle = \lim_{|i-j| \rightarrow \infty} \langle \delta \hat{n}_i e^{i\pi \sum_{l=i}^j \delta \hat{n}_l} \delta \hat{n}_j \rangle, \\ \mathcal{O}_P &= \lim_{|i-j| \rightarrow \infty} \langle \hat{\mathcal{O}}_P(i) \hat{\mathcal{O}}_P(j) \rangle = \lim_{|i-j| \rightarrow \infty} \langle e^{i\pi \sum_{l=i}^j \delta \hat{n}_l} \rangle, \end{aligned} \quad (44)$$

where the operators $\hat{\mathcal{O}}_S$ and $\hat{\mathcal{O}}_P$ are defined in Eqs. (29), with $\delta \hat{n}_j$ being the density fluctuation across the zigzag rung j . It is to be noted that these nonlocal order parameters can be measured experimentally in cold atomic setups [17, 79–82]. In Figs. 5(b) and 5(c), we show that for the topological band insulator ($m < 0$) the string correlation is nonzero, while the parity correlation vanishes [see also Fig. 6(a)]—indicating hidden nonlocal order similar to topological Haldane insulators [70–73]. The opposite is true for the trivial band insulator, i.e., $\mathcal{O}_S = 0$, $\mathcal{O}_P \neq 0$.

For further verification of the topological nature of the band insulator phases, we consider the entanglement gap $\Delta\varepsilon = \varepsilon_1 - \varepsilon_0$, where ε_0 and ε_1 are the ground- and first-excited-state energies of the entanglement Hamiltonian H_l^E , respectively. The entanglement Hamiltonian is defined as $H_l^E = -\ln \rho_l$, where ρ_l is the l -site reduced density matrix. It has been established that the entanglement Hamiltonian possesses degenerate spectra for phases with topological properties in one dimension [103]. In Fig. 5(d) we plot the the entanglement gap $\Delta\varepsilon$ in the $(m/t_0, V/t_0)$ plane. Clearly, vanishing $\Delta\varepsilon$ in the band insulator phase for $m < 0$ dictates the topological nature of this phase [see also Fig. 6(b)].

For large values of V/t_0 , we end up with a SSB phase where the \mathbb{Z}_2 symmetry corresponding to \mathcal{P} gets spontaneously broken. As a result, the relative density $\rho_{\text{rel}} = \langle \hat{n}_{j,+} - \hat{n}_{j,-} \rangle$ between two legs becomes nonzero [see Fig. 5(e)] and serves as an order parameter to detect this SSB phase, see Sec. III A 3. As discussed in Sec. III A 1, the transition from the Gaussian criticality to this SSB phase along $m = 0$ line is BKT type. This is why the order parameter ρ_{rel} varies very smoothly along the $m = 0$ line, as opposed to the case of $m \neq 0$ [Fig. 6(b)] where the transitions from the band

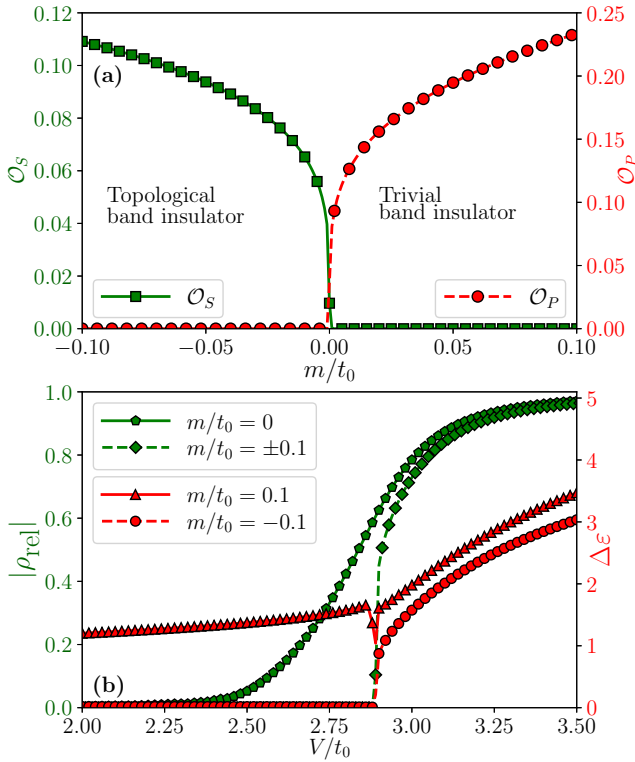


FIG. 6. (a) The string \mathcal{O}_S and parity \mathcal{O}_P correlations for varying m/t_0 and fixed $V/t_0 = 2$. (b) The variations of the order parameter ρ_{rel} and the entanglement gap $\Delta\epsilon$ with varying V/t_0 for fixed values of m/t_0 as indicated in the figure. All other details are the same as in the Fig. 5.

insulator phases to the SSB phase are of second order Ising type.

C. Bifurcation of the criticality

Now we move to carefully analyze the splitting of the critical line at $m = 0$ into two other critical lines at around $V/t_0 \simeq 2.45$ as seen in Fig. 2(b).

For this purpose, first, we determine the central charges c of the underlying conformal field theory (CFT) for these critical lines using the finite-bipartition scaling of von Neumann entanglement entropy. The von Neumann entanglement entropy of a block of l sites is defined as

$$S(l) = -\text{Tr}[\rho_l \ln(\rho_l)], \quad (45)$$

where $\rho_l = \text{Tr}_{l+1, l+2, \dots, L} |\psi\rangle\langle\psi|$ is the l -site reduced density matrix after tracing out rest of the system. In a CFT, the finite-size scaling of the entanglement entropy of a bipartition of size l in a system of length L with PBC is [104–106]

$$S(l, L) = \frac{c}{3} \ln \left[\frac{L}{\pi} \sin(\pi l/L) \right] + b', \quad (46)$$

where b' is a nonuniversal constant. In Fig. 4, we show the variations of the fitted values of the central charge, according to Eq. (46), as functions of V/t_0 for $m = 0$ [Fig. 7(a)] and $m = 0.1$ [Fig. 7(b)]. The figure clearly indicates that the critical line at $m = 0$ has central charge $c = 1$ and therefore describes $U(1)$ Gaussian criticality. On the other hand, two

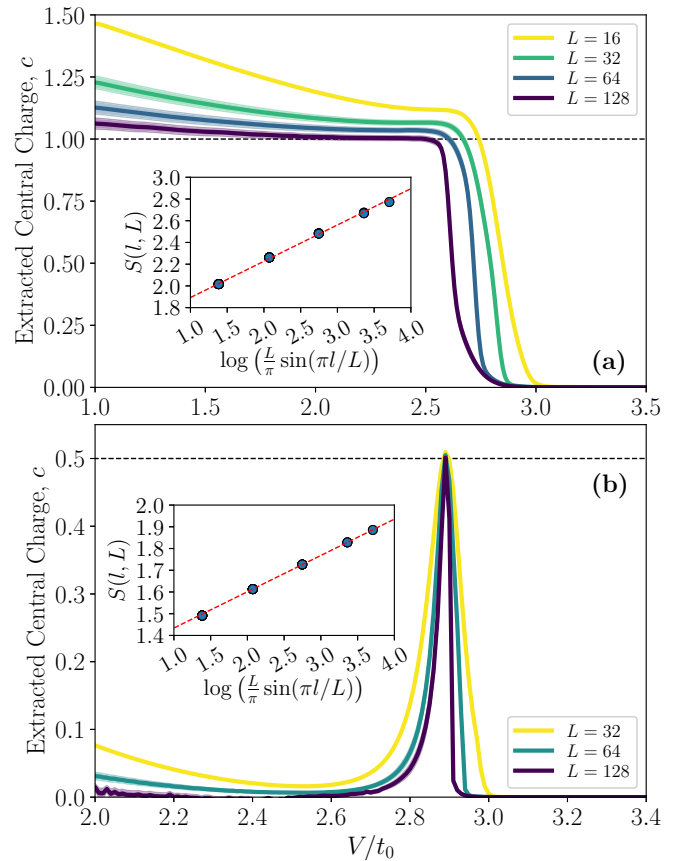


FIG. 7. The extracted values of the central charge for different system sizes using the scaling function of Eq. (46) for (a) $m = 0$ and (b) $m = 0.1t_0$. The critical line at $m = 0$ has central charge $c = 1$, i.e., a $U(1)$ Gaussian criticality, while the bifurcated critical lines at $m \neq 0$ belong to the Ising universality class having the central charge $c = 1/2$. The shaded regions mark the errors in the fitting procedure. Insets: The fitting of the entanglement entropy according to Eq. (46) for (a) $m = 0$ and $V/t_0 = 2.3$ resulting in $c = 1.00(2)$, and (b) $m = 0.1t_0$ and $V/t_0 = 2.89$ resulting in $c = 0.50(1)$. For the insets, we have chosen the data for $L = 128$.

bifurcated critical lines at $m \neq 0$ has $c = 1/2$ and thereby describes the Ising criticality. This scenario matches that of the AT model and our analytical prediction from the phenomenological analysis of the DSG model.

However, the scaling of entanglement entropy does not shed much lights on the bifurcation point, and it is unable to tell us whether this is a $SU(2)_1$ critical point. To confirm that this bifurcation point is indeed a $SU(2)_1$ critical point, we determine the Luttinger parameter K numerically and show that it tends to $1/2$ at the bifurcation point (see Sec. IV).

In this analysis, we extract the Luttinger parameter K from the scaling of the bipartite fluctuations [107–109]. In a Luttinger liquid with a global $U(1)$ conserve quantity O and with PBC, the local fluctuations

$$F_l(O) = \left\langle \left(\sum_{n \leq l} O_n \right)^2 \right\rangle - \left\langle \sum_{n \leq l} O_n \right\rangle^2 \quad (47)$$

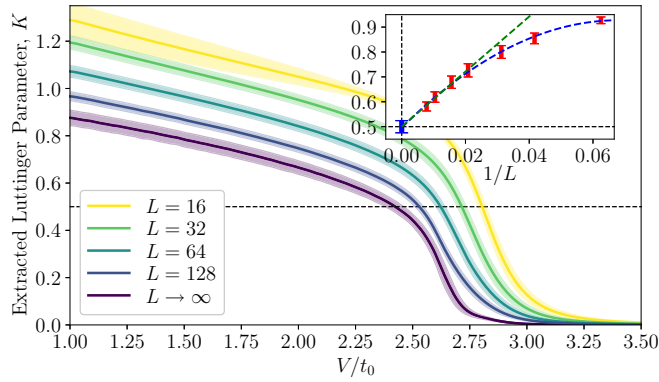


FIG. 8. The extracted values of the Luttinger parameter K for different system sizes using the scaling form of Eq. (48) along the $m = 0$ line. The shaded regions denote the error bars. The estimated values of K in the thermodynamic limit has been extracted by using a linear function $f_1(1/L) = K_\infty + b/L$ and a quadratic function $f_2(1/L) = K_\infty + b/L + d/L^2$ in $1/L$ (see inset).

obey the scaling of the form [107–109]:

$$\mathcal{F}_l(O) = \frac{K}{\pi^2} \ln \left[\frac{L}{\pi} \sin(\pi l/L) \right] + \text{const.} \quad (48)$$

For our system, the global $U(1)$ conservation corresponds to the fermionic charge $O_n = \hat{n}_{n,+} + \hat{n}_{n,-}$. In Fig. 8, we show the extracted Luttinger parameter for several system sizes $L \in [16, 128]$ with PBC across the $m = 0$ line. Interestingly, as we increase the system size L , the point in V/t_0 , where the fitted K crosses the value $1/2$, approaches towards the expected bifurcation point $V/t_0 \simeq 2.45$. We extrapolate the Luttinger parameter K in the thermodynamic limit by using both a linear function and a quadratic function in $1/L$ (see the inset of Fig. 8). By this extrapolation, we find that the Luttinger parameter K becomes $1/2$ at $V/t_0 = 2.43(4)$. This $K = 1/2$ value of the Luttinger parameter confirms the nature of the bifurcation point as the $SU(2)_1$ WZNW critical point in correspondence with the discussions of Sec. IV.

VI. CONCLUSION

In this work, we studied the phase diagram of a system of interacting spinless fermions on a two-leg triangular ladder at half-filling, with uniform t_0 intrachain and alternating $t_{1,2}$ interchain nearest-neighbor tunneling amplitudes, $f = 1/2$ magnetic flux per triangular plaquette (in units of π), and V nearest-neighbor density-density interchain interaction. At the microscopic level, the model exhibits a $U(1)$ symmetry pertained to the conservation of total fermion number and a \mathbb{Z}_2 symmetry—a combined parity transformation and the chain exchange operation. The model is based on experimental setups with cold atom gases in optical lattices, in the presence of off-resonant laser driving to Rydberg states. The regime of parameters under consideration is in principle accessible experimentally [12,26,29,51].

To obtain the phase diagram, we use the bosonization approach in the weakly interacting regime ($|V| \ll t_0$), with $0 < t_{1,2} \ll t_0$ and $|t_1 - t_2| \ll t_1 + t_2$, and map the model onto the double-frequency sine-Gordon model. We analytically predict

various properties of the system, by utilizing the symmetries of the original lattice model, and renormalization group analysis for the bosonized version. Specifically, for $t_1 \neq t_2$ and sufficiently weak repulsive interaction $V \ll V_c$, the system is a band insulator. If additionally $t_1 > t_2$ is the case, then the phase is a trivial band insulator with nonzero dimerization along t_1 links. If $t_1 < t_2$ holds, then the phase is instead a topological band insulator, with nonzero dimerization along t_2 links, and displays edge states for open boundary conditions. For $t_1 = t_2$, the system is described by a Gaussian model with central charge $c = 1$, separating two band insulator phases.

The Gaussian critical line for $t_1 = t_2$ terminates at $V = V_c$, where the symmetry of the system is enlarged from $\mathbb{Z}_2 \times U(1)$ to $SU(2)$, with the underlying field theory of the model corresponding to the $SU(2)_1$ WZNW model. This emergent non-Abelian $SU(2)$ invariance, that is absent in the microscopic description of the system, is a remarkable effect coming from the interplay between the geometric frustration, magnetic flux, and many-body correlations.

At this $t_1 = t_2$ regime, when crossing $V = V_c$ critical point, the system undergoes a Berezinskii-Kosterlitz-Thouless transition to a gapped phase, with spontaneously broken \mathbb{Z}_2 symmetry. In this phase, we observe nonzero charge imbalance (i.e., a net relative density between the two chains) and total current along the chains. Additionally, the Gaussian critical line, terminated at $SU(2)_1$ point, bifurcates into two Ising critical lines, with central charge $c = 1/2$, similar to what is seen in the Ashkin-Teller model. These Ising critical lines separate the strong-coupling symmetry-broken phase from the band insulators.

Since the bosonization approach is valid for weak-coupling regimes, we have used numerical simulations based on tensor network states to corroborate the analytical predictions. Specifically, using iDMRG method, we characterize the phase diagram and different phases of the lattice Hamiltonian directly at the thermodynamic limit in the enlarged range of interaction strength V and confirm the predictions of bosonization approach. By applying TTN-based calculations for finite systems with periodic boundary conditions, we characterize both the Gaussian $c = 1$ and Ising $c = 1/2$ critical lines by using the scaling of entanglement entropies. Furthermore, from the numerical scaling of bipartite fluctuations corresponding to the global $U(1)$ conserve quantity, we confirm the existence of $SU(2)_1$ WZNW bifurcation point similarly to what is observed in the Ashkin-Teller model.

Our work, therefore, provides a unique example where non-Abelian $SU(2)$ symmetry emerges in a fundamentally Abelian system.

ACKNOWLEDGMENTS

We thank Poetri S. Tarabunga for precious discussions and collaborations during the implementations of the TTN codes. We are grateful to Simone Montangero, Simone Notarnicola, Pietro Silvi, and Colin Egan for the useful discussions regarding the developments of the code. M.D. thanks M. Fabrizio and P. Fendley for discussions. A.N. thanks F. H. L. Essler and O. Starykh for their interest in our work and useful comments. B.B. and A.N. acknowledge fruitful cooperation with G. Japaridze on projects related to frustrated

one-dimensional quantum systems. T.C. acknowledges the support of PL-GRID infrastructure for the computational resource. M.T. thanks the Simons Foundation for supporting his Ph.D. studies through Award No. 284558FY19 to the ICTP. The work of M.D. was partly supported by the ERC under Grant No. 758329 (AGEnTh), and by the Munich Institute for Astro-, Particle and BioPhysics (MIAPbP) which is funded by the Deutsche Forschungsgemeinschaft (DFG, German Research Foundation) under Germany's Excellence Strategy – EXC-2094 – 390783311. The support of B.B and A.N. from the Shota Rustaveli National Science Foundation of Georgia, SRNSF, Grant No. FR-19-11872, is gratefully acknowledged. M.D. and E.T. further acknowledge support from the MIUR Programme FARE (MEPH), and from QUANTERA DYNAMITE PCI2022-132919. The iDMRG simulations have been performed with the TeNPy library [110], while the TTN simulations use the C++ ITensor library [111] as its backbone.

APPENDIX A: CONTINUUM FORM OF LOCAL PHYSICAL OPERATORS IN THE CHAIN AND BAND REPRESENTATIONS

In the continuum limit, after projecting onto the low-energy sector, the fluctuation parts of local physical fields, defined in the chain representation, take the following form:

Local densities on each chain:

$$\begin{aligned} \hat{n}_{n\sigma} &::= c_{n,\sigma}^\dagger c_{n,\sigma} : \rightarrow a_0 \rho_\sigma(x), \\ \rho_\sigma(x) &::= \Psi_\sigma^\dagger(x) \Psi_\sigma(x) : . \end{aligned} \quad (\text{A1})$$

Longitudinal currents on each chain at $f = 1/2$:

$$\begin{aligned} : J_{n,n+1}^\sigma &::= -it_0 (c_{n,\sigma}^\dagger c_{n+1,\sigma} : e^{-i\pi\sigma f} - \text{H.c.})|_{f=1/2} \\ &= -t_0\sigma (c_{n,\sigma}^\dagger c_{n+1,\sigma} : + \text{H.c.}) \\ &\rightarrow \sigma v_F : \Psi_\sigma^\dagger(x) \Psi_\sigma(x) : + O(v_F a_0) \equiv j_\sigma^0(x), \end{aligned}$$

implying that, due to their chiral nature, in the leading order at $a_0 \rightarrow 0$, local densities and longitudinal currents coincide up to a prefactor v_F :

$$j_\sigma^0(x) = \sigma v_F \rho_\sigma(x). \quad (\text{A2})$$

Interchain currents on t_1 and t_2 zigzag links:

$$\begin{aligned} : J_{nm}^{+-} &::= -it_1 : (c_{n,+}^\dagger c_{n,-} - \text{H.c.}) : \\ &\rightarrow t_1 a_0 \Psi^\dagger(x) \hat{\sigma}_2 \Psi(x), \\ : J_{n,n+1}^{-+} &::= -it_2 : (c_{n,-}^\dagger c_{n+1,+} - \text{H.c.}) : \\ &\rightarrow t_2 a_0 \Psi^\dagger(x) \hat{\sigma}_2 \Psi(x). \end{aligned}$$

At $t_1 = t_2$ ($m = 0$) and $a_0 \rightarrow 0$ with $v_F = 2t_0 a_0 = \text{const}$, the currents along the oriented t_1 and t_2 links coincide:

$$\begin{aligned} : J_{nm}^{+-} &:: \rightarrow j_z(x), \quad : J_{n,n+1}^{-+} :: \rightarrow j_z(x), \\ j_z(x) &= v_F \tau : \Psi^\dagger(x) \hat{\sigma}_2 \Psi(x) : . \end{aligned} \quad (\text{A3})$$

Bond-density fields:

$$\begin{aligned} B_{nm} &::= c_{n,+}^\dagger c_{n,-} : + \text{H.c.} \rightarrow a_0 B(x), \\ B_{n,n+1} &::= c_{n,+}^\dagger c_{n+1,-} : + \text{H.c.} \rightarrow -a_0 B(x), \\ B(x) &::= \Psi^\dagger(x) \hat{\sigma}_1 \Psi(x) : . \end{aligned} \quad (\text{A4})$$

In formulas (A1)–(A4), normal ordering prescription is defined as $: \hat{A} := \hat{A} - \langle \hat{A} \rangle_0$, where averaging is done over the vacuum of the noninteracting model at $f = 1/2$ and $m = 0$. From formulas (A1) and (A2) it follows that the total current $j_0 = \sum_\sigma j_\sigma^0$ of the zigzag ladder at $f = 1/2$ is proportional to the relative particle density

$$j_0(x) = v_F \rho_{\text{rel}}(x). \quad (\text{A5})$$

Using the transformations (5) and passing to the rotated basis, we obtain the expressions for all above operators in the band representation:

$$\begin{aligned} \rho_+(x) &= \frac{1}{v_F} j_0^+(x) \\ &= u^2 J_R(x) + v^2 J_L(x) - uv \mathcal{N}_2(x), \end{aligned} \quad (\text{A6})$$

$$\begin{aligned} \rho_-(x) &= -\frac{1}{v_F} j_0^-(x) \\ &= v^2 J_R(x) + u^2 J_L(x) + uv \mathcal{N}_2(x), \end{aligned} \quad (\text{A7})$$

$$\begin{aligned} j_z(x) &= v_F \tau \{2uv [J_R(x) - J_L(x)], \\ &\quad + (u^2 - v^2) \mathcal{N}_2(x)\}, \end{aligned} \quad (\text{A8})$$

$$B(x) = \mathcal{N}_1(x). \quad (\text{A9})$$

Here $J_R(x) =: R^\dagger(x)R(x) :$ and $J_L(x) =: L^\dagger(x)L(x) :$ are U(1) chiral fermionic currents defined in the band basis (see, e.g., Ref. [56]), and $\mathcal{N}_{1,2}$ are Dirac mass bilinears:

$$\begin{aligned} \mathcal{N}_1(x) &= \chi^\dagger(x) \hat{\sigma}_1 \chi(x) \\ &= R^\dagger(x)L(x) : + : L^\dagger(x)R(x) :, \end{aligned} \quad (\text{A10})$$

$$\begin{aligned} \mathcal{N}_2(x) &= \chi^\dagger(x) \hat{\sigma}_2 \chi(x) \\ &= -i[: R^\dagger(x)L(x) : - : L^\dagger(x)R(x) :]. \end{aligned} \quad (\text{A11})$$

The expressions (A8) and (A9) are the leading terms of the expansion in small a_0 . Under the \mathcal{P} transformation

$$\begin{aligned} R(x) &\rightarrow L(-x), \quad L(x) \rightarrow R(-x), \\ J_R(x) &\rightarrow J_L(-x), \quad J_L(x) \rightarrow J_R(-x), \\ \mathcal{N}_1(x) &\rightarrow \mathcal{N}_1(-x), \quad \mathcal{N}_2(x) \rightarrow -\mathcal{N}_2(-x). \end{aligned} \quad (\text{A12})$$

Here a comment is in order. In models of 1D lattice fermions with a half-filled band, operators with the structure (A10) and (A11) are associated with spatially modulated (staggered) order parameter fields. In those cases, the fermionic bilinears $R^\dagger L$, $L^\dagger R$ emerge due to hybridization of single-particle states near two opposite Fermi points, with the momentum transfer close to $2k_F = \pi$. In the present model, there is only one Dirac point in the low-energy spectrum, and the particle-hole fields with momentum transfer π are all short-ranged. In fact, the appearance of the fermionic bilinear \mathcal{N}_2 in the asymptotic expressions (A6)–(A8) is entirely due to the τ deformation of the kinetic energy (4) that is geometrical frustration of the zigzag ladder.

APPENDIX B: BOUNDARY MODES IN THE TOPOLOGICAL PHASE OF BAND INSULATOR

In Sec. III A 2 of the main text we have shown that, under the conditions $K > 1/2$ and $m \neq 0$, for both signs of the “light” mass m the ladder displays a band insulator phase with massive Dirac fermions being elementary low-energy excitations. In this Appendix, we address the topological properties of these phases by studying zero-energy boundary states in a semi-infinite sample of a triangular $1/2$ -filled flux ladder at $f = 1/2$. Since (apart from a possible formation of excitonic states) at $K > 1/2$ interaction effects basically reduce to renormalization of the single-particle mass gap, Eq. (27), it is sufficient to do the calculation for a noninteracting model.

Consider a semi-infinite sample, in which the diatomic unit cells are labeled as $n = 1, 2, \dots, \infty$. Let us adopt the continuum limit of this model by taking into account both Dirac-like low-energy modes with masses $M = t_1 + t_2$ and $m = t_1 - t_2$, $|M|, |m| \ll t_0$. Then we can write

$$c_{n,\sigma} \rightarrow \sqrt{a_0} [(-1)^n \psi_\sigma(x) + \bar{\psi}_{-\sigma}(x)], \quad (\sigma = \pm), \quad (\text{B1})$$

where $\psi_\sigma(x)$ and $\bar{\psi}_\sigma(x)$ are fermionic fields describing single-particle excitations with momenta close to π and 0 , respectively. Adding an additional rung $n = 0$ to the open end of the ladder we impose boundary conditions

$$c_{0,\sigma} = 0 \rightarrow \psi_\sigma(0) + \bar{\psi}_{-\sigma}(0) = 0, \quad (\sigma = \pm). \quad (\text{B2})$$

Denoting by $\{u(x), v(x)\}$ and $\{\tilde{u}(x), \tilde{v}(x)\}$ the components of the 2-spinor wave functions $w(x)$ and $\tilde{w}(x)$ associated with the field operators $\psi(x)$ and $\bar{\psi}(x)$, from (B2) we obtain

$$u(0) + \tilde{v}(0) = 0, \quad v(0) + \tilde{u}(0) = 0.$$

This leads to the following constraint imposed on the boundary spinors:

$$w(0) = \begin{bmatrix} u(0) \\ v(0) \end{bmatrix}, \quad \tilde{w}(0) = \begin{bmatrix} \tilde{u}(0) \\ \tilde{v}(0) \end{bmatrix} = -\hat{\sigma}_1 w(0). \quad (\text{B3})$$

The boundary zero modes corresponding to these functions satisfy the equations

$$[-iv_F(\sigma_3 + \tau\sigma_2) - m\sigma_1]w(x) = 0, \quad (\text{B4})$$

$$[-iv_F(\sigma_3 + \tau\sigma_2) - M\sigma_1]\tilde{w}(x) = 0, \quad x \geq 0. \quad (\text{B5})$$

The kinetic energy in Eqs. (B4) and (B5) is diagonalized by an SU(2) transformation of the spinors

$$\psi = U\zeta, \quad \bar{\psi} = U\tilde{\zeta}, \quad (\text{B6})$$

where

$$\zeta = \begin{pmatrix} z_1 \\ z_2 \end{pmatrix}, \quad \tilde{\zeta} = \begin{pmatrix} \tilde{z}_1 \\ \tilde{z}_2 \end{pmatrix}, \quad (\text{B7})$$

and the unitary matrix U is defined in (5). The spinors ζ and $\tilde{\zeta}$ satisfy canonical Dirac equations for zero modes:

$$(-i\tilde{v}\sigma_3\partial_x - m\sigma_1)\zeta(x) = 0,$$

$$(-i\tilde{v}\sigma_3\partial_x - M\sigma_1)\tilde{\zeta}(x) = 0.$$

On the semiaxis $x \geq 0$ their solution reads

$$\begin{aligned} \zeta(x) &= \zeta_0 \begin{pmatrix} 1 \\ is_m \end{pmatrix} \exp(-|m|x/\tilde{v}), \\ \tilde{\zeta}(x) &= \tilde{\zeta}_0 \begin{pmatrix} 1 \\ is_M \end{pmatrix} \exp(-|M|x/\tilde{v}), \end{aligned} \quad (\text{B8})$$

where ζ_0 and $\tilde{\zeta}_0$ are normalization coefficients and $s_m = \text{sgn } m$, $s_M = \text{sgn } M$.

Using the transformations (B6) we obtain

$$w(x) = \chi_0 \begin{bmatrix} u - vs_m \\ i(v + us_m) \end{bmatrix} \exp(-|m|x/\tilde{v}), \quad (\text{B9})$$

$$\tilde{w}(x) = \tilde{\chi}_0 \begin{bmatrix} u - vs_M \\ i(v + us_M) \end{bmatrix} \exp(-|M|x/\tilde{v}). \quad (\text{B10})$$

On the other hand, according to the boundary condition (B3),

$$\tilde{w}(x) = -\chi_0 \begin{bmatrix} i(v + us_M) \\ u - vs_m \end{bmatrix} \exp(-|M|x/\tilde{v}). \quad (\text{B11})$$

Then we obtain

$$\tilde{\zeta}_0(u - vs_M) = -i\zeta_0(v + us_m),$$

$$i\tilde{\zeta}_0(v + us_M) = -\zeta_0(u - vs_m),$$

implying that

$$\frac{\tilde{\zeta}_0}{\zeta_0} = \frac{-i(v + us_m)}{u - vs_M} = \frac{i(u - vs_m)}{v + us_M}. \quad (\text{B12})$$

From the last equation it follows that

$$(u - vs_m)(u - vs_M) + (v + us_m)(v + us_M) = 1 + s_m s_M = 0, \quad (\text{B13})$$

which leads to the conclusion that a normalizable boundary zero mode only exists—and hence, according to the bulk-boundary theorem, the ground state is topologically nontrivial—if the masses m and M have different signs:

$$s_m s_M = -1 \rightarrow Mm < 0. \quad (\text{B14})$$

With the convention $M > 0$ adopted in the main text, the ground state at $K > 1/2$ represents a topological insulator if $m < 0$ and is topologically trivial at $m > 0$.

The total wave function for the boundary zero mode has the structure

$$\Upsilon(x) = (-1)^{x/a_0} w(x) + \tilde{w}(x), \quad x \geq 0, \quad (\text{B15})$$

where $w(x)$ and $\tilde{w}(x)$ are given by expressions (B9) and (B10), respectively, in which the condition (B14) has to be taken into account. If $|M| \gg |m|$, then $\tilde{w}(x)$ exponentially decays at short distances, $x \sim \tilde{v}/|M|$. At longer distances, $x \gtrsim \tilde{v}/|m|$, there exists an exponential tail of the boundary wave function contributed by the light fermions.

APPENDIX C: NUMERICAL RESULTS FOR THE ATTRACTIVE INTERCHAIN INTERACTION

For the sake of completeness, we consider the attractive interaction, i.e., $V < 0$ [thus $\lambda < 0$ from Eq. (9)], between the chains.

From our analysis using bosonization, we have predicted that the scenario of attractive interaction is less interesting

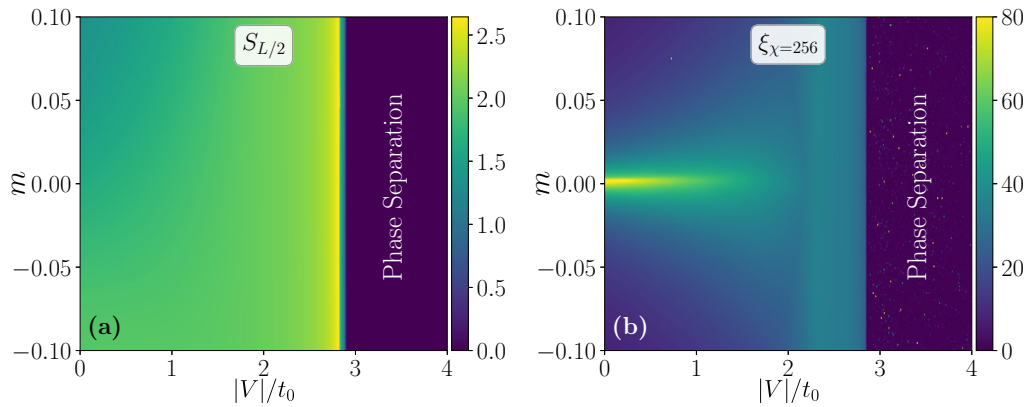


FIG. 9. The phase diagram for an attractive triangular ladder in the $(m, V/t_0 < 0)$ plane. (a) We plot half-system entanglement entropy for a finite ladder of linear size $L = 60$ with OBC using fDMRG. (b) The correlation length ξ_{χ} extracted from iDMRG simulations with iMPS bond dimension $\chi = 256$.

compared to the repulsive case. For the attractive regime, we have $\lambda < 0$ and thus $K > 1$. In this case, the λ term in Eq. (13), which describes interband pair-hopping processes, is irrelevant. This way the properties of the model are determined only by the single-particle mass perturbation. As long as the attractive interaction is weak, where the mass term is relevant, we remain in either trivial or topological band insulator phases, depending on the sign of m . For very strong interaction $|V|/t_0 \gg 1$, the mass term becomes irrelevant, and the system phase separates between density $\rho = 1$ Mott phase and density $\rho = 0$ vacuum state. Since these phase separation

states break the translational invariance over macroscopic distances, iDMRG is not suitable for these states and randomly gets stuck to higher energy states. That is why we also employ finite DMRG with OBC along with iDMRG simulations to confirm our results.

In Figs. 9(a) and 9(b), we show the half-system entanglement entropy for finite ladder with OBC and the correlation length ξ_{χ} extracted from iDMRG simulations, respectively. Clearly, apart from the appearance of the phase separation region, the situation here is not that interesting unlike the situation of repulsive interactions.

-
- [1] P. Schauß, M. Cheneau, M. Endres, T. Fukuhara, S. Hild, A. Omran, T. Pohl, C. Gross, S. Kuhr, and I. Bloch, *Nature (London)* **491**, 87 (2012).
- [2] Y.-Y. Jau, A. M. Hankin, T. Keating, I. H. Deutsch, and G. W. Biedermann, *Nat. Phys.* **12**, 71 (2016).
- [3] R. Faoro, C. Simonelli, M. Archimi, G. Masella, M. M. Valado, E. Arimondo, R. Mannella, D. Ciampini, and O. Morsch, *Phys. Rev. A* **93**, 030701(R) (2016).
- [4] J. Zeiher, R. van Bijnen, P. Schauß, S. Hild, J. yoon Choi, T. Pohl, I. Bloch, and C. Gross, *Nat. Phys.* **12**, 1095 (2016).
- [5] H. Bernien, S. Schwartz, A. Keesling, H. Levine, A. Omran, H. Pichler, S. Choi, A. S. Zibrov, M. Endres, M. Greiner, V. Vuletić, and M. D. Lukin, *Nature (London)* **551**, 579 (2017).
- [6] D. Barredo, V. Lienhard, S. de Léséleuc, T. Lahaye, and A. Browaeys, *Nature (London)* **561**, 79 (2018).
- [7] A. Keesling, A. Omran, H. Levine, H. Bernien, H. Pichler, S. Choi, R. Samajdar, S. Schwartz, P. Silvi, S. Sachdev, P. Zoller, M. Endres, M. Greiner, V. Vuletić, and M. D. Lukin, *Nature (London)* **568**, 207 (2019).
- [8] A. Browaeys and T. Lahaye, *Nat. Phys.* **16**, 132 (2020).
- [9] C. Gross and I. Bloch, *Science* **357**, 995 (2017).
- [10] S. de Léséleuc, S. Weber, V. Lienhard, D. Barredo, H. P. Büchler, T. Lahaye, and A. Browaeys, *Phys. Rev. Lett.* **120**, 113602 (2018).
- [11] P. Scholl, H. J. Williams, G. Bornet, F. Wallner, D. Barredo, L. Henriot, A. Signoles, C. Hainaut, T. Franz, S. Geier, A. Tebben, A. Salzinger, G. Zürn, T. Lahaye, M. Weidemüller, and A. Browaeys, *PRX Quant.* **3**, 020303 (2022).
- [12] A. W. Glaetzle, M. Dalmonte, R. Nath, C. Gross, I. Bloch, and P. Zoller, *Phys. Rev. Lett.* **114**, 173002 (2015).
- [13] P. Scholl, M. Schuler, H. J. Williams, A. A. Eberharter, D. Barredo, K.-N. Schymik, V. Lienhard, L.-P. Henry, T. C. Lang, T. Lahaye, A. M. Läuchli, and A. Browaeys, *Nature (London)* **595**, 233 (2021).
- [14] S. Ebadi, T. T. Wang, H. Levine, A. Keesling, G. Semeghini, A. Omran, D. Bluvstein, R. Samajdar, H. Pichler, W. W. Ho, S. Choi, S. Sachdev, M. Greiner, V. Vuletić, and M. D. Lukin, *Nature (London)* **595**, 227 (2021).
- [15] G. Semeghini, H. Levine, A. Keesling, S. Ebadi, T. T. Wang, D. Bluvstein, R. Verresen, H. Pichler, M. Kalinowski, R. Samajdar, A. Omran, S. Sachdev, A. Vishwanath, M. Greiner, V. Vuletić, and M. D. Lukin, *Science* **374**, 1242 (2021).
- [16] T. Pohl, E. Demler, and M. D. Lukin, *Phys. Rev. Lett.* **104**, 043002 (2010).
- [17] S. de Léséleuc, V. Lienhard, P. Scholl, D. Barredo, S. Weber, N. Lang, H. P. Büchler, T. Lahaye, and A. Browaeys, *Science* **365**, 775 (2019).
- [18] R. Verresen, M. D. Lukin, and A. Vishwanath, *Phys. Rev. X* **11**, 031005 (2021).
- [19] P. S. Tarabunga, F. M. Surace, R. Andreoni, A. Angelone, and M. Dalmonte, *Phys. Rev. Lett.* **129**, 195301 (2022).
- [20] Z. Jouini, N. Chepiga, L. Herviou, and F. Mila, Emergent U(1) symmetry in non-particle-conserving 1D models, [arXiv:2305.01746](https://arxiv.org/abs/2305.01746) (2023).
- [21] N. Henkel, R. Nath, and T. Pohl, *Phys. Rev. Lett.* **104**, 195302 (2010).

- [22] J. Honer, H. Weimer, T. Pfau, and H. P. Büchler, *Phys. Rev. Lett.* **105**, 160404 (2010).
- [23] G. Pupillo, A. Micheli, M. Boninsegni, I. Lesanovsky, and P. Zoller, *Phys. Rev. Lett.* **104**, 223002 (2010).
- [24] T. Macrì and T. Pohl, *Phys. Rev. A* **89**, 011402(R) (2014).
- [25] M. Mattioli, M. Dalmonte, W. Lechner, and G. Pupillo, *Phys. Rev. Lett.* **111**, 165302 (2013).
- [26] M. Dalmonte, W. Lechner, Z. Cai, M. Mattioli, A. M. Läuchli, and G. Pupillo, *Phys. Rev. B* **92**, 045106 (2015).
- [27] A. Angelone, F. Mezzacapo, and G. Pupillo, *Phys. Rev. Lett.* **116**, 135303 (2016).
- [28] A. Angelone, T. Ying, F. Mezzacapo, G. Masella, M. Dalmonte, and G. Pupillo, *Phys. Rev. A* **101**, 063603 (2020).
- [29] E. Guardado-Sanchez, B. M. Spar, P. Schauss, R. Belyansky, J. T. Young, P. Bienias, A. V. Gorshkov, T. Iadecola, and W. S. Bakr, *Phys. Rev. X* **11**, 021036 (2021).
- [30] M. Tsitsishvili, T. Chanda, M. Votto, P. Fromholz, M. Dalmonte, and A. Nersesyan, *Phys. Rev. B* **105**, 155159 (2022).
- [31] P. Fromholz, M. Tsitsishvili, M. Votto, M. Dalmonte, A. Nersesyan, and T. Chanda, *Phys. Rev. B* **106**, 155411 (2022).
- [32] T. Botzung, G. Pupillo, P. Simon, R. Citro, and E. Ercolessi, One-dimensional extended Hubbard model with soft-core potential, [arXiv:1909.12168](https://arxiv.org/abs/1909.12168) (2019).
- [33] M. Sarkar, M. Pal, A. Sen, and K. Sengupta, *SciPost Phys.* **14**, 004 (2023).
- [34] L. Eck and P. Fendley, Critical lines and ordered phases in a Rydberg-blockade ladder, [arXiv:2304.08484](https://arxiv.org/abs/2304.08484) (2023).
- [35] E. Orignac and T. Giamarchi, *Phys. Rev. B* **64**, 144515 (2001).
- [36] B. N. Narozhny, S. T. Carr, and A. A. Nersesyan, *Phys. Rev. B* **71**, 161101(R) (2005).
- [37] S. T. Carr, B. N. Narozhny, and A. A. Nersesyan, *Phys. Rev. B* **73**, 195114 (2006).
- [38] H. Miyake, G. A. Siviloglou, C. J. Kennedy, W. C. Burton, and W. Ketterle, *Phys. Rev. Lett.* **111**, 185302 (2013).
- [39] M. Atala, M. Aidelsburger, M. Lohse, J. T. Barreiro, B. Paredes, and I. Bloch, *Nat. Phys.* **10**, 588 (2014).
- [40] L. F. Livi, G. Cappellini, M. Diem, L. Franchi, C. Clivati, M. Frittelli, F. Levi, D. Calonico, J. Catani, M. Inguscio, and L. Fallani, *Phys. Rev. Lett.* **117**, 220401 (2016).
- [41] S. Barbarino, L. Taddia, D. Rossini, L. Mazza, and R. Fazio, *New J. Phys.* **18**, 035010 (2016).
- [42] J. C. Budich, A. Elben, M. Łącki, A. Sterdyniak, M. A. Baranov, and P. Zoller, *Phys. Rev. A* **95**, 043632 (2017).
- [43] M. Calvanese Strinati, E. Cornfeld, D. Rossini, S. Barbarino, M. Dalmonte, R. Fazio, E. Sela, and L. Mazza, *Phys. Rev. X* **7**, 021033 (2017).
- [44] S. Barbarino, M. Dalmonte, R. Fazio, and G. E. Santoro, *Phys. Rev. A* **97**, 013634 (2018).
- [45] J. Jünemann, A. Piga, S.-J. Ran, M. Lewenstein, M. Rizzi, and A. Bermudez, *Phys. Rev. X* **7**, 031057 (2017).
- [46] A. Bermudez, E. Tirrito, M. Rizzi, M. Lewenstein, and S. Hands, *Ann. Phys.* **399**, 149 (2018).
- [47] E. Tirrito, M. Rizzi, G. Sierra, M. Lewenstein, and A. Bermudez, *Phys. Rev. B* **99**, 125106 (2019).
- [48] E. Tirrito, M. Lewenstein, and A. Bermudez, *Phys. Rev. B* **106**, 045147 (2022).
- [49] C.-H. Huang, M. Tezuka, and M. A. Cazalilla, *New J. Phys.* **24**, 033043 (2022).
- [50] Z. Bacciconi, G. M. Andolina, T. Chanda, G. Chiriaco, M. Schirò, and M. Dalmonte, First-order superradiant phase transition in magnetic cavities: A two-leg ladder model, [arXiv:2302.09901](https://arxiv.org/abs/2302.09901) (2023).
- [51] D. Jaksch and P. Zoller, *New J. Phys.* **5**, 56 (2003).
- [52] J. Dalibard, F. Gerbier, G. Juzeliūnas, and P. Öhberg, *Rev. Mod. Phys.* **83**, 1523 (2011).
- [53] A. Celi, P. Massignan, J. Ruseckas, N. Goldman, I. B. Spielman, G. Juzeliūnas, and M. Lewenstein, *Phys. Rev. Lett.* **112**, 043001 (2014).
- [54] V. Galitski, G. Juzeliūnas, and I. B. Spielman, *Phys. Today* **72**(1), 38 (2019).
- [55] B. Beradze and A. Nersesyan, *Eur. Phys. J. B* **96**, 2 (2023).
- [56] A. O. Gogolin, A. A. Nersesyan, and A. M. Tsvelik, *Bosonization and Strongly Correlated Systems* (Cambridge University Press, Cambridge, UK, 2004).
- [57] T. Giamarchi, *Quantum Physics in One Dimension* (Oxford University Press, Oxford, 2003).
- [58] U. Schollwöck, *Ann. Phys.* **326**, 96 (2011).
- [59] R. Orús, *Ann. Phys.* **349**, 117 (2014).
- [60] P. Silvi, F. Tschirsich, M. Gerster, J. Jünemann, D. Jaschke, M. Rizzi, and S. Montangero, *SciPost Phys. Lect. Not.* **8** (2019).
- [61] P. D. Francesco, P. Mathieu, and D. Sénéchal, *Conformal Field Theory* (Springer, New York, 1997).
- [62] G. Delfino and G. Mussardo, *Nucl. Phys. B* **516**, 675 (1998).
- [63] M. Fabrizio, A. Gogolin, and A. Nersesyan, *Nucl. Phys. B* **580**, 647 (2000).
- [64] L. P. Kadanoff and A. B. Zisook, *Nucl. Phys. B* **180**, 61 (1981).
- [65] G. Delfino and P. Grinza, *Nucl. Phys. B* **682**, 521 (2004).
- [66] S. Hollerith, K. Srakaew, D. Wei, A. Rubio-Abadal, D. Adler, P. Weckesser, A. Kruckenhauser, V. Walther, R. van Bijnen, J. Rui *et al.*, *Phys. Rev. Lett.* **128**, 113602 (2022).
- [67] Y. Shapira, T. Manovitz, N. Akerman, A. Stern, and R. Ozeri, *Phys. Rev. X* **13**, 021021 (2023).
- [68] S. Coleman, *Phys. Rev. D* **11**, 2088 (1975).
- [69] K. Hida, *Phys. Rev. B* **45**, 2207 (1992).
- [70] E. G. Dalla Torre, E. Berg, and E. Altman, *Phys. Rev. Lett.* **97**, 260401 (2006).
- [71] E. Berg, E. G. Dalla Torre, T. Giamarchi, and E. Altman, *Phys. Rev. B* **77**, 245119 (2008).
- [72] G. G. Batrouni, R. T. Scalettar, V. G. Rousseau, and B. Grémaud, *Phys. Rev. Lett.* **110**, 265303 (2013).
- [73] G. G. Batrouni, V. G. Rousseau, R. T. Scalettar, and B. Grémaud, *Phys. Rev. B* **90**, 205123 (2014).
- [74] A. Montorsi and M. Roncaglia, *Phys. Rev. Lett.* **109**, 236404 (2012).
- [75] L. Barbiero, A. Montorsi, and M. Roncaglia, *Phys. Rev. B* **88**, 035109 (2013).
- [76] Y. Bahri and A. Vishwanath, *Phys. Rev. B* **89**, 155135 (2014).
- [77] G. Y. Chitov and T. Pandey, *J. Stat. Mech.: Theory Exp.* (2017) 043101.
- [78] A. A. Nersesyan, *Phys. Rev. B* **102**, 045108 (2020).
- [79] M. Endres, M. Cheneau, T. Fukuhara, C. Weitenberg, P. Schauß, C. Gross, L. Mazza, M. C. Bañuls, L. Pollet, I. Bloch, and S. Kuhr, *Science* **334**, 200 (2011).
- [80] T. A. Hilker, G. Salomon, F. Grusdt, A. Omran, M. Boll, E. Demler, I. Bloch, and C. Gross, *Science* **357**, 484 (2017).
- [81] P. Sompet, S. Hirthe, D. Bourgund, T. Chalopin, J. Bibo, J. Koepsell, P. Bojović, R. Verresen, F. Pollmann, G. Salomon,

- C. Gross, T. A. Hilker, and I. Bloch, *Nature (London)* **606**, 484 (2022).
- [82] D. Wei, D. Adler, K. Srakaew, S. Agrawal, P. Weckesser, I. Bloch, and J. Zeiher, *Phys. Rev. X* **13**, 021042 (2023).
- [83] J. B. Kogut, *Rev. Mod. Phys.* **51**, 659 (1979).
- [84] M. Kohmoto, M. den Nijs, and L. P. Kadanoff, *Phys. Rev. B* **24**, 5229 (1981).
- [85] I. Affleck, *Nucl. Phys. B* **265**, 409 (1986).
- [86] G. Mussardo, *Statistical Field Theory: An Introduction to Exactly Solved Models in Statistical Physics* (Oxford University Press, New York, 2010).
- [87] A. Luther and I. Peschel, *Phys. Rev. B* **12**, 3908 (1975).
- [88] F. D. M. Haldane, *Phys. Rev. B* **25**, 4925 (1982).
- [89] S. Peotta, L. Mazza, E. Vicari, M. Polini, R. Fazio, and D. Rossini, *J. Stat. Mech.: Theory Exp.* (2014) P09005.
- [90] G. Giudici, A. Angelone, G. Magnifico, Z. Zeng, G. Giudice, T. Mendes-Santos, and M. Dalmonte, *Phys. Rev. B* **99**, 094434 (2019).
- [91] S. Singh, R. N. C. Pfeifer, and G. Vidal, *Phys. Rev. A* **82**, 050301(R) (2010).
- [92] S. Singh, R. N. C. Pfeifer, and G. Vidal, *Phys. Rev. B* **83**, 115125 (2011).
- [93] S. R. White, *Phys. Rev. Lett.* **69**, 2863 (1992).
- [94] S. R. White, *Phys. Rev. B* **48**, 10345 (1993).
- [95] S. R. White, *Phys. Rev. B* **72**, 180403(R) (2005).
- [96] I. P. McCulloch, *J. Stat. Mech.: Theory Exp.* (2007) P10014.
- [97] I. P. McCulloch, Infinite size density matrix renormalization group, revisited [arXiv:0804.2509](https://arxiv.org/abs/0804.2509) (2008).
- [98] G. M. Crosswhite, A. C. Doherty, and G. Vidal, *Phys. Rev. B* **78**, 035116 (2008).
- [99] G. Vidal, *Phys. Rev. Lett.* **98**, 070201 (2007).
- [100] J. A. Kjäll, M. P. Zaletel, R. S. K. Mong, J. H. Bardarson, and F. Pollmann, *Phys. Rev. B* **87**, 235106 (2013).
- [101] L. Tagliacozzo, G. Evenbly, and G. Vidal, *Phys. Rev. B* **80**, 235127 (2009).
- [102] M. Gerster, P. Silvi, M. Rizzi, R. Fazio, T. Calarco, and S. Montangero, *Phys. Rev. B* **90**, 125154 (2014).
- [103] F. Pollmann, A. M. Turner, E. Berg, and M. Oshikawa, *Phys. Rev. B* **81**, 064439 (2010).
- [104] C. Callan and F. Wilczek, *Phys. Lett. B* **333**, 55 (1994).
- [105] G. Vidal, J. I. Latorre, E. Rico, and A. Kitaev, *Phys. Rev. Lett.* **90**, 227902 (2003).
- [106] P. Calabrese and J. Cardy, *J. Stat. Mech.* (2004) P06002.
- [107] H. F. Song, S. Rachel, and K. Le Hur, *Phys. Rev. B* **82**, 012405 (2010).
- [108] H. F. Song, S. Rachel, C. Flindt, I. Klich, N. Laflorencie, and K. Le Hur, *Phys. Rev. B* **85**, 035409 (2012).
- [109] S. Rachel, N. Laflorencie, H. F. Song, and K. Le Hur, *Phys. Rev. Lett.* **108**, 116401 (2012).
- [110] J. Hauschild and F. Pollmann, *SciPost Phys. Lect. Not.* **5** (2018).
- [111] M. Fishman, S. R. White, and E. M. Stoudenmire, *SciPost Phys. Codebases* **4** (2022).

Hysteresis of Dynamical Axion Insulators

Joan Bernabeu¹ and Alberto Cortijo²

¹*Departamento de Física de la Materia Condensada,
Universidad Autónoma de Madrid, Cantoblanco, E-28049 Madrid, Spain*

²*Instituto de Ciencia de Materiales de Madrid (ICMM),
Consejo Superior de Investigaciones Científicas (CSIC),
Sor Juana Inés de la Cruz 3, 28049 Madrid, Spain*

Magnetic catalysis is a known proposal for inducing dynamical axionic gapped phases by means of external magnetic fields from a Weyl or Dirac semimetal phase [1]. At a non-zero chemical potential, the phase transition is of first-order type and the magnetic field needs to reach a critical value for the transition to take place. Using the theory of bubble nucleation, we predict the order parameter features a hysteretic behavior as a function of the external magnetic field [2]. We also analyze the experimental consequences of this hysteretic behavior in several observables like magnetoconductivity, magnetic susceptibility, and nonlinear optical coefficients. This hysteretic behavior might serve as a fingerprint of magnetic catalysis in condensed matter systems.

[1] B. Roy and J. D. Sau, Phys.Rev.B 92, 125141 (2015).

[2] J. Bernabeu and A. Cortijo, Phys.Rev.B B 110(8), L081101 (2024).

Topological phase transition through electron-phonon interaction in an α - T_3 lattice

Kuntal Bhattacharyya, Mijanur Islam, and Saurabh Basu

Department of Physics, Indian Institute of Technology Guwahati, Guwahati-781039, Assam, India

We study the phenomenon of topological phase transitions induced by electron-phonon (e-ph) coupling in an α - T_3 Haldane-Holstein model that presents smooth tunability between graphene ($\alpha = 0$) and a dice lattice ($\alpha = 1$). The e-ph coupling has been incorporated via the Lang-Firsov transformation which adequately captures the polaron physics in the high frequency (anti-adiabatic) regime, and yields an effective Hamiltonian of the system through zero phonon averaging at $T = 0$. While investigating the phase transition driven by polaron and its interplay with the parameter α , we identify two regions based on the values of α , namely, the low to intermediate range ($0 < \alpha \leq 0.6$) and larger values of α ($0.6 < \alpha < 1$) where the topological transitions show distinct behaviour. There exists a single critical e-ph coupling strength for the former, below which the system behaves as a topological insulator characterized by edge modes, finite Chern number, and Hall conductivity, with all of them vanishing above this value, and the system undergoes a spectral gap closing transition. Further, the critical coupling strength depends upon α . For the latter case ($0.6 < \alpha < 1$), the scenario is more interesting where there are two critical values of the e-ph coupling at which trivial-topological-trivial and topological-topological-trivial phase transitions occur. Our studies on e-ph coupling induced phase transitions show a significant difference with regard to the well-known unique transition occurring at $\alpha = 1/2$ (or at $1/\sqrt{2}$) in the absence of the e-ph coupling, and thus underscore the importance of interaction effects on the topological phase transitions.

- [1] F. D. M. Haldane, Phys. Rev. Lett. **61**, 2015–2018 (1988).
- [2] T. Holstein, Ann. Phys. **8**, 343–389 (1959).
- [3] H. Hu, Q. Si, Sci. Adv. **9**, eadg0028 (2023).
- [4] J. D. Malcolm, E. J. Nicol, Phys. Rev. B **93**, 165433 (2016).
- [5] A. Raoux, M. Morigi, J.-N. Fuchs, F. Piéchon, G. Montambaux, Phys. Rev. Lett. **112**, 026402 (2014).
- [6] J. Wang, J.-F. Liu, Phys. Rev. B **103**, 075419 (2021).
- [7] B. Dey, T. K. Ghosh, Phys. Rev. B **99**, 205429 (2019).
- [8] A. Singh, G. Sharma, Phys. Rev. B **107**, 245150 (2023).
- [9] L. M. Cangemi, A. S. Mishchenko, N. Nagaosa, V. Cataudella, G. D. Filippis, Phys. Rev. Lett. **123**, 046401 (2019).
- [10] A. C.-Guardian, N. Goldman, P. Massignan, G. M. Bruun, Phys. Rev. B **99**, 081105 (2019).
- [11] C. Lu, M. Zhang, H. Wang, Q. Ai, T. Liu, Phys. Rev. B **107**, 125118 (2023).
- [12] S. Julià-Farré, M. Müller, M. Lewenstein, A. Dauphin, Phys. Rev. Lett. **125**, 240601 (2020).

Dispersive drumhead states in nodal-line semimetal junctions

Francesco Buccheri¹, Reinhold Egger² and Alessandro De Martino³

¹*Department of Applied Science and Technology, Polytechnic University Turin*

²*Institute for Theoretical Physics IV, HHU Düsseldorf*

³*Department of Mathematics, City, University of London*

We consider a smooth interface between a topological nodal-line semimetal [2, 3] and a topologically trivial insulator or another semimetal with a nodal ring of different radius. Using a low-energy effective Hamiltonian including only the two crossing bands, we show that these junctions accommodate a two-dimensional zero-energy level and a set of two-dimensional dispersive bands, corresponding to states localized at the interface. We characterize the spectrum, identifying the parameter ranges in which these states are present, and highlight the role of the nodal radius and the smoothness of the interface. We also suggest material-independent ways to detect and identify these states, using optical conductivity and infrared absorption spectroscopy in magnetic field [1].

- [1] F. Buccheri, R. Egger and A. De Martino, *Phys. Rev. Res.* **6** (1), 013193 (2024);
- [2] CA. A. Burkov, M. D. Hook and L. Balents, *Phys. Rev. B* **84**, 235126 (2011);
- [3] C. Fang, Y. Chen, H.-Y. Kee and L. Fu, *Phys. Rev. B* **92**, 081201(R).

Topological superconductivity in hexagonal lattice systems

Matthew Bunney^{1,2}, C. Honerkamp^{2,3} and S. Rachel¹

¹ *School of Physics, University of Melbourne, Parkville, VIC 3010, Australia*

² *Institute for Theoretical Solid State Physics, RWTH Aachen University, 52062 Aachen, Germany*

³ *JARA Fundamentals of Future Information Technology, 52062 Aachen, Germany*

Topological superconductors are amongst the most desired phase of quantum matter, as they can host so-called midgap states in their energy spectra, commonly known as Majorana zero modes. In particular, chiral – *i.e.*, time-reversal breaking – superconductors can be characterised by the Chern number, just like quantum Hall insulators.

Hexagonal lattices systems are promising platforms in the search for topological superconductors. These lattices rose to prominence following the experimental fabrication of the graphene and other two-dimensional van der Waals materials, including the recently discovered “twisted materials”.

The functional renormalisation group is well suited to discern between competing many-body instabilities in an unbiased way. We employ the truncated-unity formulation of the functional renormalisation group to calculate rich phase diagrams with magnetic, charge-density wave, and superconducting phases. Moreover, we find a surprisingly rich landscape of varying Chern numbers associated with the superconducting instabilities. [1] This is one example of the drastic effect of spin-orbit coupling to these models, with our results expected to be relevant for heterostructures and non-centrosymmetric materials.

[1] Bunney, M., et al., “Chern number landscape of spin-orbit coupled chiral superconductors.” arXiv preprint arXiv:2405.03757 (2024).

Plasmons as proxies of orbital skyrmion textures: the case of twisted MoTe_2

Lorenzo Cavicchi¹, Koen J. A. Reijnders², Mikhail I. Katsnelson², and Marco Polini^{3,4}

¹*Scuola Normale Superiore, I-56126 Pisa, Italy*

²*Institute for Molecules and Materials, Radboud University, Heyendaalseweg 135, 6525AJ Nijmegen, The Netherlands*

³*Dipartimento di Fisica dell'Università di Pisa, Largo Bruno Pontecorvo 3, I-56127 Pisa, Italy*

⁴*ICFO-Institut de Ciències Fotòniques, The Barcelona Institute of Science and Technology, Av. Carl Friedrich Gauss 3, 08860 Castelldefels (Barcelona), Spain*

We present a comprehensive theoretical investigation of the optical and plasmonic properties of twisted transition metal dichalcogenide (TMD) bilayers, with a particular focus on twisted MoTe_2 homobilayers. These materials have recently attracted significant attention due to experimental discoveries of fractional Chern insulating states in zero magnetic fields [1, 2, 3, 4] and superconductivity [5, 6]. Available continuum-model Hamiltonians [7, 8] describing their single-particle topological moiré bands—which have been recently dubbed *skyrmion Chern-band models* [9, 10]—harbor orbital (rather than spin) skyrmion lattices. The presence of this orbital skyrmion lattice enables an approximate mapping of the system onto a model of Landau levels subjected to a periodic potential [9, 11]. Using an adiabatic approximation for the layer-pseudospin degree of freedom, the twisted TMD Hamiltonian can be simplified to describe holes moving in the combined effect of a periodic potential and a periodic magnetic field. This effective magnetic field, which has a non-zero average, is directly linked to the topological charge of the skyrmion lattice [7, 9, 11].

A key result of our study is that plasmons in twisted TMD bilayers could serve as a sensitive probe of orbital skyrmion textures. While the effective magnetic field description captures the qualitative features of the system, we show that a more precise quantum mechanical treatment is necessary to obtain quantitatively accurate results. Additionally, we provide an alternative derivation of the mapping onto a single pseudospin sector, distinct from previous works [9, 11], by employing semiclassical techniques. This leads to a formal series expansion that systematically incorporates higher-order corrections in the adiabatic parameter.

Our findings enlarge the understanding of the optical and plasmonic properties of twisted TMD bilayers and suggest potential experimental approaches for probing topological textures in these systems.

- [1] Cai, J. et al. *Nature* **622**, 63 (2023).
- [2] Park, H. et al. *Nature* **622**, 74 (2023).
- [3] Zeng, Y. et al. *Nature* **622**, 69 (2023).
- [4] Xu, F. et al. *Phys. Rev. X* **13**, 031037 (2023).
- [5] Xia, T., et al. arXiv:2405.14784.
- [6] Guo, Y., et al. arXiv:2406.03418 (2024).
- [7] Wu, F., et al. *Phys. Rev. Lett.* **122**, 086402 (2019).
- [8] Pan, H., et al. *Phys. Rev. Research* **2**, 033087 (2020).
- [9] Morales-Durán, N., et al. *Phys. Rev. Lett.* **132**, 096602 (2024).
- [10] Reddy, A. P., et al. arXiv:2403.00059.
- [11] Shi, J., et al. *Phys. Rev. B* **110**, 035130 (2024).

Light-Induced Electronic States in Thin Topological Insulators

S. S. Dabiri¹, H. Cheraghchi^{2,3}

¹ *Department of Physics, Shahid Beheshti University, Tehran, Iran*

² *School of Physics, Damghan University, Damghan, Iran*

³ *School of Physics, Institute for Research in Fundamental Sciences (IPM), Tehran, Iran*

Recent technological advancements in mid-infrared lasers have opened up exciting new possibilities for engineering electronic band structures. The interplay between lattice periodicity and time, arising from the oscillating electromagnetic field, extends the Hilbert space, leading to the emergence of **Floquet-Bloch states**. These states allow for the modification of band structures, including gap opening, and enable the engineering of phase transitions through photon-assisted processes. Notably, light-induced states have been experimentally observed on the surfaces of irradiated topological insulators, optical lattices, and graphene.

An intriguing case involves **magnetically doped topological insulator thin films**, such as Cr-doped (Bi,Sb) $_2$ Te $_3$ family, irradiated by circularly polarized electromagnetic fields. The resulting phase diagram exhibits fascinating features, including the **quantum anomalous Hall insulator** and the **quantum pseudo-spin Hall insulator**, which depend on the frequency, intensity of light, system parameters, and magnetic field. By engineering these light-induced states, one can design an electronic switch. Additionally, using the extended Kubo formula, we investigate the **time-averaged optical conductivity** of this driven system in two driven regimes and two occupation models.

Furthermore, we explore **dichroism** and **optical conductivity** in irradiated bilayer graphene under illumination by linear or circularly polarized light. Remarkably, when circularly polarized light is applied in conjunction with a perpendicular bias, **valley asymmetry** introduces the potential for generating a **valley-polarized current**.

[1] S. S. Dabiri, H. Cheraghchi, A. Sadeghi, Phys. Rev. B. 103, 205130 (2021); S. Dabiri, H. Cheraghchi, Phys. Rev. B. 104, 245121 (2021).

[2] S. S. Dabiri, H. Cheraghchi, A. Sadeghi, Phys. Rev. B. 106 (16), 165423 (2022).

[3] Z. Askarpour, H. Cheraghchi, Phys. Scr. 98, 055917 (2023).

[4] S. S. Dabiri, H. Cheraghchi, F. Adinehvand, and R. Asgari, Phys. Rev. B 109, 115431 (2024).

Dynamics of spiral magnetic order in an electrically-biased Kondo chain

Xiaohu Han¹, Pedro Ribeiro², and Stefano Chesi¹

¹*Beijing Computational Science Research Center, Beijing 100193, China*

²*CeFEMA-LaPMET and Physics Department, Instituto Superior Técnico, Universidade de Lisboa Av. Rovisco Pais, 1049-001 Lisboa, Portugal*

We have analyzed a one-dimensional system of localized magnetic moments coupled to itinerant electrons under an external bias voltage. In equilibrium, the system supports spiral magnetic order, leading to chiral electronic states. This magnetic phase has been proposed, in conjunction with proximity-induced superconductivity, to realize a self-organized topological superconductor. Here we study a Kondo chain without superconductivity, showing that non-equilibrium conditions induced by the external bias can significantly affect the spiral order.

More specifically, within an adiabatic approximation for the dynamics of the localized spins, and in the presence of a phenomenological damping term, we demonstrate the occurrence of various dynamical regimes: At small bias a rigidly-rotating non-coplanar magnetic structure is realized which, by increasing the applied voltage, transitions to a quasi-periodic and, finally, fully chaotic evolution. These phases give distinct signatures in transport measurements of the charge and spin current. In particular, the rigidly-rotating state results in an average transfer of electronic spin polarization, oriented along the rotation axis. For this rigidly-rotating state, we analyze in detail the dependence of the rotation axis and frequency on system's parameters. We show that the spin dynamics slows down in the thermodynamic limit, when a static conical state persists to arbitrarily long times.

Our results suggest the possibility of discovering non-trivial dynamics in other symmetry-broken quantum states under bias. Extending our analysis in the presence of electron interactions or superconductivity are other interesting directions of future research.

Topological Semimetals via Internal Symmetry

Faruk Abdulla^{1,2}, Gapathy Murthy³, and Ankur Das^{4,5}

¹*Harish-Chandra Research Institute, A CI of Homi Bhabha National Institute, Chhatnag Road, Jhansi, Prayagraj (Allahabad), India*

²*Physics Department, Technion - Israel Institute of Technology, Haifa, Israel*

³*Department of Physics and Astronomy, University of Kentucky, Lexington, KY, USA*

⁴*Department of Condensed Matter Physics, Weizmann Institute of Science, Rehovot, Israel*

⁵*Department of Physics, Indian Institute of Science Education and Research (IISER) Tirupati, India*

It has been realized over the past two decades that topological nontriviality can be present not only in insulators but also in gapless semimetals, the most prominent example being Weyl semimetals in three dimensions. Key to topological classification schemes are the three “internal” symmetries, time reversal T , charge conjugation C , and their product, called chiral symmetry $S=TC$. In this work, we show that robust topological semimetal phases occur in $d=3$ in systems without invoking crystalline symmetries other than translations. These topological semimetals naturally appear as an intermediate gapless phase between the topological and the trivial insulators; a sufficient condition for topological semimetals to exist is that the symmetry class must have a nontrivial topological insulator in $d=3$. We argue and show that the topological semimetals can be classified using winding number on a loop for nodal line semimetals and Chern number for point node semimetals (i.e. Weyl Semimetals). A nonzero winding number on a nodal loop implies robust gapless drumhead states on the surface Brillouin zone. Similarly, for point nodes, it will be Fermi arcs.

[1] Topological nodal line semimetals with chiral symmetry, arXiv: 2311.18667

[2] Stable nodal line semimetals in the chiral classes in three dimensions, arXiv: 2401.02966

Altermagnets are crystallographic rotational symmetry breaking spin-ordered states, possessing a net zero magnetization despite manifesting Kramers non-degenerate bands. Here, we show that momentum-independent local spin nematic orders in monolayer, Bernal bilayer and rhombohedral trilayer graphene give rise to p -wave, d -wave and f -wave altermagnets, respectively, thereby inheriting the free-fermion topology of linear, bi-quadratic and bi-cubic band touchings that are

also described in terms of angular momentum $\ell = 1, 2$ and 3 spherical harmonics in the reciprocal space. The same conclusions also hold inside a nematic spin-triplet superconductor, featuring Majorana altermagnets. Altogether, these findings highlight the importance of electronic band structure in identifying such exotic magnetic orders in real materials. We depict the effects of in-plane magnetic fields on altermagnets, and showcase a novel spin-disordered alter-valleymagnet phase.

Topological signatures of a p-wave superconducting wire through light

Frederick del Pozo¹, Karyn Le Hur^{1,2}

¹*(Ecole Polytechnique (IP Paris))*

²*CNRS*

We show in [1] how the topological index of a one-dimensional topological p-wave superconductor can be revealed when driving with a classical vector potential i.e. an electromagnetic wave, through the light-induced transition probabilities and the profile of the induced quasiparticles population. As a function of driving frequency ω , it is possible to obtain a measure of this topological invariant from the resonance envelope, similar to [2], classifying the two distinct topological phases of the short-range Kitaev wire. We also propose to probe the topological phase transition in the model through the responses of the global capacitance in the presence of the light field and also through the Josephson current between the wire and the proximity coupled bulk superconductor. The system may also be implemented on the Bloch sphere [3, 4] allowing alternative ways to measure the \mathbb{Z} and \mathbb{Z}_2 topological invariants through circuit or cavity quantum electrodynamics.

- [1] F. del Pozo, K. Le Hur, arXiv preprint [arXiv:2401.14501](https://arxiv.org/abs/2401.14501) (2024) (accepted in PRB for publication)
- [2] T. Goren, K. Plekhanov, F. Appas, K. Le Hur, Phys. Rev. B **97**, 041106 (2018)
- [3] J. Hutchinson, K. Le Hur, Commun. Physics **4**, 144 (2021)
- [4] F. del Pozo, L. Herviou, K. Le Hur, Phys. Rev. B **107** (15), 155134 (2023)

Magnon transmission across $\nu=1|-1|1$ mono-layer graphene junction as a probe of electronic structure

Suman Jyoti De^{1,2}, Sumathi Rao³ and Ganpathy Murthy⁴

¹*Department of Physics, McGill University, Canada*

²*Harish-Chandra Research Institute, India*

³*International Centre for Theoretical Sciences, India*

⁴*Department of Physics & Astronomy, University of Kentucky, USA*

We study magnon transmission across gate-controlled junctions in the $n=0$ manifold of Landau levels in monolayer graphene, in the presence of both spin and valley Zeeman fields. Specifically, we consider the $1|-1|1$ sandwich geometry. The nature of the interfaces between regions of different filling turns out to be crucial for magnon transmission. Using the Hartree-Fock approximation, we find that either the spin or the valley degrees of freedom of the occupied one-body states rotate across the interfaces. If the interfaces exhibit spin rotation, magnon transmission is suppressed at high energies, while if the interfaces have valley rotation, magnon transmission becomes perfect at high energies.

The valley Zeeman coupling, which arises from partial alignment with the encapsulating Boron Nitride, is independent of the perpendicular magnetic field B , while the spin Zeeman and other anisotropic couplings scale linearly with B . This allows the tuning of the relative strength of the valley Zeeman coupling in situ by varying B , which can drive phase transitions of the interfaces between spin-rotated and valley-rotated phases, leading to magnon transmission being either vanishing or perfect at high energies. Our analysis[1], along with the experimental measurements, can be used to determine the anisotropic couplings in the sample.

[1] Suman Jyoti De, Sumathi Rao, Ganpathy Murthy, Phys. Rev. B. **110**, 085417 (2024).

Valley-contrasting magnetoresistance beyond the relaxation-time approximation

A. Faridi¹, and R. Asgari^{1,2}

¹ *School of Physics, Institute for Research in Fundamental Sciences (IPM), Tehran 19395-5531, Iran*

² *School of Physics, University of New South Wales, Kensington, NSW 2052, Australia*

In this work, we study the magnetotransport properties in a 2D multivalley system in the presence of orbital magnetic moment (OMM). Going beyond the simple time-relaxation approximation and solving accurately (up to the lowest Born approximation) the Boltzmann equation following an integral equation approach[1], we have included the “in-scattering” terms and the “intervalley scattering” in our calculations both of which have been completely ignored in previous studies on 2D multivalley systems.

Our calculations show that when time-reversal symmetry is preserved in the system, the inclusion of “in-scattering” terms has a profound impact on the magnetotransport such that in high-density regime it can change the sign of the magnetoresistance. Also, in the presence of the “intervalley” scattering, when the Fermi energy is near the band-edge, we find a sharp drop in the magnetoresistance at a specific magnetic field where one of the valleys is depleted. The discontinuity of the magnetoresistance at this point grows with the intervalley scattering and therefore it can be thought of as an experimental measure of the existence and the magnitude of the intervalley scattering in a system.

Furthermore, we have studied the magnetoresistance in a multivalley time-reversal-broken system which is modeled by considering a valley polarization in the system. We find that not only the OMM-induced terms substantially change the absolute value of the magnetoresistance, but also in this case it behaves completely different depending on the polarization sign. While for negative polarization, the magnetoresistance stays negative for $B > 0$, it changes sign from positive to negative in the case of positive polarization and this shift occurs in low-field limit[2].

[1] Karel Vyborny, Alexey A. Kovalev, Jairo Sinova, and T. Jungwirth, Phys. Rev. B **79**, 045427 (2009).

[2] A. Faridi, and R. Asgari, Phys. Rev. B **107**, 235417 (2023).

Topological phase diagram of two-band fermionic chain in presence of Hubbard interaction

R. Favata¹, D. Piccioni², A. Parola³ and F. Becca¹

¹*Dipartimento di Fisica, Università di Trieste, Strada Costiera 11, I-34151 Trieste, Italy*

²*Scuola Internazionale Superiore di Studi Avanzati (SISSA), Via Bonomea 265, I-34136 Trieste, Italy*

³*Dipartimento di Scienza e Alta Tecnologia, Università dell'Insubria, Via Valleggio 11, I-22100 Como, Italy*

Topological insulators are an emerging class of intriguing materials with unique electronic properties. The topological features of a material are commonly established at the non-interacting level and the fate of topology in strongly correlated systems is a relevant topic of current research in the field. Here, we explore the ground-state properties of a two-band fermionic chain supporting a symmetry-protected topological insulator phase, in the presence of Hubbard interaction, inspired by the model proposed in [1]. Starting from the non-interacting ground state, we define a two-orbital Jastrow-Slater wave function and show how it provides a proper variational description of the topological phase diagram. The topological properties in the presence of interaction are detected by the many-body marker introduced by Resta and Sorella [2]. We find that the topologically non-trivial behaviour of the system persists in the large U limit, where the spin-1 Haldane chain, characterized by string order, emerges as an effective spin Hamiltonian[3].

[1] S. Barbarino, G. Sangiovanni, and J. C. Budich, Phys. Rev. B **99**, 075158 (2019).

[2] R. Resta and S. Sorella, Phys. Rev. Lett. **82**, 370 (1999).

[3] S. R. White Phys. Rev. B **53**, 52 (1996)

Non-Hermitian Topological Phase Transition of the Bosonic Kitaev Chain

C. Fortin¹, **A. McDonald**², **K. Wang**¹, **T. Pereg-Barnea**¹

¹ *Department of Physics, McGill University, Montréal, Québec H3A 2T8, Canada*

² *Institut Quantique and Département de Physique, Université de Sherbrooke, Sherbrooke, Québec J1K 2R1, Canada*

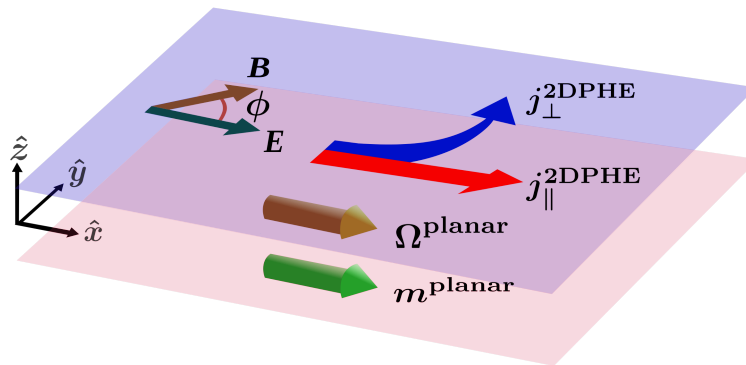
The bosonic Kitaev chain (BKC) is a 1D system with nearest-neighbor hopping and parametric coupling that exhibits exponential amplification in the field quadratures depending on whether the (complex) spectrum of the periodic chain winds around the origin. When it does not, the field quadratures are exponentially suppressed. We study the topological phase transition of the BKC whose unit cell is subject to different configurations in the on-site bath coupling constants. We show that there is neither amplification nor suppression at the critical point separating two topological phases. When the unit cell's size is even, we find that the BKC exhibits exponential amplification for arbitrarily large dissipation on odd sites. On the other hand, even when subject to mild dissipation, the BKC undergoes a topological phase transition when the size of its unit cell is odd.

Planar Hall Effect in Quasi-Two-Dimensional Materials

(<https://doi.org/10.48550/arXiv.2405.00379>)

Koushik Ghorai¹, Sunit Das¹, Harsh Varshney¹ and Amit Agarwal¹

¹ *Department of Physics, Indian Institute of Technology Kanpur, Kanpur-208016, India*



Schematic for 2D planar Hall effect (2DPHE)

The planar Hall effect (PHE) is the generation of longitudinal and transverse voltages in the plane of the applied electric (\mathbf{E}) and magnetic fields (\mathbf{B}). The planar Hall effect in 3D systems is an effective probe for their Berry curvature, topology, and electronic properties. However, the Berry curvature-induced conventional planar Hall effect is forbidden in 2D systems as the out-of-plane Berry curvature cannot couple to the band velocity of the electrons moving in the 2D plane. Here, we demonstrate a unique 2D planar Hall effect (2DPHE) originating from the hidden planar components of the Berry curvature (Ω^{planar}) and orbital magnetic moment ($\mathbf{m}^{\text{planar}}$) in quasi-2D materials. We identify all planar band geometric contributions to 2DPHE and classify their crystalline symmetry restrictions. Using gated bilayer graphene as an example, we show that in addition to capturing the hidden band geometric effects, 2DPHE is also sensitive to the Lifshitz transitions. Our work motivates further exploration of hidden planar band geometry-induced 2DPHE and related transport phenomena for innovative applications

[1] Kyoung-Wan Kim, Hogyun Jeong, J. Kim, and Hosub Jin, Phys. Rev. B **104**, L081114 (2021).

[2] S. Nandy, G. Sharma, A. Taraphder, and Sumanta Tewari, Phys. Rev. Lett. **119**, 176804 (2017).

Local and energy-resolved topological invariants for Floquet systems

Arnob Kumar Ghosh, Rodrigo Arouca, and Annica M. Black-Schaffer

Department of Physics and Astronomy, Uppsala University, Box 516, 75120 Uppsala, Sweden

Periodically driven systems offer a perfect breeding ground for out-of-equilibrium engineering of topological boundary states at zero energy (0-mode), as well as finite energy (π -mode), with the latter having no static analog. The Floquet operator and the effective Floquet Hamiltonian, which encapsulate the stroboscopic features of the driven system, capture both spectral and localization properties of the 0- and π -modes but sometimes fail to provide complete topological characterization, especially when 0- and π -modes coexist. In this work [1], we utilize the spectral localizer, a powerful local probe that can provide numerically efficient, spatially local, and energy-resolved topological characterization [2]. In particular, we apply the spectral localizer to the effective Floquet Hamiltonian for driven one- and two-dimensional topological systems with no or limited symmetries and are able to assign topological invariants, or local markers, that characterize the 0- and the π -boundary modes individually and unambiguously. Due to the spatial resolution, we also demonstrate that the extracted topological invariants are suitable for studying driven disordered systems and can even capture disorder-induced phase transitions.

[1] A. K. Ghosh, R. Arouca, and A. M. Black-Schaffer, arXiv:2408.08548.

[2] T. A. Loring, *Annals of Physics* **356**, 383 (2015).

Title: Spin-triplet superconductivity in topological semimetals

By Sudeep Kumar Ghosh

Affiliation: Department of Physics, IIT Kanpur

Abstract: Topological semimetals are three dimensional materials with symmetry-protected massless bulk excitations. In this talk, I will present our recent discoveries of time-reversal symmetry breaking superconductivity in two different families of topological semimetals: a) LaNiSi, LaPtSi and LaPtGe - Weyl nodal-line semimetals [1] and b) (Ta, Nb)OsSi – 3D Dirac semimetals [2]. I will present detailed theoretical and experimental results to establish that the superconducting ground state in both of these families is most likely a nonunitary triplet state. These materials thus provide promising platforms to investigate the rich physics arising from an interplay between topological nodal fermions and unconventional TRS-breaking superconductivity.

[1] T. Shang*, Sudeep Kumar Ghosh*, M. Smidman*, D. J. Gawryluk, C. Baines, A. Wang, W. Xie, Y. Chen, M. O. Ajeesh, M. Nicklas, E. Pomjakushina, M. Medarde, M. Shi, J. F. Annett, H. Yuan, J. Quintanilla* and T. Shiroka*- “Spin-triplet superconductivity in Weyl nodal-line semimetals” npj Quantum Mater. 7, 35 (2022).

[2] Sudeep Kumar Ghosh*, P. K. Biswas*, C. Xu, B. Li, J. Z. Zhao, A. D. Hillier and X. Xu*- “Time-Reversal Symmetry Breaking Superconductivity in Three-Dimensional Dirac Semimetallic Silicides” Phys. Rev. Research (Letters) 4, L012031 (2022).

Skyrmion Stripes in Twisted Double Bilayer Graphene

Debasmita Giri^{1,2}, Dibya Kanti Mukherjee^{3,4}, H.A. Fertig^{4,5,6}, Arijit Kundu²

¹*Institute for Theoretical Physics, University of Regensburg, Regensburg, Germany*

²*Department of Physics, Indian Institute of Technology Kanpur, Kanpur 208016, India*

³*Laboratoire de Physique des Solides, CNRS UMR 8502,*

Université Paris-Saclay, 91405 Orsay Cedex, France

⁴*Department of Physics, Indiana University, Bloomington, IN 47405*

⁵*Quantum Science and Engineering Center, Indiana University, Bloomington, IN, 47408*

⁶*Instituto de Ciencia de Materiales de Madrid, (CSIC), Cantoblanco, 28049, Madrid, Spain*

Two dimensional moiré systems have recently emerged as a platform in which the interplay between topology and strong correlations of electrons play out in non-trivial ways. Among these systems, twisted double bilayer graphene (TDBG) is of particular interest as its topological properties may be tuned via both twist angle and applied perpendicular electric field. In this system, energy gaps are observed at half filling of particular bands, which can be associated with correlated spin polarized states. In this work, we investigate the fate of these states as the system is doped away from this filling. We demonstrate that, for a broad range of fractional fillings, the resulting ground state is partially valley polarized, and supports multiple broken symmetries, including a textured spin order indicative of skyrmions, with a novel stripe ordering that spontaneously breaks C3 symmetry.

[1] [Debasmita Giri](#), [Dibya Kanti Mukherjee](#), [H.A. Fertig](#), [Arijit Kundu](#), [arXiv:2310.01185](#) (2023).

Layer-polarized ferromagnetism and electrical switching of chirality in rhombohedral multilayer graphene

Giannan Hua^{1,2}, Wenqiang Zhou^{1,2}, Jing Ding^{1,2}, and Shuigang Xu^{1,2}

¹*(Presenting author underlined) Department of Physics, School of Science, Westlake University, Hangzhou, Zhejiang 310024 China.*

²*Institute of Natural Sciences, Westlake Institute for Advanced Study, Hangzhou, Zhejiang 310024 China.*

Flat-band systems with strongly correlated electrons can exhibit a variety of phenomena, such as correlated insulating and topological states, unconventional superconductivity, and ferromagnetism. Rhombohedral multilayer graphene has recently emerged as a promising platform for investigating exotic quantum states due to its hosting of topologically protected surface flat bands at low energy, which have a layer-dependent energy dispersion. While the complex relationship between the surface flat bands and the highly dispersive high-energy bands makes it difficult to study correlated surface states.

In this study [1], we introduce (double aligned) moiré superlattices as a method to isolate the surface flat bands of rhombohedral multilayer graphene. Notably, we observe tunable layer-polarized ferromagnetism, which is evidenced by a hysteretic anomalous Hall effect. This is achieved by polarizing the surface states with finite displacement fields.

Furthermore, in [2], we report electrically switchable chirality in rhombohedral multilayer graphene-based Chern insulators. The surface flat band and giant Berry curvature in (single aligned) moiré superlattices rhombohedral multilayer graphene provide a highly tunable platform for engineering the topological states. The Chern number can be continuously tuned from 0, -1, 1 to 2 by electric fields, manifesting as a large anomalous Hall effect and following Streda's formula. Sign reversal and the anomalous Hall effect also occurred at non-integer fillings, suggesting the possibility of electrically tunable topological phase transitions within the regime of fractional Chern insulators.

[1] W. Zhou, J. Ding, J. Hua, et al. Nat. Commun. **15**, 2597 (2024).

[2] J. Ding, H. Xiang, J. Hua, et al. arXiv preprint arXiv:2406.14289 (2024).

The Development of Adjustable Exceptional Points in p - wave Altermagnets

Jorge H. Correa¹, Michal P. Nowak¹

¹ AGH University of Krakow, Academic Centre for Materials and Nanotechnology,
al.A.Mickiewicza30,30-059 Krakow, Poland

We theoretically study the role of non-hermitian ferromagnetic lead coupled to an altermagnetic material and we find the exceptional points where the eigenenergies and eigenvalues coalesce. The hamiltonian of the system is given by $H_{\text{ALM-FERR}} = H_{\text{AM}} + \Sigma^R(\omega = 0)$, where the first term represent the p-wave altermagnet, given by [1]

$$H_{\text{AM}} = t(k_x^2 + k_y^2 + \alpha_x^2 + \alpha_y^2)\sigma_0 + 2t(k_x\alpha_x + k_y\alpha_y)\sigma_z - \mu\sigma_0 \quad (1)$$

while the second part gives the coupling of a ferromagnetic lead [2]

$$\Sigma^R(\omega = 0) = -i\epsilon^+\sigma_0 - i\epsilon^-\sigma_z \quad (2)$$

the energies are given by

$$E_{1,2} = t(k_x^2 + k_y^2 + \alpha_x^2 + \alpha_y^2) - i\epsilon^\pm - \mu \pm \sqrt{\lambda_R^2(k_x^2 + k_y^2) + [2t(k_x\alpha_x + k_y\alpha_y) - i\epsilon^-]^2} \quad (3)$$

the exceptional points can be obtained when the square root is zero. In Fig. 1, we see the Fermi surfaces of the p-wave altermagnet and the energy differences, likewise, we can obtain two exceptional points as depicted in dark blue.

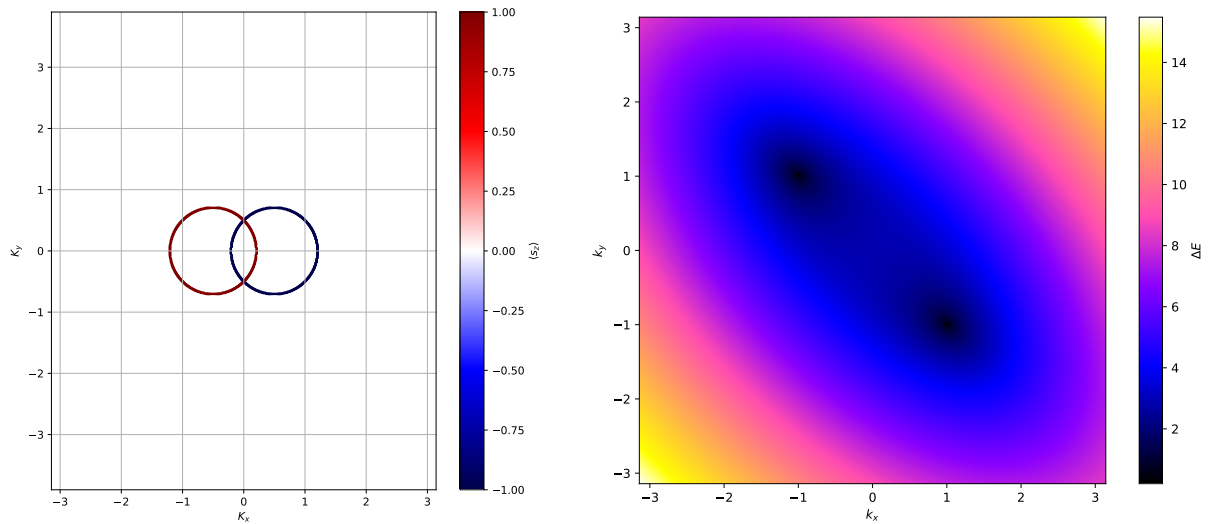


Figure 1: Left: Fermi surfaces of p-wave altermagnet where the blue and red represent the expectation values for spin-up and down respectively. Right : Difference of the energies given by Eq. 3

[1] K. Maeda, Bo Lu, K. Yada, Y. Tanaka, arXiv:2403.17482v1 (2024).

[2] Jorge Cayao, J. Phys.: Condens. Matter **35**, 254002A (2023).

Topological superconductivity in Fibonacci quasicrystals

Aksel Kobińska¹, Oladunjoye A. Awoga², Martin Leijnse², Tadeusz Domański³, Patric Holmvall¹, and Annica M. Black-Schaffer¹

¹*Department of Physics and Astronomy, Uppsala University, Box 516, 75120 Uppsala, Sweden*

²*Solid State Physics and NanoLund, Lund University, Box 118, 22100 Lund, Sweden*

³*Institute of Physics, M. Curie-Skłodowska University, 20-031 Lublin, Poland*

We investigate the properties of a Fibonacci quasicrystal (QC) arrangement of a one-dimensional topological superconductor, such as a magnetic atom chain deposited on a superconducting surface. We uncover a general mutually exclusive competition between the QC properties and the topological superconducting phase with Majorana bound states (MBS): there are no MBS inside the QC gaps and the MBS never behaves as QC subgap states, and likewise, no critical, or winding, QC subgap states exist inside the topological superconducting gaps. Surprisingly, despite this competition, we find that the QC is still highly beneficial for realizing topological superconductivity with MBS. It both leads to additional large nontrivial regions with MBS in parameter space, that are topologically trivial in crystalline systems, and increases the topological gap protecting the MBS. We also find that shorter approximants of the Fibonacci QC display the largest benefits. As a consequence, our results promote QCs, and especially their short approximants, as an appealing platform for improved experimental possibilities to realize MBS as well as generally highlights the fundamental interplay between different topologies.

Josephson-Current Signatures of Unpaired Floquet Majorana Bound States

Rekha Kumari^{1,2}, Babak Seradjeh^{3,4,5}, and Arijit Kundu²

¹*(Presenting author underlined) International Centre for Theoretical Sciences, Tata Institute of Fundamental Research, Bangalore 560089, India*

²*Department of Physics, Indian institute of technology, Kanpur, India*

³*Department of Physics, Indiana University, Bloomington, Indiana 47405, USA*

⁴*Quantum Science and Engineering Center, Indiana University, Bloomington, Indiana 47405, USA*

⁵*IU Center for Spacetime Symmetries, Indiana University, Bloomington, Indiana 47405, USA*

In this work we theoretically study the transport signatures of unpaired Floquet Majorana bound states in the Josephson current of weakly linked, periodically driven topological superconductors. We obtain the occupation of the Floquet Majorana modes in the presence of weak coupling to thermal leads analytically, and show that, similar to static superconductors, the Josephson current involving Floquet Majorana bound states is also 4π -periodic in the phase difference across the junction, and also depends linearly on the coupling between superconductors. Moreover, unlike the static case, the amplitude of the Josephson current can be tuned by setting the unbiased chemical potential of the driven superconductors at multiple harmonics of the drive frequency. As a result, we uncover a Josephson Floquet sum rule for driven superconductors. We confirm our analytical expressions for Josephson current, the occupation of Floquet bands, and a perturbative analysis of the quasienergies with numerically exact results.

[1] Rekha Kumari, Babak Seradjeh, and Arijit Kundu, arXiv:2301.07707v1 (2023).

Competing topological phases in a non-Hermitian time-reversal symmetry-broken Bernevig-Hughes-Zhang model

Srijata Lahiri, Dipendu Halder and Saurabh Basu

Department of Physics, Indian Institute of Technology Guwahati, Guwahati-781039, Assam, India

The Bernevig-Hughes-Zhang (BHZ) model is one of the most celebrated examples of a quantum spin Hall (QSH) insulator exhibiting helical edge states characterized by a Z_2 invariant. The Z_2 topology is primarily protected by the presence of time reversal symmetry (TRS) in the system which is responsible for the robustness of the helical states. In the presence of an in-plane magnetic field, which breaks TRS, these first-order helical states gap out to be replaced by second-order corner states under suitable open-boundary conditions. Here, we show that the inclusion of a spin-dependent non-Hermitian balanced gain/loss potential, in addition to the in-plane magnetic field, induces a competition between the first and second-order topological phases. We observe that the first-order helical edge states that were gapped out in a nanoribbon geometry, resurface as the non-Hermitian effect intensifies, effectively neutralizing the role played by the magnetic field. By employing the projected spin spectra and the spin Chern number, we conclusively explain the resurgence of the first-order topological properties in the time-reversal symmetry-broken BHZ model in presence of non-Hermiticity. Finally, the biorthogonal spin-resolved Berry phase, exhibiting a non-trivial winding, definitively establishes the topological nature of these revived edge states, emphasizing the triumph of non-Hermiticity over the magnetic field.

Spin-orbit splitting and piezoelectric properties of Janus Ge_2XY (X and $Y = \text{P, As, Sb and Bi}$)

Hui-Ying Liu,¹ Yue-Yi Wang,¹ Ze-Yan Chen,² Ting-Ping Hou,^{1,2} Kai-Ming Wu^{1,2} and Heng-Fu Lin^{1,2}

¹ Hubei Province Key Laboratory of Systems Science in Metallurgical Process, and College of Science, Wuhan University of Science and Technology, Wuhan 430081, China

² The State Key Laboratory for Refractory Material and Metallurgy, International Research Institute for Steel Technology, and Collaborative Center on Advanced Steels, Wuhan University of Science and Technology, Wuhan 430081, China

The coexistence of spin-orbit coupling and piezoelectricity in a single material may have potential application in multifunctional devices, including spintronics, nanorobotics and piezotronics. Spin-orbit coupling provides a new mean to manipulate electron's spin without additional external magnetic field, while the piezoelectricity is referred to the interplay between mechanical stresses and electric polarizations. Using first-principles calculations, the structural, electronic, optical, spin, and piezoelectric properties of the Janus Ge_2XY ($X \neq Y = \text{P, As, Sb, and Bi}$) monolayers were systematically investigated. All the Ge_2XY are energetically and dynamically stable in α phase. Under GW level, the Ge_2AsSb , Ge_2AsBi , and Ge_2SbBi have direct fundamental band gaps of 0.65, 0.64, and 0.91 eV. Under GW+BSE level, their optical gaps are 0.42, 0.45, and 0.63 eV, and the optical absorption coefficients can reach about 10^{-5} cm^{-1} in the infrared light region, which reveal that they have the potential application in the infrared photodetectors. For the Ge_2PBi , Ge_2AsBi , and Ge_2SbBi containing heavy Bi element, the lowermost conduction band and uppermost valence band have large spin splitting along the M - K and K - Γ lines, and the bands near the fermi level possess Rashba spin splitting at the Γ point. The Ge_2PBi and Ge_2SbBi have both large in-plane piezoelectric coefficients d_{11} (-0.75 and -3.18 pm/V) and out-of-plane piezoelectric coefficients d_{31} (0.37 and 0.30 pm/V). Our findings are helpful to understand the mechanism of the spin-orbit physics and piezoelectricity on Janus Ge_2XY monolayers and guide experiments in exploring novel multifunctional materials.

[1] Hui-Ying Liu, Yue-Yi Wang, Ze-Yan Chen, Ting-Ping Hou, Kai-Ming Wu and **Heng-Fu Lin**, *Physical Chemistry Chemical Physics*, **25**, 16559 – 16569(2023).

Poster title: Fermi arcs and Landau levels in superconducting topological semimetals

Tianyu Liu^{1,2} and Hai-Zhou Lu^{1,2,3,4}

*¹Shenzhen Institute of Quantum Science and Engineering and Department of Physics,
Southern University of Science and Technology, Shenzhen, 518055, China*

²International Quantum Academy, Shenzhen, 518048, China

*³Quantum Science Center of Guangdong-Hong Kong-Macao Greater Bay Area
(Guangdong), Shenzhen 518045, China*

⁴Shenzhen Key Laboratory of Quantum Science and Engineering, Shenzhen 518055, China

Topological semimetals can acquire superconductivity under pressure or sufficiently low temperature. When the superconducting gaps are opened away from the band crossings, the Dirac nature persists. On the one hand, the Dirac cones can support superconducting Fermi arcs when boundaries are created and may result in superconducting Weyl orbits for exotic transport. On the other hand, the Dirac cones can be broken into superconducting Landau levels by strain, while such a reconciliation of Landau quantization and superconductivity is not achievable through the ordinary magnetic field. These features suggest that superconducting topological semimetals can serve as the playground for new quantum states and transport phenomena.

[1] T. Liu, H.-Z. Lu, unpublished, (2024).

Talk Title: Pseudo Electromagnetic Fields in Dirac Matter

Tianyu Liu^{1,2}, **Zheng Shi**³, and **Hai-Zhou Lu**^{1,2,4,5}

¹*Shenzhen Institute of Quantum Science and Engineering and Department of Physics, Southern University of Science and Technology, Shenzhen, 518055, China*

²*International Quantum Academy, Shenzhen, 518048, China*

³*Institute for Quantum Computing and Department of Physics and Astronomy, University of Waterloo, Waterloo, Ontario, N2L 3G1, Canada*

⁴*Quantum Science Center of Guangdong-Hong Kong-Macao Greater Bay Area (Guangdong), Shenzhen 518045, China*

⁵*Shenzhen Key Laboratory of Quantum Science and Engineering, Shenzhen 518055, China*

Dirac matter encodes both relativistic and quantum mechanical effects and its remarkable response to elastic strain in the form of pseudo electromagnetic fields has attracted great attentions from the physics community. In this talk, I will systematically discuss pseudo electromagnetic fields in various Dirac materials. In semimetals (e.g., graphene, Dirac/Weyl semimetals, and kagome metals), static (dynamic) strain can induce a pseudo magnetic (electric) field, giving rise to quantum oscillations and chiral anomaly in the complete absence of applied electromagnetic fields. In Dirac magnets, pseudo electromagnetic fields are also induced but exhibit an exotic duality to their counterparts in semimetals. The non-conservation of magnons further gives rise to new types of quantum anomalies. In Dirac superconductors, strain also causes Landau quantization, which cannot be produced by magnetic fields because of the Meissner effect. The strain-induced pseudo electromagnetic fields serve as extra tuning knobs of Dirac matter and should be beneficial for the quantum devices based on straintronics.

[1] [T. Liu](#), D. I. Pikulin, and M. Franz, Phys. Rev. B **95**, 041201(R) (2017).

[2] [T. Liu](#), M. Franz, and S. Fujimoto, Phys. Rev. B **96**, 224518 (2017).

[3] T. Matsushita, [T. Liu](#), T. Mizushima, and S. Fujimoto, Phys. Rev. B **97**, 134519 (2018).

[4] [T. Liu](#) and Z. Shi, Phys. Rev. B **99**, 214413 (2019).

[5] [T. Liu](#), Phys. Rev. B **102**, 045151 (2020).

[6] [T. Liu](#) and Z. Shi, Phys. Rev. B **103**, 144420 (2021).

[7] Z. Shi, H.-Z. Lu, and [T. Liu](#), Phys. Rev. Research **3**, 033139 (2021).

[8] [T. Liu](#) and H.-Z. Lu, Phys. Rev. Research **4**, 023137 (2022).

[9] J. Sun, [T. Liu](#), Y. Du, and H. Guo, Phys. Rev. B **106**, 155417 (2022).

[10] J. Sun, X. Zhu, [T. Liu](#)^{*}, S. Feng, and H. Guo[†], Phys. Rev. B **108**, 205149 (2022).

Dynamics of the molecular geometric phase

R. Martinazzo¹, Irene Burghardt²

¹*Department of Chemistry, Università degli Studi di Milano, Via Golgi 19, 20133 Milano, Italy*

²*Institute of Physical and Theoretical Chemistry, Goethe University Frankfurt, Max-von-Laue-Straße 7, D-60438 Frankfurt/Main, Germany*

This work explores the molecular geometric phase within an exact dynamical framework, using the exact factorization of the $e - n$ wavefunction [1] combined with a recent quantum hydrodynamical description of its dynamics [2]. This approach introduces instantaneous, gauge-invariant phases, $\Gamma_{el}[\gamma]$ and $\Gamma_n[\gamma]$, for electrons and nuclei respectively, applicable to arbitrary nuclear configuration paths.

For closed paths, these phases are opposite to each other, with $\Gamma_{el}[\gamma]$ extending the conventional adiabatic geometric phase, which it reduces to under adiabatic conditions. The evolution of this closed-path phase over time adheres to a Maxwell-Faraday-like induction law, where non-conservative forces arising from electron dynamics play the role of effective electromotive forces. Among these, pseudo-electric forces are the most significant in driving phase changes when the dynamics is quasi-adiabatic [3].

For open paths, $\Gamma_{el}[\gamma]$ and $\Gamma_n[\gamma]$ contribute separately to the phase difference of the total $e - n$ wavefunction, and represent useful tools to track the phase evolution between different portions of the total wave function. We show this by analyzing the dynamics of a wavepacket that encircles a conical intersection between adiabatic surfaces, monitoring its phase along the path and examining the transition to a closed-path limit [4].

Overall, this work presents a time-dependent view of the molecular geometric phase, illustrating its emergence from an exact dynamical framework and its impact on electron-nuclear dynamics.

- [1] A. Abedi, N. T. Maitra, and E. K. U. Gross, *Exact Factorization of the Time-Dependent Electron-Nuclear Wave Function*, Phys. Rev. Lett. **105**, 123002 (2010).
- [2] R. Martinazzo and I. Burghardt, *Quantum Hydrodynamics of Coupled Electron-Nuclear Systems*, arXiv:2310.08766 (2023).
- [3] R. Martinazzo, and I. Burghardt, *Dynamics of the molecular geometric phase*, Phys. Rev. Lett. **132**, 243002 (2024).
- [4] R. Martinazzo, and I. Burghardt, *Emergence of the molecular geometric phase from exact electron-nuclear dynamics*, J. Phys. Chem. Lett. **15**, 10416 (2024).

Giant chirality-induced spin polarization in twisted transition metal dichalcogenides

Guido Menichetti¹, Lorenzo Cavicchi², Leonardo Lucchesi^{1,3}, Fabio Taddei^{4,2}, Giuseppe Iannaccone³, Pablo Jarillo-Herrero⁵, Claudia Felser⁶, Frank H. L. Koppens^{7,8}, and Marco Polini^{1,7}

¹*Dipartimento di Fisica dell'Università di Pisa, Largo Bruno Pontecorvo 3, I-56127 Pisa, Italy*

²*Scuola Normale Superiore, Piazza dei Cavalieri 7, I-56126 Pisa, Italy*

³*Dipartimento di Ingegneria dell'Informazione dell'Università di Pisa, Via Girolamo Caruso 16, I-56122 Pisa, Italy*

⁴*NEST, Istituto Nanoscienze-CNR, Piazza S. Silvestro 12, I-56126 Pisa, Italy*

⁵*Department of Physics, Massachusetts Institute of Technology, Cambridge, Massachusetts, USA*

⁶*Max Planck Institute for Chemical Physics of Solids, Nöthnitzer Str. 40, Dresden 01187, Germany*

⁷*ICFO-Institut de Ciències Fotòniques, The Barcelona Institute of Science and Technology, Av. Carl Friedrich Gauss 3, 08860 Castelldefels (Barcelona), Spain*

⁸*ICREA-Institució Catalana de Recerca i Estudis Avançats, Passeig de Lluís Companys 23, 08010 Barcelona, Spain*

In 1999, under the leadership of R. Naaman, a team made a significant observation: films composed of chiral organic molecules exhibit an asymmetrical scattering of polarized electrons [1]. This phenomenon, now widely known as the chirality-induced spin selectivity (CISS) effect, has garnered considerable attention in the field of chiral chemistry, yet much of its intricacies remain to be fully grasped [2]. Essentially, the CISS effect entails electrons passing through chiral molecules gaining a notable degree of spin polarization. In this study, we explore the behavior of atomically-thin chiral crystals formed by twisting van der Waals heterostructures. In this work, we demonstrate that this effect can be remarkably pronounced even in systems comprising just two monolayers, particularly those with spin-orbit coupling. Its emergence is attributed to the interplay between structural chirality and spin-flipping spin-orbit coupling. Through calculations involving twisted homobilayer transition metal dichalcogenides [3-6], we illustrate that the chirality-induced spin polarization can reach staggering proportions, exceeding 50% for materials like MoTe₂. Additionally, we introduce a theoretical framework for this phenomenon based on the microscopic Hamiltonian of twisted homobilayer transition metal dichalcogenides and a spin-resolved scattering matrix approach [7,8]. Our findings suggest that twisted quantum materials offer a versatile platform for investigating and manipulating the CISS effect in both condensed matter physics and chiral chemistry [9].

[1] K. Ray, S. P. Ananthavel, D. H. Waldeck, and R. Naaman, *Science* **283**, 814(1999).

[2] S. H. Yang, R. Naaman, Y. Paltiel, and S. S P. Parkin, *Nat. Rev. Phys.* **3**, 328 (2021).

[3] J. M. Lopes dos Santos, N. M. R. Peres, A. H. Castro Neto, *Phys. Rev. Lett.* **99**, 256802 (2007).

[4] G. T. de Laissardière, D. Mayou, and L. Magaud, *Phys. Rev. B* **86**, 125413 (2012).

- [5] D. Kochan, S. Irmer, and J. Fabian, *Phys. Rev. B* **95**, 165415 (2017).
- [6] F. Wu, T. Lovorn, E. Tutuc, I. Martin, and A. H. MacDonald, *Phys. Rev. Lett.* **122**, 086402 (2019).
- [7] C. W. Groth, M. Wimmer, A. R. Akhmerov, and X. Waintal, *New J. Phys.* **16**, 063065 (2014).
- [8] Y. V. Nazarov and Y. M. Blanter, *Quantum Transport*, (Cambridge University Press, 2012).
- [9] G. Menichetti, L. Cavicchi, L. Lucchesi, F. Taddei, G. Iannaccone, P. Jarillo-Herrero, C. Felser, F. H. L. Koppens, and M. Polini, arXiv:2312.09169.

Topological phase transition in non-Hermitian gauge fields

Bikashkali Midya¹

¹*Indian Institute of Science Education and Research Berhampur, India*

We will describe the point-gap topological phase transitions and skin-effect in non-Hermitian lattice models. These models incorporate site-dependent nonreciprocal hoppings facilitated by a spatially fluctuating complex gauge field that disrupts translational symmetry. We propose an analytical framework that offers a comprehensive method for analytically predicting spectral topological invariance and associated boundary localization phenomena for bond-disordered nonperiodic lattices, based on imaginary gauge-transformed mean-field periodic lattices. Notably, for a lattice with quasiperiodic gauge-field $g_n = \log |\lambda \cos 2\pi\alpha n|$ and an irrational α , a previously unknown topological phase transition is unveiled. It is observed that the topological spectral index W assumes values of $-N$ or $+N$, leading to all N open-boundary eigenstates localizing either at the right or left edge, solely dependent on the strength of the gauge field, where $\lambda < 2$ or $\lambda > 2$. A phase transition is identified at the critical point $\lambda \approx 2$, at which all eigenstates undergo delocalization. The theory has been shown to be relevant for long-range hopping models and for higher dimensions.

[1] [B. Midya](#), Phys. Rev. A 109, L061502 (2024).

[2] Z. Gao, X. Qiao, M. Pan, S. Wu, J. Yim, K. Chen, [B. Midya](#), L. Ge, L. Feng, Phys. Rev. Lett. 130, 263801 (2023).

[3] [B. Midya](#), Physical Review A 106 (5), 053513.

Interaction-induced strong zero modes in short quantum dot chains with time-reversal symmetry

A. Mert Bozkurt¹, Sebastian Miles¹, Sebastiaan L. D. ten Haaf¹, Chun-Xiao Liu¹, Fabian Hassler², Michael Wimmer¹

¹*QuTech and Kavli Institute of Nanoscience, Delft University of Technology, P.O. Box 4056, 2600 GA Delft, The Netherlands*

²*Institute for Quantum Information, RWTH Aachen University, 52056 Aachen, Germany*

We theoretically explore the emergence of strong zero modes [1] in a two-site chain consisting of two quantum dots coupled due to a central dot that mediates electron hopping and singlet superconducting pairing. In the presence of time-reversal symmetry, the on-site Coulomb interaction leads to a three-fold ground-state degeneracy when tuning the system to a sweet spot as a function of the inter-dot couplings. This degeneracy is protected against changes of the dot energies in the same way as “poor man’s” Majorana bound states [2] in short Kitaev chains [3]. In the limit of strong interactions, this protection is maximal and the entire spectrum becomes triply degenerate, indicating the emergence of a “poor man’s” version of a strong zero mode. We explain the degeneracy and protection by constructing corresponding Majorana Kramers-pair operators and Z_3 -parafermion operators. The strong zero modes share many properties of Majorana bound states in short Kitaev chains, including the stability of zero-bias peaks in the conductance and the behavior upon coupling to an additional quantum dot. However, they can be distinguished through finite-bias spectroscopy and they exhibit a different behavior when scaling to longer chains.

- [1] J. Alicea and P. Fendley, Topological phases with parafermions: Theory and blueprints, *Annu. Rev. Condens. Matter Phys.* 7(1), 119 (2016).
- [2] M. Leijnse and K. Flensberg, Parity qubits and poor man’s Majorana bound states in double quantum dots, *Phys. Rev. B* 86(13), 134528 (2012).
- [3] A Yu Kitaev, Unpaired Majorana fermions in quantum wires, *Physics-uspekhi* 44, 131 (2001).

\mathbb{Z}_2 Topological Order in Strongly Correlated Systems

Fatemeh Mohammadi¹, Mojtaba Tabatabaei², Mehdi Kargarian¹ and Abolhassan Vaezi¹

¹*Department of Physics, Sharif University of Technology, Tehran 14588-89694, Iran*

²*Department of Physics, Kharazmi University, Tehran 1571914911, Iran*

Topology, symmetry, electron correlations, and the interplay between them have formed the cornerstone of our understanding of quantum materials in recent years and are used to identify new emerging phases. In this work, we investigate \mathbb{Z}_2 topological order within two model systems that showcase the role of electron correlations: the superconducting Kondo lattice model and the Kitaev-Hubbard model. These models provide a fertile ground for merging topology and strong correlations where topologically ordered phases arise. First, we study a superconducting Kondo lattice model, a network of 1D Kitaev superconductors Kondo coupled to a lattice of magnetic moments [1]. Using slave-particle representation of spins and exact numerical calculations, we obtain the phase diagram of the model in terms of Kondo coupling J_K and identify an invertible topological phase for $J_K > J_K^c$. Decreasing J_K leads to a Mott insulating transition into a stable topological order phase for $J_K < J_K^c$, where J_K^c is the critical point.

This construction provides a framework to realize various topological orders. By utilizing accessible ingredients, we show that \mathbb{Z}_2 topological order and also $\mathbb{Z}_2 \times \mathbb{Z}_2$ topological order, with enhanced computational capabilities [2], can be engineered in architecture patterns of semiconductor nanowires hosting Majorana bound states [3]. The basic blocks of these patterns are the time-reversal Majorana Cooper boxes [4, 5] coupled to each other by metallic leads, and the Majorana states are allowed to tunnel to quantum dots sitting on the vertices of the lattices. In the limit of strong onsite Coulomb interactions, the magnetic moments of dots on the square and honeycomb lattices are described by topologically ordered spin models.

Additionally, we investigate electron correlations in the Kitaev-Hubbard (KHu) model [6] and demonstrate how these interactions lead to the emergence of \mathbb{Z}_2 topological order. Recent experiments show that the ground state of some layered materials with localized moments is in close proximity to the Kitaev spin liquid, calling for a proper model to describe the measurements. The KHu model is the minimal model that captures the essential ingredients of these systems; it yields the Kitaev-Heisenberg spin model at strong coupling limit and contains the charge fluctuations present in these materials as well. Despite its relevance, the phase diagram of the KHu model has not been rigorously revealed yet. In this work, we study the full phase diagram of the KHu model using the \mathbb{Z}_2 slave-spin mean-field theory [7] as well as the auxiliary field quantum Monte Carlo (QMC) on rather large systems and at low temperatures. The Mott transition is signaled by a vanishing quasiparticle weight evaluated using the slave-spin construction. Moreover, we show using both QMC and slave-spin approaches that there are multiple magnetic phase transitions within the Mott phase including magnetically ordered phases and most notably a \mathbb{Z}_2 spin liquid phase for $1.0 \lesssim t'/t \lesssim 1.11$ at $U/t = 5$ consistent with recent studies of the KHu model [8].

[1] T. H. Hsieh, Y.-M. Lu, and A. W. W. Ludwig, *Science Advances* **3**, 10 (2017).

[2] H. Bombin and M. A. Martin-Delgado, *Phys. Rev. Lett.* **97**, 180501 (2006).

[3] R. M. Lutchyn, J. D. Sau, and S. Das Sarma, *Phys. Rev. Lett.* **105**, 077001 (2010).

[4] X.-L. Qi, T. L. Hughes, S. Raghu, and S.-C. Zhang, *Phys. Rev. Lett.* **102**, 187001 (2009).

[5] B. Beri and N. R. Cooper, *Phys. Rev. Lett.* **109**, 156803 (2012).

[6] L.-M. Duan, E. Demler, and M. D. Lukin, *Phys. Rev. Lett.* **91**, 090402 (2003).

[7] S. D. Huber and A. Rugg, *Phys. Rev. Lett.* **102**, 065301 (2009).

[8] S. Dong, H. Zhang, C. Wang, M. Zhang, Y.-J. Han, and L. He, *Chin. Phys. Lett.* **40**, 126403 (2023).

Superconducting Diode Effect in Josephson Junction with Zeeman Field and Rashba Spin-Orbit Coupling

Sayan Mondal¹, Pei-Hao Fu², and Jorge Cayao¹

¹ *Department of Physics and Astronomy, Uppsala University, Box 516, S-751 20 Uppsala, Sweden*

² *Science, Mathematics and Technology, Singapore University of Technology and Design, Singapore 487372, Singapore*

A semiconducting nanowire with Rashba spin-orbit coupling, when coupled to a superconductor, offers a promising platform for observing the superconducting diode effect, when a Zeeman field is applied at specific range of angles to the spin-orbit axis. Such systems are promising candidates for exploring Majorana physics. In this work, we investigate the evolution of the Josephson diode effect as the system transitions from a trivial to a topological phase [1]. The component of the Zeeman field parallel to the spin-orbit axis introduces asymmetry in the Andreev bound states, which in turn leads to an asymmetry in the Josephson current, giving rise to the diode effect. In this study, we analyze the forward and backward currents, which differ due to the presence of the parallel Zeeman field. We discover that the diode's efficiency as a function of the Zeeman field exhibits a rich structure strongly dependent on the Andreev bound states. This dependence reveals clear signatures at the topological phase transition. Notably, in the topological phase, the diode efficiency develops an oscillatory pattern that reflect the formation of Majorana bound states. We have also verified that the functionality of the obtained Josephson diode is robust against finite temperatures, below the superconducting gap. Our findings help understanding the realization of Josephson diodes in topological superconductors and can be also useful for identifying the emergence of Majorana bound states.

[1] : S. Mondal, P. -H. Fu, and J. Cayao, In preparation.

Heat-charge separation in a hybrid superconducting quantum Hall setup (Poster)

C.Panu^{1,2}, **F. Taddei**³, **M. Polini**^{1,4} and **Amir Yacoby**⁵

¹ *Institute of Condensed Matter Theory and Solid State Optics, Friedrich-Schiller-Universität Jena, Max-Wien-Platz 1, 07743 Jena, Germany*

² *Dipartimento di Fisica dell'Università di Pisa, Largo Bruno Pontecorvo 3, I-56127 Pisa, Italy*

³ *NEST, Istituto Nanoscienze-CNR and Scuola Normale Superiore, I-56126 Pisa, Italy*

⁴ *ICFO-Institut de Ciències Fotòniques, The Barcelona Institute of Science and Technology, Av. Carl Friedrich Gauss 3, 08860 Castelldefels (Barcelona), Spain*

⁵ *Department of Physics, Harvard University, Cambridge, Massachusetts 02138, USA*

Separating heat from charge in a material is an extremely challenging task since they are transported by the very same carriers, i.e. electrons or holes. In Ref. [1] we show that such separation can reach 100% efficiency in a hybrid superconducting quantum Hall setup, provided that the quantum Hall system is tuned to integer filling factor. We present microscopic calculations for a three-terminal setup to illustrate our idea.

[1] C. Panu, F. Taddei, M. Polini, and A. Yacoby, arXiv preprint arXiv:2402.19198 (2024).

Spin- and orbital-charge conversion at the surface states of Bi_{1-x}Sb_x Topological insulators

Armando Pezo^a, Jean-Marie George^a, Henri Jaffres^a

^a Laboratoire Albert Fert, universit  Paris-Saclay 1 Avenue Augustin Fresnel, 91767 Palaiseau Cedex, France

Topological insulators are quantum materials characterized by Time-reversal protected surface states (TSS) which make them appealing candidates for the design of next generation of highly efficient spintronic devices. The very recent demonstration of large transient spin-charge conversion (SCC) and subsequent powerful THz emission from Co|Bi_{1-x}Sb_x bilayers clearly demonstrate such potentiality and feasibility for the near future [1-3]. Amongst the exotic properties appearing in and at the surface of such quantum materials, spin-momentum locking (SML) remains as a key ingredient to effectively convert the spin degree of freedom into a charge or a voltage signal. In that sense, in this work we will provide some clear theoretical and numerical insights implemented by multi-orbital and multi-layered tight-binding methods (TB). These developments clarify our recent experimental results obtained by THz-TDS spectroscopy techniques in the time domain [2]; and allows us to disentangle the various magnetic SCC contributions. Taking advantage of their spin-momentum locking property, we also postulate the occurrence of Orbital-to-charge conversion (OCC) taking place also in these aforementioned experiments at equal footing to SCC.

By extending the spin-to-charge conversion theory, we postulate the emergence of its orbital counterpart, namely the Orbital-charge conversion (OCC), covering different contributions in terms of the orbital degree of freedom. Our results unveil the interest and prospects for the use of specific materials as source of both spin and orbital current (as Ni); and we may anticipate the advantage of using lighter elements with the restricting requirement of large SOC would be avoided in the latter case.

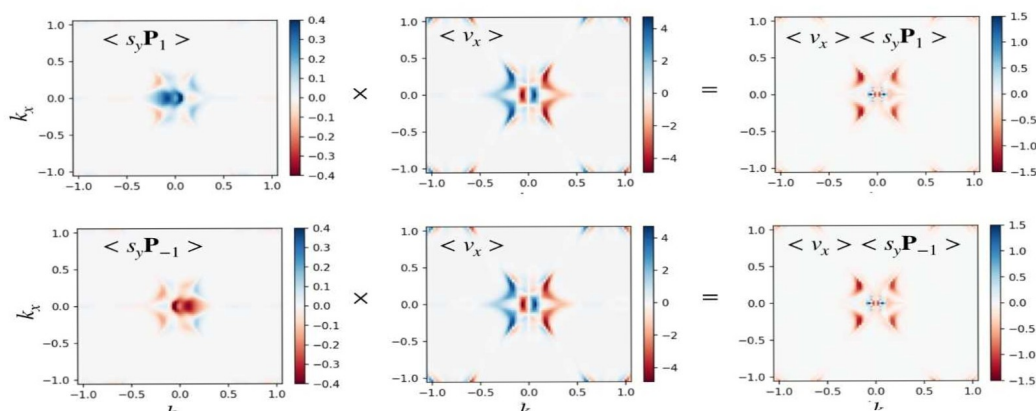


Fig. 1. Velocity and Fermi surface projection of the Orbital operator showing the distribution over the Brillouin zone.

- [1] H. Park et al., , Topological Surface-Dominated Spintronic THz Emission in Topologically Nontrivial Bi_{1-x}Sb_x Films. *Adv. Sci.* 2022, 9, 2200948
- [2] E. Rongione et al., Spin-Momentum Locking and Ultrafast Spin-Charge Conversion in Ultrathin Epitaxial Bi_{1-x}Sb_x Topological Insulator. *Adv. Sci.* 2023, 10, 2301124.
- [3] S. Rho et al., Exceptional Spin-to-Charge Conversion in Selective Band Topology of Bi/Bi_{1-x}Sb_x with Spintronic Singularity. *Adv. Funct. Mater.*, 33: 2300175.
- [4] A. Pezo, J. M. George, H. Jaffres, Theory of spin and orbital charge conversion at the surface states of Bi_{1-x}Sb_x topological insulator.

Insulating and metallic phases in the 1D Hubbard-Su-Schrieffer-Heeger model: Insights from a backflow-inspired variational wave function

Davide Piccioni¹, Francesco Ferrari², Michele Fabrizio¹, Federico Becca³

¹*Scuola Internazionale Superiore di Studi Avanzati (SISSA), Via Bonomea 265, Trieste, Italy*

²*Institute for Theoretical Physics, Goethe University, Frankfurt, Germany*

³*Dipartimento di Fisica, Università di Trieste, Strada Costiera 11, Trieste, Italy*

The Su–Schrieffer–Heeger model[1] was introduced to describe how electrons deal with lattice distortions; by modeling phonons as quantum harmonic oscillators located on each lattice site and considering electron hopping modulated by the phonon displacements, interesting physics can appear. Specifically, for interacting electrons at half-filling, there is a competition between the Peierls insulator (with finite lattice distortion) and an undistorted Mott insulating phase. The behavior of such a system in the doped regime is still an open problem.

We introduce a new variational wave function[2] for electron-phonon systems. The fermionic part of the variational state depends on the phonon configuration in a backflow-inspired way, thus going beyond simple Jastrow-Slater approaches. We show that this wave function can capture correctly the physical properties of the system at half-filling, showing a transition between Peierls and Mott insulators. In this respect, we also benchmark our results against density matrix renormalization group calculations. Furthermore, studying the hole-doped regime, we report the presence of a conventional Luttinger liquid (gapless in all excitation channels) upon doping the Mott insulating phase; instead, when lightly doping the Peierls insulator, we observe that the resulting metallic phase retains a finite spin gap (Luther Emery liquid[3]).

[1] W. P. Su, J. R. Schrieffer, and A. J. Heeger, *Phys. Rev. Lett.* **42**, 1698 (1979).

[2] M. Capello, F. Becca, M. Fabrizio, S. Sorella, E. Tosatti, *Phys. Rev. Lett.* **94**, 026406 (2005).

[3] A. Luther and V. J. Emery, *Phys. Rev. Lett.* **33**, 589 (1974).

Signatures of topological phase transition on a quantum critical line

Ranjith R Kumar¹, Nilanjan Roy², Y. R. Kartik¹, S. Rahul¹ and Sujit Sarkar¹

¹*Theoretical Sciences Division, Poornaprajna Institute of Scientific Research, Bidalur, Bengaluru-562164, India.*

²*Centre for Condensed Matter Theory, Department of Physics, Indian Institute of Science, Bengaluru-560012, India.*

Recently topological states of matter have witnessed a new physical phenomenon where both edge modes and gapless bulk coexist at topological quantum criticality [1-3]. The presence and absence of edge modes on a critical line can lead to an unusual class of topological phase transition between the topological and non-topological critical phases [4,5]. We explore the existence of this new class of topological phase transitions in a generic model representing the topological insulators and superconductors and we show that such transition occurs at a multicritical point, i.e., at the intersection of two critical lines. To characterize these transitions we reconstruct the theoretical frameworks, which include bound state solution of the Dirac equation, winding number, correlation factors, and scaling theory of the curvature function to work for the criticality. Critical exponents and scaling laws are discussed to distinguish between the multicritical points, which separate the critical phases. Entanglement entropy and its scaling in the real space provide further insights into the unique transition at criticality revealing the interplay between fixed point and critical point at the multicriticalities.

[1] R. Verresen, N. G. Jones, and F. Pollmann, Phys. Rev. Lett. **120**, 057001 (2018).

[2] R. Verresen, R. Thorngren, N. G. Jones, and F. Pollmann, Phys. Rev. X. **11**, 041059 (2021).

[3] R. R. Kumar, Y. R. Kartik, S. Rahul, and S. Sarkar, Sci. Rep. **11**, 1 (2021).

[4] R. R. Kumar, Nilanjan Roy, Y. R. Kartik, S. Rahul and Sujit Sarkar, Phys. Rev. B, **107**, 205114 (2023).

[5] R. R. Kumar, Y. R. Kartik and Sujit Sarkar, New. J. Phys. **25**, 083027 (2023).

Non-Abelian fractionalization in topological minibands

Aidan P. Reddy

Department of Physics, Massachusetts Institute of Technology

Motivated by the recent discovery of fractional quantum anomalous Hall states in moiré systems, we consider the possibility of realizing non-Abelian phases in topological minibands. We study a family of moiré systems, skyrmion Chern band (SCB) models, which can be realized in two-dimensional semiconductor/magnetic skyrmion heterostructures and also capture the essence of twisted transition metal dichalcogenide (TMD) homobilayers. We show using many-body exact diagonalization that, in spite of strong Berry curvature variations in momentum space, the non-Abelian Moore-Read state can be realized at half filling of the second miniband. These results demonstrate the feasibility of non-Abelian fractionalization in moiré systems without Landau levels and shed light on the desirable conditions for their realization. In particular, we highlight the prospect of realizing the Moore-Read state in twisted semiconductor bilayers.

[1] Reddy, A. P., Paul, N., Abouelkomsan, A., & Fu, L. (2024). Non-Abelian fractionalization in topological minibands. *Physical Review Letters*, *in press*.

Emerging Spintronic and Valleytronic Phenomena in Non-Centrosymmetric Variants of the Kane-Mele $X_4Y_2Z_6$ Materials Family ($X=\text{Pt, Pd, Ni}$; $Y=\text{Hg, Zn, Cd}$; $Z=\text{S, Se, Te}$)

Majeed Ur Rehman¹, Zia Ur Rahman,² and Maryam Kiani²

¹ *Songshan Lake Materials Laboratory, Dongguan, Guangdong 523808, China*

² *College of Physics and Optoelectronic Engineering, Shenzhen University, Shenzhen, Guangdong 518060, China*

The Kane-Mele model's implementation in Xene solids is limited by weak spin-orbit coupling (SOC). However, the recently discovered $X_4Y_2Z_6$ family ($X=(\text{Pt, Pd, Ni})$, $Y=(\text{Hg, Zn, Cd})$, and $Z=(\text{S, Se, Te})$), known as the Jantiguaite family, presents a promising alternative with enhanced SOC. Yet, the centrosymmetric nature of this family restricts the realization of certain spintronics and valleytronics phenomena. This presentation will explore various methods to break centrosymmetry in this family. We will also discuss a newly explored, non-centrosymmetric version of the Kane-Mele family, [$X_4YY'Z_6$ and $X_4YY'(ZZ')_3$], consisting of over 16 experimentally accessible members. These materials exhibit intertwined phenomena involving topology, spin, and valley degrees of freedom, including the quantum valley/spin Hall effect, spin-valley locking, and spin-valley selective optical transitions. Notably, Rashba coupling coexists with Ising spin splitting, enabling valley spin valve functionality and out-of-plane spontaneous electric polarization. Quantum valley Hall kink states are achievable on domain walls between these non-centrosymmetric monolayers due to opposite spin-valley Berry curvatures. Additionally, external factors like electric fields and strain can induce various topological phase transitions. This study provides a foundational framework for exploring spin-valley physics in low-dimensional topological materials with non-centrosymmetry, paving the way for advancements in quantum devices.

Generic control of measurement induced topological phase transitions

Ritu Nehra

Department of Physics, Ben Gurion University of the Negev, Beer-Sheva 84105, Israel

Abstract

The dynamics of entanglement under measurement in many-body quantum systems is a topic under intensive study recently. Unitary dynamics typically lead to thermalization due to high entanglement, while continuous monitoring destroys entanglement. These competing dynamics drive intriguing phase transitions in quantum systems, analyzed through entanglement entropy scaling. The experimental probing of these measurements is independent of environmental feedback, which restricts its applicability to a few open systems. In recent work, the measuring device is modeled as a continuous Gaussian probe to capture a large class of environments. It modifies the detector state and uses it as feedback to the systems. I will discuss the role of the feedback control measurements in the context of topological phase transitions of the free Fermionic chains.

Reference-

Ritu Nehra, Alessandro Romito and Dagnit Meidan, arXiv:2404.07918v2 (2404)

First-principles study of photocurrents in non-centrosymmetric magnetic Weyl semimetal CeAlSi

Abhirup Roy Karmakar^{1,2}, A. Taraphder², and G. P. Das³

¹*Dipartimento di Chimica, Università degli Studi di Milano, MI 20133, Italy*

²*Department of Physics, Indian Institute of Technology Kharagpur, WB 721302, India*

³*Research Institute for Sustainable Energy (RISE), TCG Centres for Research and Education in Science and Technology, Salt Lake, WB 700091, India*

The recent identification of the Weyl semimetal CeAlSi¹, which exhibits simultaneous breaking of inversion and time-reversal symmetries, has paved the way for exciting new research into the interplay between light and topologically protected bands. In this study, we conduct a comprehensive analysis of both the shift current and injection current that contribute to the photocurrents in CeAlSi, utilizing advanced first-principles calculations. Our findings reveal a notably high injection current² of approximately 4 mA/V² across a wide range in the near-infrared spectrum, significantly surpassing earlier reports in this field.

In addition to characterizing the photocurrent, we systematically explored various externally adjustable parameters that could further enhance its magnitude². Among these, we found that applying uniaxial strain along the c-axis of the crystal leads to a substantial increase in injection current; specifically, a 5% uniaxial strain results in an impressive 64% boost in performance. This enhancement underscores the tunability of the photocurrent response in CeAlSi.

The exceptional photocurrent response observed in CeAlSi not only highlights its unique electronic properties but also suggests that magnetic non-centrosymmetric Weyl semimetals may provide considerable opportunities for innovative photogalvanic applications. These findings could have significant implications for future research and development in optoelectronic devices, positioning CeAlSi as a promising candidate for harnessing light-matter interactions in advanced technological applications.

[1] Guoqing Chang, Bahadur Singh *et al.*, Phys. Rev. B **97**, 041104(R) (2018).

[2] Abhirup Roy Karmakar, A. Taraphder, G. P. Das, arXiv:2308.00045 (2023).

Dualities of Paired Quantum Hall Bilayer States at $\nu_T = \frac{1}{2} + \frac{1}{2}$

Luca Rüegg¹, Gaurav Chaudhary¹, and Robert-Jan Slager¹

¹*TCM Group, Cavendish Laboratory, University of Cambridge, J. J. Thomson Avenue, Cambridge CB3 0HE, United Kingdom*

Density-balanced, widely separated quantum Hall bilayers at $\nu_T = 1$ can be described as two copies of composite Fermi liquids (CFLs). The two CFLs have interlayer weak-coupling BCS instabilities mediated by gauge fluctuations, the resulting pairing symmetry of which depends on the CFL hypothesis used. If both layers are described by the conventional Halperin-Lee-Read (HLR) theory-based composite electron liquid (CEL) [1], the dominant pairing instability is in the $p + ip$ channel [2, 3]; whereas if one layer is described by CEL and the other by a composite hole liquid (CHL, in the sense of anti-HLR) [4], the dominant pairing instability occurs in the s -wave channel [5]. Using the Dirac composite fermion (CF) picture [6], we show that these two pairing channels can be mapped onto each other by particle-hole (PH) transformation. Furthermore, we derive the CHL theory as the non-relativistic limit of the PH-transformed massive Dirac CF theory. Finally, we prove that an effective topological field theory for the paired CEL-CHL in the weak-coupling limit is equivalent to the exciton condensate phase in the strong-coupling limit.

- [1] B. I. Halperin, P. A. Lee, and N. Read, *Phys. Rev. B* **47**, 7312 (1993).
- [2] N. E. Bonesteel, I. A. McDonald, C. Nayak, *Phys. Rev. Lett.* **77**, 3009 (1996).
- [3] H. Isobe, L. Fu, *Phys. Rev. Lett.* **118**, 166401 (2017).
- [4] M. Barkeshli, M. Mulligan, and M. P. A. Fisher, *Phys. Rev. B* **92**, 165125 (2015).
- [5] L. Rüegg, G. Chaudhary, R.-J. Slager, *Phys. Rev. Research* **5**, L042022 (2023).
- [6] D. T. Son, *Phys. Rev. X* **5**, 031027 (2015).

Abstract for “Conference on Advances in Topological Condensed Matter”

Martina Minutillo¹, Procolo Lucignano¹, Gabriele Campagnano², and
Angelo Russomanno^{3, 1}

¹ *Dipartimento di Fisica “E. Pancini”, Università di Napoli Federico II, Complesso di Monte S. Angelo, via Cinthia, I-80126 Napoli, Italy*

² *CNR-SPIN, c/o Complesso di Monte S. Angelo, via Cinthia, I-80126 Napoli, Italy*

³ *Scuola Superiore Meridionale, Università di Napoli Federico II, Largo San Marcellino 10, I-80138 Napoli, Italy*

We study a superconducting Kitaev ring pierced by a magnetic flux, with and without disorder, in a quantum ring configuration, and in a rf-SQUID one, where a weak link is present. In the rf-SQUID configuration, in the topological phase, the supercurrent shows jumps at specific values of the flux $\Phi^* = \frac{hc}{e}(1/4 + n)$, with $n \in \mathbb{N}$. In the thermodynamic limit Φ^* are constant inside the topological phase, independently of disorder, and we analytically predict this fact using a perturbative approach in the weak-link coupling. The weak link breaks the topological ground-state degeneracy, and opens a spectral gap for $\Phi \neq \Phi^*$, that vanishes at Φ^* with a cusp providing the current jump. Looking at the quasiparticle excitations, we see that they are Anderson localized, so they cannot carry a resistive contribution to the current, and the localization length shows a peculiar behavior at a flat-band point for the quasiparticles. In the absence of disorder, we analytically and numerically find that the chemical-potential derivative of the supercurrent logarithmically diverges at the topological-to-trivial transition, in agreement with the transition being of the second order. These findings are reported in [1]

- [1] Martina Minutillo, Procolo Lucignano, Gabriele Campagnano, and Angelo Russomanno, *Physical Review B* **109**, 064504 (2024).

Transverse chirality current in the magnetic Weyl semimetal/ superconductor junction

Morteza Salehi¹

¹*Physics department, Faculty of Basic Science, Bu-Ali Sina University, Hamadan, Iran.*

In this work, we theoretically investigate the Andreev reflection in a junction comprising magnetic Weyl semimetal and superconductors. We show that in the presence of magnetization, Dirac semimetals convert to the magnetic Weyl, and the separation between Weyl nodes depends on the magnitude of magnetization. This conversion from Dirac to Weyl fermions has important implications for the electronic properties and transport phenomena in these materials.

Our findings reveal that the Andreev reflection, which is a crucial process in superconductor-based devices, depends on the incident angle of the incoming fermion. This angle-dependent Andreev reflection is a direct consequence of the unique electronic structure of the magnetic Weyl semimetal. Interestingly, we also discover that due to the reverse action between different nodes with different chirality, a transverse chirality current flows parallel to the interface if the magnetization has a component parallel to the junction's interface. This transverse chirality current has the potential to be utilized in spintronic and chirotronics applications.

The theoretical insights provided in this work advance our understanding of the interplay between magnetism, topology, and superconductivity in Weyl semimetals. These findings pave the way for the design and development of novel superconducting devices and spintronic technologies based on magnetic Weyl semimetals.

[1] Morteza Salehi, *Physica Scripta* **98**, 025822 (2023).

[2] Razieh Beiranvand and Morteza Salehi, *J. Phys. Cond. Matt.* **33**, 32541 (2021).

Topological characterization of monolayer jacutingaite

Abstract:

Monolayer jacutingaite (Pt_2HSe_3) has been predicted to be the first large-gap Kane-Mele quantum spin Hall insulator. Materials in the jacutingaite family undergo topological phase transitions (TPTs), *i.e.*, from a topologically non-trivial to a semimetallic phase and further to the normal insulating phase when exposed to electric fields and off-resonance, high-frequency and high-intensity laser irradiation. In this article, we investigate the rich tapestry of topological phases in this unique material in the presence of an appropriate choice of off-resonance circularly polarized laser fields and staggered sublattice potentials. The interplay of these stimuli with large spin-orbit coupling, due to the buckled structure of jacutingaite materials, results in the emergence of quantum spin Hall insulator, valley-spin-polarized metal, spin-polarized metal, photo-induced quantum Hall insulator, anomalous quantum Hall insulator and band insulator phases. By analyzing the band structures, we compute Berry curvatures in different topological regimes for the K and K' valleys. Furthermore, by using the Kubo formula, we calculate the spin-valley resolved longitudinal and Hall conductivities as a function of photon energies showing that the conductivities exhibit a strong topological state dependence. The photon energy of the intraband and interband optical transitions can be tuned by varying the electric and optical fields. Finally, we demonstrate that by modulating the chemical potential, some of the allowed optical transitions become Pauli blocked due to the optical selection rules.

Emerging topology in a hybrid SSH model due to the competition between higher order hopping and spin-orbit coupling*

Hemant Kumar Sharma

Institute of Physics, Sachivalaya Marg, Bhubaneswar-751005, India

Arijit Saha[†] and Saptarshi Mandal[‡]

Institute of Physics, Sachivalaya Marg, Bhubaneswar-751005, India and

Homi Bhabha National Institute, Training School Complex, Anushakti Nagar, Mumbai 400094, India

(Dated: July 10, 2024)

The Su-Schrieffer-Heeger (SSH) model is a widely used theoretical model for studying electronic properties and topology in one-dimensional systems. In the present work we theoretically investigate emergent topological phases in single as well as multiple coupled SSH chains in presence of different types of modulated hoppings. First we show that simultaneous consideration of next to next nearest neighbour hopping and a modulated Rashba interaction can enable one to realize topological index as zero, one and two hosting multiple pairs of zero energy localized edge modes. Further we generalize our scheme to multiple coupled chains and show the emergence of all possible higher topological indices bounded by the number of chains.[1–11]

-
- [1] F. D. M. Haldane, Nobel lecture: Topological quantum matter, *Rev. Mod. Phys.* **89**, 040502 (2017).
- [2] K. v. Klitzing, G. Dorda, and M. Pepper, New method for high-accuracy determination of the fine-structure constant based on quantized hall resistance, *Phys. Rev. Lett.* **45**, 494 (1980).
- [3] K. von Klitzing, T. Chakraborty, P. Kim, V. Madhavan, X. Dai, J. McIver, Y. Tokura, L. Savary, D. Smirnova, A. M. Rey, C. Felser, J. Gooth, and X. Qi, 40 years of the quantum hall effect, *Nature Reviews Physics* **2**, 397 (2020).
- [4] A. Altland and M. R. Zirnbauer, Nonstandard symmetry classes in mesoscopic normal-superconducting hybrid structures, *Phys. Rev. B* **55**, 1142 (1997).
- [5] C.-K. Chiu, J. C. Y. Teo, A. P. Schnyder, and S. Ryu, Classification of topological quantum matter with symmetries, *Rev. Mod. Phys.* **88**, 035005 (2016).
- [6] M. Nakahara, *Geometry, topology and physics* (CRC Press, 2018).
- [7] J. Cayssol and J. N. Fuchs, Topological and geometrical aspects of band theory, *Journal of Physics: Materials* **4**, 034007 (2021).
- [8] R. B. Laughlin, Anomalous quantum hall effect: An incompressible quantum fluid with fractionally charged excitations, *Phys. Rev. Lett.* **50**, 1395 (1983).
- [9] W. P. Su, J. R. Schrieffer, and A. J. Heeger, Solitons in polyacetylene, *Phys. Rev. Lett.* **42**, 1698 (1979).
- [10] M. Atala, M. Aidelsburger, J. T. Barreiro, D. Abanin, T. Kitagawa, E. Demler, and I. Bloch, Direct measurement of the zak phase in topological bloch bands, *Nature Physics* **9**, 795 (2013).
- [11] S. de Léséleuc, V. Lienhard, P. Scholl, D. Barredo, S. Weber, N. Lang, H. P. Büchler, T. Lahaye, and A. Browaeys, Observation of a symmetry-protected topological phase of interacting bosons with rydberg atoms, *Science* **365**, 775 (2019), <https://www.science.org/doi/pdf/10.1126/science.aav9105>.

* A footnote to the article title

[†] arijit@iopb.res.in

[‡] saptarshi@iopb.res.in

Characterization of Silicon Carbide Biphenylene Network Through GW-BSE Simulations

Arushi Singh¹, Vikram Mahamiya², and Alok Shukla¹

¹*Indian Institute of Technology Bombay, 400076 India*

²*International Centre for Theoretical Physics (ICTP)-Trieste, Italy*

Two-dimensional silicon carbide stands out among 2D materials, primarily due to its notable band gap, unlike its carbon-based counterparts. However, the binary nature and non-layered structure of bulk SiC present challenges in fabricating its 2D counterpart. Recent advancements in technology have led to the successful synthesis of atomically thin, large-scale epitaxial monolayers of hexagonal-SiC [1] and Si₉C₁₅ [2], marking a significant milestone in semiconductor research. Inspired by these advancements, we have computationally designed another stable phase of 2D-SiC in the popular biphenylene network, termed SiC-biphenylene. This structure is characterized by inter-connected polygons of octagons, hexagons, and tetragons arranged periodically. The dynamical and thermal stability has been confirmed through ab initio phonon dispersion and molecular dynamics simulations. The structure demonstrates a high melting point of approximately 3475 K and a “direct” band gap of 2.16 eV using the HSE06 functional. Upon considering many-body effects, the quasiparticle band gap widens to 2.89 eV at the G₀W₀ level, indicating pronounced electron correlation effects within the material. Our analysis further reveals that the effective mass of charge carriers exhibits higher values along the $\Gamma \rightarrow Y$ compared to the $\Gamma \rightarrow X$. Moreover, the optical spectrum obtained from solving the Bethe-Salpeter equation (G₀W₀+BSE) identifies the first optically active exciton peak at 2.07 eV, corresponding to a strongly bound exciton with a binding energy of 0.82 eV. The effective mass and Bohr radius of the exciton are calculated to be 1.01 m_0 and 2.14 Å, respectively, demonstrating the characteristic of a Frenkel exciton. Furthermore, the investigation into stable bilayer structures across various stacking configurations (AA, AA', and AB-stacked) highlights the impact of stacking patterns on excitonic binding energies, with AA-stacked configuration indicating the presence of Mott-Wannier exciton. Our investigation extends to identifying the stable bulk phase of SiC-biphenylene, revealing lower self-energy corrections compared to monolayer and bilayer structures, attributed to increased electron delocalization in bulk structures.

[1] Polley et al., Phys. Rev. Lett. 130, 076203 (2023).

[2] Gao et al., Adv. Mater. 34, 2204779 (2022).

Investigating Topological Phase Transition in Rare-Earth Monopnictide Semimetals: A *first-principles* Approach

Mukhtiyar Singh

Department of Applied Physics, Delhi Technological University, Delhi-110042, India

Email: mukhtiyarsingh@dtu.ac.in, msphysik09@gmail.com

Topological materials (TMs) are interesting materials which are insulating in bulk but have exotic metallic states. These materials are attracting significant research efforts in condensed matter physics. These materials have potential applications in spintronics, quantum computing, Chemical catalysts, and thermoelectric energy harvesting. TMs can be divided into several categories e.g., topological Insulators (TIs), topological semimetals (TSMs), topological crystalline insulators (TCIs) and many more. Time reversal symmetry (TRS) and spin-orbit coupling (SOC) play an important role in TMs. Consequently, inversion in bulk bands is observed at high symmetric points in the bulk Brillion zone which are protected by TRS and inversion symmetry. The Z_2 topological invariants and surface Dirac cones are used to identify the topological nature of materials. The surface states are doubly protected and do not allow backscattering in the absence of an external magnetic field.

We demonstrated the topological quantum phase transition (TPT) in two binary rare-earth monopnictides i.e., YbAs and YBi under hydrostatic pressure in the presence of SOC. We used hybrid density functional theory to probe the structural, electronic, and topological properties of these rare-earth monopnictides. These materials exist in stable rocksalt structure (*NaCl-type*) and were experimentally reported to be topologically trivial semimetal at ambient pressure conditions. Our calculations shows that the topological band inversion take place at an applied pressure of 20 GPa and 6.5 GPa, respectively; and these binary systems turn into Z_2 topological semimetal. We discussed the evolution of the surface states and the bulk band structure of these systems. The Surface density of states of these systems contain a Dirac cone observed near the Fermi level. The odd number of topological band inversions close to the Fermi level are verified with the help of the product of parities of all the filled eigen states and the evolution of Wannier Charge Centers (WCCs). These quantum phase transitions are well within the structural phase transitions of YbAs (52GPa) and YBi (24.5 GPa).

[1] Fu L, Kane C L and Mele E J, Phys. Rev. Lett. **98** 106803 (2007).

[2] Yu R, Qi X L, Bernevig A, Fang Z and Dai X, Phys. Rev. B **84** 075119 (2011).

[3] Singh M, Kumar R and Bibiyan R K, Eur. Phys. J. Plus **137** 6332022 (2022).

[4] Kumar R and Singh M, J. Phys.: Condens. Matter **36** 345601 (2024).

Exploring Novel Topological Phases in 3D Materials: Theoretical Insights and Predictions

Poorva Singh¹, Shivendra Kumar Gupta¹, Ashish Kore², and Saurabh Kumar Sen¹

¹Department of Physics, Visvesvaraya National Institute of Technology, Nagpur, 440010, India

²Physics Division, National Center for Theoretical Sciences, National Taiwan University, Taipei 106319, Taiwan

The interest in the role of topology in condensed matter physics has witnessed significant rise over the last decade, with topological insulators and Dirac/Weyl semimetals acquiring the centre-stage [1]. Specifically, topological insulators (TIs) are emerging materials for next generation nano-electronic devices, thanks to the non-trivial spin-momentum locking of their topological surface states. We have recently predicted materials (SrCaX, X = Bi, Sb, As and P) in which topological Dirac nodal line semimetal phase and type II Dirac point coexists. Multiple nodal lines present in these materials are confirmed by Z_2 Berry phase and drumhead-like surface states that pop out from the bulk and originates from the nodal point. Coexisting characteristics of nodal line semimetal and type II Dirac point have the potential to unveil new physical phenomena.

References:

[1] M. Z. Hasan and C. L. Kane, *Rev. Mod. Phys.* **82**, 3045 (2010).

[2] S. K. Gupta, A. Kore, S. K. Sen, and P. Singh, arXiv preprint arXiv:2406.03952 (2024).

Evidence of Magnetism Induced by Drumhead Surface States in the Dirac Line-Nodal Semimetal CaAgP

Hidemitsu Takahashi¹, Shunsaku Kitagawa¹, Kenji Ishida¹, and Yoshihiko Okamoto²

¹*Department of Physics, Kyoto University, Japan*

²*ISSP, University of Tokyo, Japan*

Topological semimetal is a group of materials characterized by topologically protected band crossing. When the crossing points form lines in the reciprocal space, it is called a line-nodal semimetal. In the line-nodal semimetals, remarkable phenomena such as extremely high mobility and quasitopological electromagnetic responses [1] are expected. Furthermore, unique topological surface states called drumhead surface states [2] appear. Despite the intensive experimental research, the properties of the line-nodal semimetal have remained elusive, partly because topologically trivial band often coexists with nodal lines in actual materials. CaAgP is one of the ideal candidates for the Dirac line-nodal semimetal [3]. The nodal line surrounding the Γ point solely locates near the Fermi energy and the drumhead surface states emerge inside the nodal line. The drumhead surface states have nearly flat energy dispersion, resulting in the large density of states and introduce the strong correlation effect. Therefore, CaAgP is a good platform to study such novel topological quantum phenomena. As a matter of fact, unconventional surface superconductivity was reported in $\text{CaAg}_{1-x}\text{Pd}_x\text{P}$ [4]. However, angle-resolved photoemission-spectroscopy measurements reported that CaAgP has topologically trivial bands [5], and the electronic structure of CaAgP is under debate. In this study, we performed ^{31}P -nuclear magnetic resonance (NMR) measurements on a single crystal CaAgP to investigate the electronic properties microscopically. We succeeded in observing NMR signals corresponding to two nonequivalent P sites in Fig. 1. The observed behaviors of Knight shift K and nuclear spin-lattice relaxation rate $1/T_1$ are consistent with the Dirac line-nodal semimetal rather than usual metal. Prominently, $1/T_1$ exhibits the anomalous behavior, which suggests magnetic transition, even though CaAgP is nonmagnetic. This result is considered to be the evidence of magnetism induced by the drumhead surface states [6, 7].

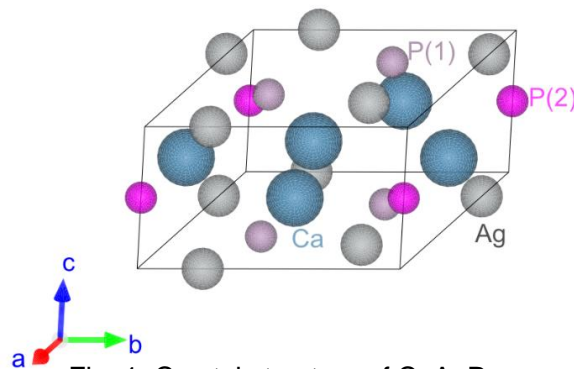


Fig. 1. Crystal structure of CaAgP.

- [1] S. T. Rammamurthy *et al.*, Phys. Rev. B **95**, 075138 (2017).
- [2] Y. Kim *et al.*, Phys. Rev. Lett. **115**, 036806 (2015).
- [3] A. Yamakage *et al.*, J. Phys. Soc. Jpn. **85**, 013708 (2016).
- [4] R. Yano *et al.*, Nat. Comm. **14**, 6817 (2023).
- [5] N. Xu *et al.*, Phys. Rev. B **97**, 161111(R) (2018).
- [6] J. Liu *et al.*, Phys. Rev. B **95**, 075426 (2017).
- [7] B. Roy *et al.*, Phys. Rev. B **96**, 04113(R) (2017).

Dependence of the conserved quantities in tilted Dirac material on the amount of tilting

M. Titandari^{1,2}, S. A. Jafari³

¹*KNT University of Technology, Tehran, Iran*

²*Department of Physics, Sharif University of Technology, Tehran 11155-9161, Iran*

³*2nd Physics Institute C, RWTH Aachen University, Aachen, Germany*

The effective Hamiltonian of Dirac/Weyl materials have an emergent Lorentz invariance which is tantamount to an emergent Minkowski spacetime in Dirac/Weyl materials albeit with the speed of light c replaced by the Fermi velocity v which is a material property [1]. From this point of view, the tilted Dirac cone materials can be associated with a deformation of the Minkowski spacetime [2] whose isometries are expected to be generalizations of Lorentz transformations. Identification of the isometries of such a new spacetime is equivalent to construction of the conserved quantities for tilted Dirac material. In this work we accomplish this for boson and Fermions and obtain explicit dependence of the conserved quantities of tilted Dirac cone materials on the dimensionless tilting parameter ζ . These results can be useful in understanding the behavior and quantum transport of electrons in heterostructure of two Dirac materials across which the tilting parameters are different. In particular we obtain how the spin current is modified by the presence of tilt which might have implications for spintronics.

[1] N. P. Armitage, E. J. Mele, and A. Vishwanath, *Rev. Mod. Phys.* **90**, 015001 (2018).

[2] G. E. Volovik, *JETP Letters* 104, 645 (2016).

Probing valley phenomena with gate-defined valley splitters

Juan Daniel Torres Luna^{1,2}, Kostas Vilkelis^{1,2}, and Antonio Liucas Rigotti Manesco²¹*Qutech, Delft University of Technology, Delft 2600 GA, The Netherlands*²*Kavli Institute of Nanoscience, Delft University of Technology, Delft 2600 GA, The Netherlands*

Despite many reports of valley-related phenomena in graphene and its multilayers, current transport experiments cannot probe valley phenomena without the application of external fields. Here we propose a gate-defined valley splitter as a direct transport probe for valley phenomenon in graphene multilayers. First, we show how the device works, its magnetotransport response, and its robustness against fabrication errors. Secondly, we present two applications for valley splitters: (i) resonant tunnelling of quantum dots probed by a valley splitter shows the valley polarization of dot levels; (ii) a combination of two valley splitters resolves the nature of order parameters in mesoscopic samples.

Emerging Majorana bound states in superconducting Haldane nanoribbons

Simone Traverso¹, Niccolò Traverso Ziani^{1,2}, Maura Sassetti^{1,2}, and Fernando Dominguez³

¹(Presenting author underlined) Physics Department, University of Genoa, 16146 Genoa, Italy

²CNR-SPIN, 16146 Genoa, Italy

³Technische Universität Braunschweig, Institut für Mathematische Physik, 38106 Braunschweig, Germany

In the ever growing landscape of quantum technologies, topological insulators and topological superconductors play a key role as promising platforms for applications in spintronics, superconducting spintronics and topologically protected quantum computation. Particularly for the latter, the ability to manipulate Majorana Bound States (MBSs) would represent a significant breakthrough.

In this contribution, we describe a novel approach to designing of MBSs, based on the dimensional reduction of two-dimensional (2D) nodal topological superconductors [1]. To illustrate this mechanism, we focus on the p -wave superconducting Haldane model and thoroughly explore its topological phase diagram.

In two dimensions, this model exhibits a topological nodal superconducting phase, characterized by a chiral Majorana mode propagating along the edges of nanoribbons with cylindrical boundary conditions. However, this phase is unstable in a finite 2D rectangular-cropped lattice, leading to corner states close to zero energy in a flake with alternating zigzag and armchair edges.

By reducing one of the dimensions, quantum confinement gaps out the bulk bands more rapidly than the edge states. This allows for the hybridization of the edge states [2], potentially resulting in Majorana zero modes. Their emergence is assessed by computing the topological invariant for the quasi-one-dimensional setup and by directly inspecting the energy spectrum of (long) open flakes. Additionally, we confirm their topological nature by computing the zero bias conductance in a normal-superconducting junction, which is found to be sharply quantized to $2e^2/h$ in presence of an MBS at the interface. Our findings hence suggest quantum confinement as a crucial ingredient in building quasi-one-dimensional topological superconducting phases starting from two-dimensional nodal topological superconductors.

[1] Traverso, S., Ziani, N. T., Sassetti, M., and Dominguez, F. Emerging Majorana bound states in superconducting Haldane nanoribbons. arXiv preprint arXiv:2407.06925.

[2] Traverso, S., Sassetti, M., and Ziani, N. T. Emerging topological bound states in Haldane model zigzag nanoribbons. npj Quantum Mater. **9**, 9 (2024)

Shuttling of Majorana zero modes in disordered and noisy topological superconducting wires

Bill Truong¹, Kartiek Agarwal^{1,2}, and T. Pereg-Barnea¹

¹*Department of Physics, McGill University*

²*Materials Science Division, Argonne National Laboratory*

Majorana zero modes (MZMs) have been the subject of intense study in recent times partly due to the prospect of their use as building blocks for a topological quantum computer. In particular, Majorana-based quantum computing takes advantage of the topological protection that MZMs are endowed, the non-locality that they display, and their non-Abelian exchange statistics. In order to perform gate operations, MZMs must be manipulated and braided, processes which ideally takes place solely within the ground state subspace of a given system. Away from this ideal setting, transitions to excited states will occur and lead to decoherence, constituting a “diabatic error.” Braiding protocols are often envisioned on a network of topological superconducting wires where MZMs are shuttled by tuning wire sections (“piano keys”) between topologically trivial and topologically non-trivial phases.

Our work studies the behaviour of the diabatic error as MZMs are shuttled in this wire setting. It has previously been established that the error from a single piano key can be adequately described by Landau-Zener physics [1] and that the use of multiple piano keys may be optimal in reducing the error in certain situations [2]. In this current work, we extend upon these studies and consider the response of the error when MZMs are transported through wires which contain disorder and are subjected to external noise. Through numerical simulation, we find that the error is generally enhanced in both cases, and we demonstrate that the minimum bulk gap plays a central role in this enhancement.

[1] B. Bauer, T. Karzig, R. V. Mishmash, A. E. Antipov, and J. Alicea, *SciPost Phys.* 5, 004 (2018)

[2] B. P. Truong, K. Agarwal, T. Pereg-Barnea, *Phys. Rev. B* 107, 104516 (2023)

Topological phase transitions of generalized Brillouin zones in Hermitian and non-Hermitian systems

Sonu Verma¹, and Moon Jip Park^{2,3}

¹*Center for Theoretical Physics of Complex Systems, Institute for Basic Science (IBS), Daejeon 34126, Republic of Korea.*

²*Department of Physics, Hanyang University, Seoul, 04763, Republic of Korea.*

³*Research Institute for Natural Science, Hanyang University, Seoul, Republic of Korea.*

A generic feature of symmetry-protected topological phases of matter is the bulk-boundary correspondence (BBC), which connects the concept of bulk topology to the emergence of robust boundary states. In recent years, non-Hermitian systems have shown unconventional properties and phenomena such as exceptional points, non-Hermitian skin effect, and many more in different research fields without Hermitian analogs. Therefore, the topological Bloch band theory with the notion of the Brillouin zone (BZ) has been extended to the non-Bloch band theory with the notion of the generalized Brillouin zone (GBZ) defined by generalized momenta, which can take complex values. The non-Bloch band theory has successfully proven that non-Hermitian systems show two types of modified BBC: (i) complex eigenvalue topology of the bulk leads to non-Hermitian skin effect, where all bulk states localize at one boundary of the system, and (ii) the wave function topology leads to the conventional topological boundary modes.

In this seminar, I will discuss a different type of BBC that originates from the intrinsic topology of the generalized Brillouin zone (GBZ) [1]. Topologically non-trivial GBZ appears due to general boundary conditions that break the system's translation symmetry locally. In our case, the topological phase transition is characterized by the generalized momentum touching of GBZ, which accompanies the emergence of exceptional points.

Furthermore, I will also discuss a simple extension of our work to Hermitian systems [2]. Firstly, we found that the intrinsic topology of GBZ successfully characterizes the symmetry-protected topological phases. In this case, the topological phase transition of GBZ is characterized by the generalized momenta touching of GBZ, which accompanies the emergence of band touching points or diabolic points. Moreover, the non-Bloch band theory provides a natural topological invariant characterizing the sub-symmetry-protected topological phases that a conventional Bloch topological invariant (winding number) fails to characterize.

[1] Sonu Verma, and Moon Jip Park, *Communication Physics* **7**, 21 (2024).

[2] Sonu Verma, and Moon Jip Park, *arXiv:2405.06240*, (2024).

Geometric measure of entanglement in systems with poor man's Majorana modes

Vimalesh Kumar Vimal¹, Jorge Cayao¹

¹*Uppsala University*

Entanglement is a quantum effect describing non-classical correlations between quantum systems and central to quantum information processing. Apart from the well-known entanglement quantifiers, such as concurrence and entanglement entropy, the degree of entanglement can also be characterized geometrically. For a pure state, the geometric measure of entanglement is defined by its distance from the nearest separable state. In this talk, I will discuss the application of the geometric measure of entanglement [3] in a system with Poor man's Majorana modes, quasiparticles that exhibit Majorana-like properties but are not protected by topology. In particular, I will focus on a two-site Kitaev chain [1, 2], where two such quasiparticles emerge. I will contrast the geometric entanglement signatures with those appearing in common entanglement quantifiers.

[1] M. Leijnse and K. Flensberg, Phys. Rev. B 86, 134528 (2012).

[2] T. Dvir et al., Nature 614, 445-459 (2023).

[3] T.-C. Wei and P. M. Goldbart, Phys. Rev. A 68, 042307 (2003).

Dynamical Hall responses of disordered superconductors

A. Hijano^{1,2}, S. Vosoughi-nia^{3,4,5}, F. S. Bergeret^{1,6}, P. Virtanen³, and T. T. Heikkilä³

¹ *Centro de Física de Materiales Centro Mixto CSIC-UPV/EHU, E-20018 Donostia–San Sebastián, Spain*

² *Department of Condensed Matter Physics, University of the Basque Country UPV/EHU, 48080 Bilbao, Spain*

³ *Department of Physics and Nanoscience Center, University of Jyväskylä, P.O. Box 35 (YFL), FI-40014 Jyväskylä, Finland*

⁴ *AGH University of Krakow, Academic Centre for Materials and Nanotechnology, al. A. Mickiewicza 30, 30-059 Krakow, Poland*

⁵ *Institute of Physics, Marie Curie-Skłodowska University, 20-031 Lublin, Poland*

⁶ *Donostia International Physics Center, 20018 Donostia–San Sebastián, Spain*

We extend the Mattis-Bardeen theory [1] for the dynamical response of superconductors to include different types of Hall responses. This is possible thanks to a recent modification of the quasiclassical Usadel equation [2, 3], which allows for analyzing Hall effects in disordered superconductors and including the precise frequency dependence of such effects. Our results form a basis for analyzing dynamical experiments especially on novel thin-film superconductors, where ordinary Hall and spin Hall effects can both show up.

[1] D. C. Mattis and J. Bardeen, Phys. Rev. **111**, 412 (1958).

[2] P. Virtanen, F. S. Bergeret, and I. V. Tokatly, Phys. Rev. B **104**, 064515 (2021).

[3] P. Virtanen, F. S. Bergeret, and I. V. Tokatly, Phys. Rev. B **105**, 224517 (2022).

Quantum geometric analysis of non-Hermitian Kitaev chain with long-range couplings

Y R Kartik¹, Jhih-Shih You^{1,2}, and H. H. Jen²

¹ *Institute of Atomic and Molecular Sciences, Academia Sinica, Taipei 10617, Taiwan*

² *Department of Physics, National Taiwan Normal University, Taipei 11677, Taiwan*

Long-range couplings play an important role in understanding the non-local behaviour of systems in nature. Here we consider a non-Hermitian PT symmetric version of Kitaev chain with long-range couplings to understand the quantum geometric aspects. We adopt the bi-orthonormal vector basis to construct the extended quantum geometry and conduct the related scaling of fidelity susceptibility. Due to long-range effect, the model exhibits different correlation behaviour at different parameter spaces, and we explore them through Wannier state correlation function with related critical exponents. The interplay of quantum geometry and long-range interactions with non-Hermitian effects are less explored in the past, which is the highlighted part in this work.

[1] YR Kartik, RR Kumar, S Sarkar, Scientific Reports 14 (1), 4504 (2024)

Topological defects in Rydberg-dressed Bose gases with spin-orbit coupling

Xiao-Fei Zhang^{1,2}

¹*School of Physics & Information Science, Shaanxi University of Science and Technology, Xi'an 710021, China*

²*National Time Service Center, Chinese Academy of Sciences, Xi'an 710600, China*

Very recently, there are growing theoretical and experimental interests in observing supersolid phases in cold atom systems, where the concept of supersolid is generalized to superfluid with spontaneous translation symmetry breaking. Previous works have shown that the cold atoms with supersolid properties can be realized in a quantum gas with dipolar interaction, spin-orbit coupling, or the nonlocal Rydberg interaction. For the ultra-cold atom system with only nonlocal Rydberg interaction, the observed topological excitations show trivial topology, and thus it is of particular interest to consider a system with both spin-orbit coupling and nonlocal Rydberg interactions.

We find a variety of novel topological defects in Rydberg-dressed Bose gas with spin-orbit coupling theoretically. A quantized vortex spontaneously breaks its azimuthal invariance, leading to the formation of discrete vortex around the supersolid crystal cells with discrete rotational symmetry. For strongly interacting case, high-order vortex characterized by a nonzero radial quantum number, can be stabilized in the unit cell within the supersolid phase. These topological defects are self-trapping and sustained by balancing the nonlocal Rydberg interaction and spin-orbit coupling, which are generally inaccessible in a conventional superfluid and observable by in situ imaging.

[1] W. Han, **X.-F. Zhang***, D.-S. Wang, H.-F. Jiang, W. Zhang, and S.-G. Zhang, Phys. Rev. Lett. **121**, 030404 (2018).

[2] **X.-F. Zhang***, L. Wen, L.-X. Wang, G.-P. Chen, R.-B. Tan, and H. Saito, Phys. Rev. A **105**, 033306 (2022) .

[3] Si-Lin Chen, H. Guo, P. Tu, L. Wen, X.-Y. Yang, **X.-F. Zhang***, To be submitted to Phys. Rev. A.

Scattering theory of higher order topological insulators

R. Johanna Zijderveld¹, Isidora Araya Day^{1,2}, and Anton R. Akhmerov¹

¹*Kavli Institute of Nanoscience, Delft University of Technology, P.O. Box 4056, 2600 GA Delft, The Netherlands*

²*QuTech, Delft University of Technology, Delft 2600 GA, The Netherlands*

Intrinsic higher order topological insulators (HOTIs) have edge states protected by the global symmetry of the sample. We advance the understanding of HOTIs by developing a theory of scattering topological invariants. Because our approach utilizes the global symmetry properties, it establishes the bulk-edge correspondence. This allows researchers to study intrinsic HOTIs in the presence of disorder as well as quasi-crystalline and amorphous HOTIs. In addition, the scattering approach enables analysis of network models, where Hamiltonian topological invariants are insufficient. In this poster, I will demonstrate the general approach by using $C_4\mathcal{T}$ symmetry as an example.